Palacký University
Faculty of Science

Quantum correlations of light produced in spontaneous parametric frequency down-conversion process

Ph.D Thesis

Ievgen Arkhipov

supervisor:

doc. RNDr. Ondřej Haderka, Ph.D.

Submitted in part fulfilment of the requirements for the degree of
Doctor of Philosophy in Applied Physics of the Palacký University, 2017

Declaration of originality

I hereby declare that this thesis is my own work and that, to the best of my knowledge and belief, it contains no material previously published or written by another person nor material which to a substantial extent has been accepted for the award of any other degree or diploma of the university or other institute of higher learning, except where due acknowledgement has been made in the text.

In Olomouc, ..., 2017 .....

Submitted on ....., 2017

The author grants permission to Palacký University in Olomouc to store and display this thesis and its electronic version in university library and on official website.

Acknowledgements

First of all, I want to express my gratitude to my supervisor Ondřej Haderka for his indespensible guidence throughout my doctoral study. Special thanks belong to my colleague Jan Peřina Jr., whose help made the impossible possible and discussions with whom motivated me a lot. I am also thankful to all co-authors of my publications (in alphabetical order) Alesia Allevi, Maria Bondani,Václav Michálek, Adam Miranowicz, Jan Peřina and Jiří Svozilík.

And, especially, I want to thank my family and my girlfriend Anna for support and inspiration in writing this Thesis and to whom this work is dedicated.

Contents

Chapter 1

Introduction

The concept of the quantum nature of light first came in 1900, when Planck in order to solve the problem of the spectral distribution of the black body arrived to the idea that the energy of harmonic oscillator is quantized. Later, in 1905, Einstein studying the photoelectric effect came to the conclusion that it could be explained by the assumption that the energy of a light beam was distributed in discrete bundles later named photons [1]. Despite the early achievements of quantum theory, for a long time there had been no experimental evidence of quantumness of light, since all experimental results could be explained from the point of view of classical physics.

In 1963 Glauber and independently Sudarshan developed the quantum theory of coherence [2, 3], where a qualitative theoretical description of the nonclassicality of light was given. Namely, they introduced the P function which serves as a quasiprobability function of the quantum light.

The first evidence of nonclassical nature of light was observed in 1976 in an experiment by Kimble, Dagenais and Mandel [4] and launched a new era in quantum optics. In that experiment the antibunching statistics was observed by the light generated by resonance fluorescence from a two-level atom. A classical theory of light would require negative probabilities in order to give photon antibunching.

Later, the new sources of nonclassical light were found, such as squeezed light. In a squeezed state one phase quadrature may reduce quantum fluctuations at the expense of increased quantum fluctuations in the other phase quadrature such that the product of the fluctuations still obeys Heisenberg's uncertainty relation. Squeezed states offer the possibility of beating the quantum limit in optical measurements by making phase-sensitive measurements which utilize only the quadrature with reduced quantum fluctuations. The first observation of squeezed states was achieved by Slusher in 1985 in four-wave mixing in atomic sodium [5]. This was soon followed by demonstrations of squeezing in an optical parametric oscillator by Kimble [6] and by four-wave mixing in optical fibres by Levenson [7]. The squeezing effect was then also found in parametric frequency down-conversion process. The intensity difference fluctuations in the twin beams produced in such a process have been shown to be considerably below the shot-noise level.

One of the most intriguing manifistations of the nonclassicality of quantum light is entanglement. The notion of the entanglement refers to the quantum correlations between different parts of the system, which cannot be described by the classical physics. Historically, the term of entanglement first appeared in the literature in 1935. The entangled states treated in the paper by Einstein, Podolsky, and Rosen [8] were two-particle states quantum-mechanically correlated with respect to their positions and momenta. Ironically, the considered quantum state in that article was intended to show incompleteness of quantum theory, because of apparent violation of causality, and thus leading to nonlocality of the quantum physics. The same year, in the journal Naturwissenschaften, Schrödinger coins the term *Verschränkung*, meaning "entanglement," and develops his famous thought experiment of a cat that exists simultaneously in a state of being alive and dead [9].

Experimental proposal to test the nonlocality and thus the entanglement was first made by Bell in 1964. Bell introduced the inequality which, if violated, would indicate the properties of nonlocality of a quantum system. Such an experiment was implemented first by Freedman in 1972 [10] and later with considerable improvements in 1982 by Aspect [11]. Those and other experiments have confirmed that entanglement and therefore nonlocal effects do indeed exist.

Later, in 1993, Bennett with colleagues proposed a scheme, where it was shown how the entanglement can be utilized to realize a quantum teleportation of the state of the photon [12]. In the same decade the experiment proving the possibility of the state teleportation was carried out by the team lead by Zeilinger from Vienna University in 1997 [13].

The entanglement has proved to be indispensible in quantum information theory and is considered as the main source in the implementation of quantum telecommunications and quantum computations [14].

So far, the most convenient and practical source of the entanglement have been the twin beams generated in a spontaneous parametric frequency down-conversion process. Twin beams are Gaussian states, i.e., their characteristic function is a Gaussian function. Although the twin beam is a bipartite system, by making use of various passive optical elements, such as beam splitters, phase shifters etc., one is able to produce multipartite nonclassical, entangled, and even hyperentangled Gaussian states [15, 16].

At present, the twin beam is a workhorse in the study of the both nonclassicality and entanglement of quantum light. It can be used as a source for discrete variable domain systems as qubits (for very low intensities) as well as for continuous variable domain as quadratures of the field.

Despite the great attention the twin beams have drawn, still the following questions need to be answered, namely

- What is the exact relationship between nonclassicality and entanglement of twin beams? And does entanglement of twin beams completely constitute the nonclassicality of their state?

Another interesting question regarding a twin beam is:

- What kind of nonclassical states can be generated from the twin beam? And how the initial nonclassicality of the twin beam can be transfered among the newly obtained states?

One of the most convenient ways to generate new states from the initial given state, especially for a two-mode state, is by means of a beam splitter. Here, one can also ask:

- Is there any nonclassicality invariant for a twin beam which would include single-mode nonclassicality and two-mode entanglement when a twin beam is subjected to unitary transformations, e.g., it is transformed by the beam splitter?

The last question has a fundamental importance, because the question about unification of the nonclassicality measures for single-mode and entanglement measure between modes for a state subjected to unitary transformations is still open.

In this Thesis we attempt to give answers to those questions.

The Thesis is organized as follows. In Chapter 2 we give a quick review of the basics of quantum optics, namely a quantization of optical fields and notions of the Fock and Gaussian states. We also give a brief introduction to the concepts of nonclassicality and entanglement and consider the appropriate measures for their quantification. Additionally, we shortly discuss the nature of the spontaneous parametric frequency down-conversion process.

Chapter 3 is devoted to the comparative study of nonclassicality, entanglement and dimensionality of multimode twin beams. In this chapter we derive the relation which unifies the entanglement measure such as negativity and nonclassicality measure - nonclassicality depth, and thus we prove that the only source of the nonclassicality for the twin beams is their entanglement. Moreover, we also show that that relation holds true also when noise is included.

In Chapter 4 we investigate the behaviour of the twin beams, single-mode squeezed light and their combinations at the beam splitter. We introduce a new integral of nonclassicality, which incorporates the entanglement between two modes and nonclassicality of one-mode states, and we prove that that integral is invariant under any unitary photon-number-preserving operations.

In Chapter 5 we study the nonclassicality of the state which is generated from the twin beam by postselection based on detecting a given number of photocounts in one arm. The nonclassicality

is derived from the high order intensity moments based on the majorization theory for single-mode states. We experimentally show the presence of the nonclassicality up to the fifth order of the intensity moments, and thus experimentally confirm that the nonclassicality for such a state resides in the intensity domain.

In Chapter 6 we investigate a four-mode state generated in spontaneous parametric frequency down-conversion and frequency up-conversion processes. We show, that the main source of the nonclassicality of the considered state is given by the twin beams and how that nonclassicality expressed by means of entanglement can "flow" from the twin beams into up-converted beams and vice versa by changing the strength of the pump fields.

Chapter 7 is dedicated to the potential application of twin beams to the problem of the reconstruction of Gaussian states. The reconstruction scheme is applied to the Gaussian fields generated from vacuum by utilizing the nonclassical properties of the twin beam. We also demonstrate, that the proposed reconstruction method enables one to avoid a homodyne detection, and it relies exlusively on photon-counting detectors.

Chapters 3 - 7 are based on published papers with considerable contribution of the author of this Thesis.

Conclusions are drawn in Chapter 8.

Chapter 2

Background Theory

2.1 Quantization of the electromagnetic field

From classical theory of electromagnetism for a plane electromagnetic wave of frequency ω_k propagating in the direction $\vec{k}$ the electric $\vec{E}$ and magnetic $\vec{B}$ fields are given by

$$\vec{E}(\vec{r},t) = \vec{\varepsilon} E_0 \mathrm{e}^{\mathrm{i}\vec{k}\vec{r}-\mathrm{i}\omega_k t} + c.c, \quad \vec{B}(\vec{r},t) = \frac{\vec{k}\times\vec{\varepsilon}}{k} E_0 \mathrm{e}^{\mathrm{i}\vec{k}\vec{r}-\mathrm{i}\omega_k t} + c.c, \tag{2.1}$$

$k = |\vec{k}| = \omega_k/c$, where c is the speed of light, $\vec{\varepsilon}$ accounts for the polarization vector of the electromagnetic wave, and thus it is perpendicular to the propogation direction z of the wave and can attain two possible projections onto the plane xy. The symbol $c.c$ denotes a complex conjugate.

The energy of the electromagnetic field contained in the volume V is given by

$$U \equiv \frac{1}{8\pi} \int\limits_V \left(|\vec{E}|^2(\vec{r},t) + |\vec{B}|^2(\vec{r},t) \right) \mathrm{d}^3 r. \tag{2.2}$$

Important role in electromagnetic theory is played by a vector potential $\vec{A}(\vec{r},t)$, which is related

to the electric and magnetic fields as

$$\vec{E} = -\frac{1}{c}\frac{\partial \vec{A}}{\partial t}, \quad \vec{B} = \vec{\nabla} \times \vec{A}. \tag{2.3}$$

The Coulomb gauge is used, i.e., the scalar potential is set to zero and therefore $\mathrm{div}\vec{A}(\vec{r},t) = 0$. By applying Coulomb gauge one makes electric and magnetic vectors completely dependent on vector potential only.

Thus, for the case of plane waves one can write

$$\vec{A}(\vec{r},t) = \vec{\varepsilon} A_0 \mathrm{e}^{\mathrm{i}\vec{k}\vec{r} - \mathrm{i}\omega_k t} + c.c., \quad E_0 = \frac{\mathrm{i}\omega_k}{c} A_0. \tag{2.4}$$

Now by considering the electromagnetic field expanded into a set of plane waves confined in the cube with linear size equal to L, and by applying the boundary periodic conditions, one obtaines the following allowed values for the components of the wave vector $\vec{k}$

$$k_x = \frac{2\pi n_x}{L}, \quad k_y = \frac{2\pi n_y}{L}, \quad k_z = \frac{2\pi n_z}{L}, \quad n_x, n_y, n_z = 0, \pm 1, \pm 2, \ldots \tag{2.5}$$

The vector potential for such a field thus can be written in the form

$$\vec{A}(\vec{r},t) = \sum_{\vec{k},s} \frac{A_{\vec{k}s}}{\sqrt{V}} \vec{\varepsilon}_{\vec{k}s} \mathrm{e}^{\mathrm{i}\vec{k}\vec{r} - \mathrm{i}\omega_k t} + c.c. \tag{2.6}$$

Combining Eqs. (2.2), (2.6) and utilizing the orthogonality property of the plain waves, i.e.,

$$\frac{1}{V} \int\limits_V \mathrm{e}^{\mathrm{i}\vec{k}\vec{r} - \mathrm{i}\vec{k}'\vec{r}} \mathrm{d}^3 r = \delta_{n_x n'_x} \delta_{n_y n'_y} \delta_{n_z n'_z}, \tag{2.7}$$

one arrives at the expression for the energy

$$U = \frac{1}{2\pi} \sum_{\vec{k},s} \left(\frac{\omega_k^2}{c^2} \right) |\vec{A}_{\vec{k}s}|^2. \tag{2.8}$$

From quantum theory we know, that the energy of the electromagnetic oscillators should be

quantized by the number of modes $n_{\vec{k}s}$, i.e.,

$$U = \sum_{\vec{k},s} \hbar\omega_{\vec{k}} n_{\vec{k}s}. \tag{2.9}$$

Now, comparing Eq. (2.8) and Eq. (2.9) we can find a correspondence

$$n_{\vec{k}s} \leftrightarrow \frac{\omega_k}{2\pi\hbar c^2} |\vec{A}_{\vec{k}s}|^2. \tag{2.10}$$

In quantum optics electric, magnetic and potential vectors become operators. And as such the energy becomes a Hermitian operator, with the mode number operator

$$\hat{n}_{\vec{k}s} = \hat{a}^\dagger_{\vec{k}s} \hat{a}_{\vec{k}s}, \tag{2.11}$$

where the non-Hermitian operator $\hat{a}^\dagger_{\vec{k}s}$ ($\hat{a}_{\vec{k}s}$) is called creation (annihilation) operator. Those operators also satisfy the following commutation relations

$$\left[\hat{a}_{\vec{k}s}, a^\dagger_{\vec{k}'s'}\right] = \delta_{\vec{k}\vec{k}'}\delta_{ss'}, \quad \left[\hat{a}_{\vec{k}s}, a_{\vec{k}'s'}\right] = 0. \tag{2.12}$$

By inspecting Eqs. (2.10), (2.11) we find that the relation between the operator of vector potential and non-Hermitian annihilation operator has a simple form $\hat{A}_{\vec{k}s} = \sqrt{\frac{2\pi\hbar c^2}{\omega_k}}\hat{a}_{\vec{k}s}$. The exact form for the field's vector operators is as following

$$\begin{aligned}
\hat{A}(\vec{r},t) &= \sum_{\vec{k},s} \sqrt{\frac{2\pi\hbar c^2}{\omega_k V}} \vec{\varepsilon}_{\vec{k}s} \hat{a}_{\vec{k}s} \mathrm{e}^{\mathrm{i}\vec{k}\vec{r} - \mathrm{i}\omega_k t} + H.c., \\
\hat{E}(\vec{r},t) &= \mathrm{i}\sum_{\vec{k},s} \sqrt{\frac{2\pi\hbar\omega_k}{V}} \vec{\varepsilon}_{\vec{k}s} \hat{a}_{\vec{k}s} \mathrm{e}^{\mathrm{i}\vec{k}\vec{r} - \mathrm{i}\omega_k t} + H.c., \\
\hat{B}(\vec{r},t) &= \mathrm{i}\sum_{\vec{k},s} \sqrt{\frac{2\pi\hbar\omega_k}{V}} \frac{\vec{k}\times\vec{\varepsilon}_{\vec{k}s}}{k} \hat{a}_{\vec{k}s} \mathrm{e}^{\mathrm{i}\vec{k}\vec{r} - \mathrm{i}\omega_k t} + H.c.,
\end{aligned} \tag{2.13}$$

where $H.c.$ means Hermitian conjugate. The Hamiltonian of the electromagnetic field which

corresponds to the energy operator given Eq. (2.2) and Eq. (2.13) can be expressed as

$$\hat{H} = \sum_{\vec{k},s} \hbar\omega_k \left(\hat{a}^\dagger_{\vec{k}s} \hat{a}_{\vec{k}s} + \frac{1}{2} \right). \tag{2.14}$$

Therefore, in contrast to the classical physics, the quantum mechanics predicts a non-zero energy for the vacuum even in the absence of the electromagnetic field, which equals $\sum_{\vec{k},s} \hbar\omega_k/2$.

2.2 Quantum states of light

Since in the following chapters we will deal with Fock and Gaussian states, here we present a brief introduction in the theory of such states.

2.2.1 Fock states

The Fock states are photon number states and can be written as a ket vector $|n\rangle$ in the Dirac representation, where n denotes the number of light quanta.

The action of the annihilation (creation) operator on the Fock state decreases (increases) a number of photons on one in the state, i.e.,

$$\hat{a}|n\rangle = \sqrt{n}|n-1\rangle, \quad \hat{a}^\dagger|n\rangle = \sqrt{n+1}|n+1\rangle. \tag{2.15}$$

And for a photon number operator one has

$$\hat{n}|n\rangle = \hat{a}^\dagger\hat{a}|n\rangle = n|n\rangle. \tag{2.16}$$

The state $|0\rangle$ is called the vacuum state, thus it does not contain any photons in the radiation field.

Making use of the expressions given in Eq. (2.15) one can generate n-photon state from the

vacuum by applying n times the creation operator $\hat{a}^\dagger$, namely

$$|n\rangle = \frac{(\hat{a}^\dagger)^n}{\sqrt{n!}}|0\rangle. \tag{2.17}$$

2.2.2 Gaussian states

For a system consisting of M modes, the phase space is determined by coordinate- and momentum-like operators $\hat{x}$, $\hat{p}$ (which are also called as amplitude and phase quadrature, respectively) expressed via boson operators as follows

$$\hat{x}_k = \frac{1}{\sqrt{2}}\left(\hat{a}_k + \hat{a}_k^\dagger\right), \quad \hat{p}_k = \frac{1}{\sqrt{2}i}\left(\hat{a}_k - \hat{a}_k^\dagger\right), \quad k = 1 \dots M, \tag{2.18}$$

and which obey a commutation rule

$$[\hat{x}_k, \hat{p}_l] = \mathrm{i}\delta_{kl}. \tag{2.19}$$

An M-mode state described by the density matrix $\hat{\rho}$ is a Gaussian state if its symmetrically-ordered characteristic function is Gaussian:

$$C_{\mathcal{S}}(\mathcal{B}) = \mathrm{Tr}\left[\hat{\rho}\exp\left\{-\mathrm{i}\mathcal{B}^T\mathbf{\Sigma}\hat{\boldsymbol{R}}\right\}\right], \tag{2.20}$$

where Tr stands for a trace operation, $\mathcal{B} = (\beta_{1x}, \beta_{1y}, \dots, \beta_{Mx}, \beta_{My})^T \in \mathbb{R}^{2M}$, $\mathbf{\Sigma}$ is the symplectic matrix, i.e., $\mathbf{\Sigma}^T = -\mathbf{\Sigma} = \mathbf{\Sigma}^{-1}$, which is defined as

$$\mathbf{\Sigma} = \bigoplus_{i=1}^{M} \boldsymbol{\omega}_i, \quad \boldsymbol{\omega}_i = \begin{pmatrix} 0 & 1 \\ -1 & 0 \end{pmatrix}, \tag{2.21}$$

and $\hat{\boldsymbol{R}} = (\hat{x}_1, \hat{p}_1, \dots, \hat{x}_M, \hat{p}_M)^T$ is a vector of operators.

$$C_{\mathcal{S}}(\mathcal{B}) = \exp\left\{-\frac{1}{2}\mathcal{B}^T\mathbf{\Sigma}\boldsymbol{\sigma}_{\mathcal{S}}\mathbf{\Sigma}^T\mathcal{B} - \mathrm{i}\mathcal{B}^T\mathbf{\Sigma}\langle\hat{\boldsymbol{R}}\rangle\right\} \tag{2.22}$$

where we defined the covariance matrix of symmetrical ordering

$$\sigma_{\mathcal{S}kl} \equiv [\boldsymbol{\sigma}_{\mathcal{S}}]_{kl} = \frac{1}{2}\langle \hat{R}_k \hat{R}_l + \hat{R}_l \hat{R}_k \rangle - \langle \hat{R}_k \rangle \langle \hat{R}_l \rangle. \tag{2.23}$$

Note that because of the noncommutativity of the boson operators $\hat{a}$, $\hat{a}^\dagger$, one deals with different ordering of operators. For example, for normal ordering of boson operators, which we denote by ::, all the creation operators are put to the left, and annihilation operators to the right, respectively, when acting on a certain state, i.e., $:\hat{a}\hat{a}^\dagger: = \hat{a}^\dagger\hat{a}$, thus $:\hat{a}\hat{a}^\dagger: \neq \hat{a}^\dagger\hat{a} + 1$. The opposite rule applies to the antinormal ordering.

It is worth noting, that Gaussian states can be completely determined by their covariance matrix, since by applying the approapriate displacement operator to the state $\hat{\rho}$, one can dispose of the first-moment vector $\hat{\boldsymbol{R}}$.

The uncertainty relations among canonical operators impose a constraint on the covariance matrix, corresponding to the inequality

$$\boldsymbol{\sigma}_{\mathcal{S}} + \frac{\mathrm{i}}{2}\boldsymbol{\Sigma} \geq 0, \tag{2.24}$$

that expresses the positivity of the density matrix $\hat{\rho}$.

In analogy with symmetrically ordered characteristic function in Eq. (2.22) we can define normally-ordered characteristic function, which also plays a crucial role in our later analysis, namely

$$C_{\mathcal{N}}(\boldsymbol{\beta}) = \exp\left\{-\frac{1}{2}\boldsymbol{\beta}^\dagger \boldsymbol{\Sigma} \boldsymbol{\sigma}_{\mathcal{N}} \boldsymbol{\Sigma}^T \boldsymbol{\beta} - \boldsymbol{\beta}^\dagger \boldsymbol{\Sigma} \langle \hat{\boldsymbol{A}} \rangle\right\}, \tag{2.25}$$

with $\boldsymbol{\beta} = (\beta_1, \beta_1^*, \ldots, \beta_M \beta_M^*)^T \in \mathbb{C}^{2M}$ and normally-ordered covariance matrix

$$\sigma_{\mathcal{N}kl} \equiv [\boldsymbol{\sigma}_{\mathcal{N}}]_{kl} = \langle :\hat{A}_k^\dagger \hat{A}_l: \rangle - \langle \hat{A}_k^\dagger \rangle \langle \hat{A}_l \rangle, \tag{2.26}$$

where $\hat{\boldsymbol{A}} = \left(\hat{a}_1, \hat{a}_1^\dagger, \ldots, \hat{a}_M, \hat{a}_M^\dagger\right)^T$ is a column vector of boson operators.

By Fourier transforming the characteristic function in Eq. (2.22), we obtain the so-called Wigner

function of $\hat{\rho}$

$$W(\boldsymbol{X}) = \frac{1}{(2\pi^2)^M} \int\limits_{\mathbb{R}^{2M}} \mathrm{d}^{2M}\mathcal{B} \exp\left\{\mathrm{i}\mathcal{B}^T \boldsymbol{\Sigma} \boldsymbol{X}\right\} C_{\mathcal{S}}(\mathcal{B}) \tag{2.27}$$

Substituting Eq. (2.22) into Eq. (2.27) one obtains

$$W(\boldsymbol{X}) = \frac{1}{\pi^M \sqrt{\det[\boldsymbol{\sigma}_{\mathcal{S}}]}} \exp\left\{-\frac{1}{2}\left(\boldsymbol{X} - \langle \hat{\boldsymbol{R}} \rangle\right)^T \boldsymbol{\sigma}_{\mathcal{S}}^{-1} \left(\boldsymbol{X} - \langle \hat{\boldsymbol{R}} \rangle\right)\right\}. \tag{2.28}$$

Therefore, the Wigner function is Gaussian whenever $C_{\mathcal{S}}(\mathcal{B})$ is Gaussian. This is in contrast with normally-ordered characteristic function, which, under certain circumstances, can lack the Gaussian behaviour because of the nonpositivity of the covariance matrix in Eq. (2.25). Since $C_{\mathcal{N}}(\boldsymbol{\beta})$ determines the Glauber-Sudarshan P function [17, 18] via Fourier transform, this can lead to highly nonregular behaviour of P function. The latter case indicates the nonclassicality of the quantum state, and we proceed to its discussion in the next section.

2.3 Nonclassicality of quantum light

For optical fields, a commonly accepted criterion for distinguishing nonclassical states from the classical ones is expressed as follows: a quantum state is nonclassical if its Glauber-Sudarshan P function fails to have all the properties of a probability density. The Glauber-Sudarshan P function for a bosonic state $\hat{\rho}$ can be defined as

$$\hat{\rho} = \int P(\alpha, \alpha^*) |\alpha\rangle\langle\alpha| \mathrm{d}^2\alpha, \tag{2.29}$$

It is worth noting that the negativity of the P function is the necessary and sufficient condition for nonclassicality, while the irregularity of the P function is only a sufficient condition. Therefore, if the P function is more singular or more irregular than Dirac's δ-function for a given state, then it is also nonpositive (semidefinite). As an example of such an irregular function is the P function for an n-photon Fock state (with $n = 1, 2, ...$), which is given by the nth derivative of $\delta(\alpha)$.

Based on this definition of nonclassicality, various operational criteria have been proposed for testing the nonclassicality. In what follows, for the sake of simplicity, we consider nonclassicality measures defined for a single-mode state, the generalization to the multimode case is straightforward.

One of the first measures of the nonclassicality of light was introduced by Mandel in 1979 [19]. He introduced the following parameter

$$Q_M = \frac{\langle :\hat{n}^2: \rangle - \langle \hat{n} \rangle^2}{\langle \hat{n} \rangle}. \tag{2.30}$$

In terms of the P function the parameter Q_M can be expressed as

$$Q_M = \frac{\langle (\alpha^* \alpha - \langle \alpha^* \alpha \rangle)^2 \rangle_P}{\langle \alpha^* \alpha \rangle_P}, \tag{2.31}$$

where $\langle \rangle_P$ stands for the avarage over $P(\alpha)$, namely

$$\langle \alpha^{*m} \alpha^n \rangle_P = \int P(\alpha) \alpha^{*m} \alpha^n \mathrm{d}^2 \alpha. \tag{2.32}$$

The quantity in Eq. (2.31) is positive if Glauber-Sudarshan P function is a positive function. Therefore, if $Q_M < 0$ then the state should be nonclassical, since P function fails to be a probability function. For coherent states one has $Q_M = 0$, i.e., the state exhibits pure Poissonian statistics, for Fock states $Q_M = -1$ and thus, the state is nonclassical. As it is seen from the definition of Q_M in Eq. (2.30), the Mandel parameter can detect nonclassicality only in the intensity domain, and cannot answer if the state is nonclassical in the phase space.

The extension of the Mandel parameter, which is based on the second-order intensity moments of the light field, to the higher-order intensity moments was done by Lee [20] with an introduced normalized nonclassicality parameter derived from the majorization theory:

$$R_k(l,m) \equiv \frac{\langle :\hat{n}^{l+k}: \rangle \langle :\hat{n}^{m-k}: \rangle}{\langle :\hat{n}^l: \rangle \langle :\hat{n}^m: \rangle} - 1, \quad l \geq m \geq k. \tag{2.33}$$

In the same way the nonclassicality of a state is revealed by the condition $R_k(l,m) < 0$.

To detect the nonclassicality expressed in the phase space, the following parameter can be utilized [21]:

$$S_\theta = \langle : (\hat{X}_\theta)^2 : \rangle_P - \langle \hat{X}_\theta \rangle_P^2, \tag{2.34}$$

where $\hat{X}_\theta$ is the generalized quadrature of the field

$$\hat{X}_\theta = \frac{\hat{a}\mathrm{e}^{-\mathrm{i}\theta} + \hat{a}^\dagger \mathrm{e}^{\mathrm{i}\theta}}{\sqrt{2}}. \tag{2.35}$$

For $\theta = 0$ $(\pi/2)$, the $\hat{X}_\theta$ reduces to well-known coordinate- (momentum-) like operator $\hat{x}$ $(\hat{p})$.

Therefore, whenever $S_\theta < 0$ it is said that the corresponding quantum state is nonclassical. The nonclassical measure S_θ is often used to detetect a squeezed light, i.e., light, where the variance of one of its quadratures ($\hat{x}$ or $\hat{p}$) is squeezed compared to the deviation of the vacuum, namely

$$\langle \Delta \hat{X}_\theta^2 \rangle < \frac{1}{2}. \tag{2.36}$$

Based on the definition of the nonclassicality measures derived from the nonclassicality of the P function mentioned above, in general, one can construct any such a $\hat{f}$ operator decomposed into a series of m photon number (quadrature) operators $\hat{f} = \sum_k c_k \hat{n}^k$ $\left(\hat{f} = \sum_k c_k \hat{X}_\theta^k\right)$. The quadratic normally-ordered form of $\hat{f}$ would then lead to the nonclassicality measure

$$\langle : \hat{f}^\dagger \hat{f} : \rangle_P < 0. \tag{2.37}$$

The latter condition leads to the negativity of the matrix M with elements $M_{jk} = \langle : \hat{n}^{j+k} : \rangle$ $\left(M_{jk} = \langle : \hat{X}_\theta^{j+k} : \rangle\right)$, which implies the negativity of the principal minors of the matrix M, namely

$$\mathrm{det} M^{(k)} < 0, \quad 1 \leq k \leq m. \tag{2.38}$$

The condition given in Eq. (2.38) is called the nonclassicality condition in terms of higher-order moments of the number or quadrature operators.

Another suggestion how to measure nonclassicality came from Lee in 1991 [22]. He introduced

the following general distribution function

$$R(\alpha,\tau)=\frac{1}{\pi\tau}\int \mathrm{d}^2\beta \exp\left(-\frac{1}{\tau}|\alpha-\beta|^2\right)P(\beta) \tag{2.39}$$

where parameter τ serves as nonclassical measure of a state and $0\leq\tau\leq 1$. P is the Glauber-Sudarshan function.

The idea behind the introduction of the convolution function R in Eq. (2.39) is to find such a minimal value of τ at which the function $R(\alpha,\tau)$, if being a nonpositive and a more nonregular than Dirac delta function, becomes a positive function, i.e., it satisfies the requirements imposed on a classical probability function. When $\tau=0,\frac{1}{2},1$ the R function is transformed into the Glauber-Sudarshan function P, the Wigner function W and Hashimi function Q, respectively. Whenever $\tau>0$ the state is considered to be nonclassical, and the larger the τ the larger the nonclassicality of the state.

2.4 Entanglement

Quantum entanglement is a remarkable phenomenon and it is at the heart of the current development of quantum information processing. It emerges from the quantum superposition principle lying at the heart of quantum mechanics.

So far, the most well known systems displaying entanglement are bipartite states, i.e. states consisting of two subsystems. The theory regarding multiparitite entanglement still needs further investigation and development, since it can be studied only for a limited number of states [23]. There are two types of systems which are at the center of the entanglement theory, namely discrete variable and continuous variable systems. The former deals with the finite Hilbert space, e.g., qubits of photons, whereas the latter considers the systems in the infinite Hilbert space like coordinate and momentum quadratures of the optical field.

For any entangled pure bipartite state with orthonormal bases of each subsystem $\{|u_n\rangle\}$ and

$\{|v_n\rangle\}$, the total state vector can be written in the Schmidt decomposition as

$$|\psi\rangle = \sum_n c_n |u_n\rangle |v_n\rangle . \tag{2.40}$$

The form of Eq. (2.40) implies that the state vector $|\psi\rangle$ can not be presented as a product of two parties, and thus it is entangled.

The definition of pure-state entanglement via the non-factorizability of the total state vector is generalized to mixed states through nonseparability of the total density operator. A general quantum state of a two-party system is separable if its total density operator is a mixture of product states

$$\hat{\rho}_{12} = \sum_i \eta_i \hat{\rho}_{i,1} \otimes \hat{\rho}_{i,2} \tag{2.41}$$

Otherwise, it is inseparable. In general, it is a difficult question whether a given density operator is separable or inseparable. One of the methods to test the state for inseparability is Peres' partial transpose criterion [24]. For a separable state as in Eq. (2.41), transposition of either density matrix gives again a non-negative density operator

$$\hat{\rho}_{12}^{\Gamma} = \sum_i \eta_i \hat{\rho}_{i,1}^{T} \otimes \hat{\rho}_{i,2}. \tag{2.42}$$

The operation T in Eq. (2.42), called a partial transpose, corresponds to transposition of indices corresponding to the first subsystem and has an interpretation as a partial time reversal [23].

The Eq. (2.42) gives a necessary condition for a separable state, and therefore if one of the eigenvalues of the density matrix $\hat{\rho}_{12}^{\Gamma}$ is negative it is, in general, a sufficient condition for inseparability (entanglement). But there are cases, when violation of equality given in Eq. (2.42) is both sufficient and necessary condition for the entanglement, namely for 2×2 and 2×3-dimensional systems, as well as for $1 \times N$-mode Gaussian and $m \times n$-mode bisymmetric Gaussian states [25].

For Gaussian states the time reversal operation mentioned earlier corresponds to the change of

the sign of the momentum operator. Such a transformation in the phase space is described as

$$\hat{\boldsymbol{R}} \to \Gamma\hat{\boldsymbol{R}} = (\hat{x}_1, -\hat{p}_1, \ldots, \hat{x}_M, -\hat{p}_M)^T. \tag{2.43}$$

The covariance matrix of the M-mode Gaussian state reduces then to $\boldsymbol{\sigma}_{\mathcal{S}} \to \Gamma\boldsymbol{\sigma}_{\mathcal{S}}\Gamma$.

The condition, that the partially transposed Gaussian state is physical can be written as follows:

$$\Gamma_a\boldsymbol{\sigma}_{\mathcal{S}}\Gamma_a \geq \frac{\mathrm{i}}{4}\boldsymbol{\Sigma}, \tag{2.44}$$

where operator $\Gamma_a = \Gamma \otimes \mathbb{I}$, i.e., it changes signs of the momenta in the first subsystem a.

The violation of the condition given in Eq. (2.44) is sufficient for entanglement between Gaussian subsytems a and b, and as was mentioned earlier is also necessary for $1 \times N$-mode Gaussian and $m \times n$-mode bisymmetric Gaussian states.

There are several measures of entanglement, which apply either to discrete or continuous variable domain. Since in our present work we deal with Gaussian states, i.e., continuous variable states, below we consider the most used quantitative entanglement measures.

One such a measure is called *negativity* N. Since the inseparable state exhibits the negativity of the partial transpose density matrix, in that way one can utilize such a non-positivity property as a measure for the entanglement. Based on that, negativity N can be defined as an absolute sum of negative eigenvalues of the density matrix $\hat{\rho}_{12}^{\Gamma}$. And it can be written as

$$N = \frac{||\hat{\rho}^{\Gamma}||_1 - 1}{2}, \tag{2.45}$$

where $||\cdot||_1$ is the trace norm, i.e., the sum of absolute values of eigenvalues.

For Gaussian states the negativity N can also be obtained directly from its partially transposed covariance matrix $\Gamma_a\boldsymbol{\sigma}_{\mathcal{S}}\Gamma_a$. Any two-mode covariance matrix $\boldsymbol{\sigma}_{\mathcal{S}}$ can be written as

$$\boldsymbol{\sigma}_{\mathcal{S}} = \begin{pmatrix} \boldsymbol{A} & \boldsymbol{C} \\ \boldsymbol{C}^T & \boldsymbol{B} \end{pmatrix} \tag{2.46}$$

where $\boldsymbol{A}$, $\boldsymbol{B}$, and $\boldsymbol{C}$ are 2×2 matrices. Then we can define four local symplectic invariants, i.e., quantities that are left unchanged by local symplectic transformations:

$$I_{\mathcal{S}1} = \det[\boldsymbol{A}], \quad I_{\mathcal{S}2} = \det[\boldsymbol{B}], \quad I_{\mathcal{S}3} = \det[\boldsymbol{C}], \quad I_{\mathcal{S}4} = \det[\boldsymbol{\sigma}_{\mathcal{S}}]. \tag{2.47}$$

Another important symplectic invariant is defined as follows

$$\Delta(\boldsymbol{\sigma}_{\mathcal{S}}) = I_{\mathcal{S}1} + I_{\mathcal{S}2} + 2I_{\mathcal{S}3}. \tag{2.48}$$

For partial transpose covariance matrix those invariants become

$$\tilde{I}_{\mathcal{S}1} = I_{\mathcal{S}1}, \quad \tilde{I}_{\mathcal{S}2} = I_{\mathcal{S}2}, \quad \tilde{I}_{\mathcal{S}3} = -I_{\mathcal{S}3}, \quad \tilde{I}_{\mathcal{S}4} = I_{\mathcal{S}4}, \quad \tilde{\Delta}(\boldsymbol{\sigma}_{\mathcal{S}}) = I_{\mathcal{S}1} + I_{\mathcal{S}2} - 2I_{\mathcal{S}3}. \tag{2.49}$$

The symplectic eigenvalues of $\Gamma_a \boldsymbol{\sigma}_{\mathcal{S}} \Gamma_a$ are defined then as follows

$$\tilde{d}_{\pm} = \sqrt{\frac{\tilde{\Delta}(\boldsymbol{\sigma}_{\mathcal{S}}) \pm \sqrt{\tilde{\Delta}(\boldsymbol{\sigma}_{\mathcal{S}})^2 - 4I_{\mathcal{S}4}}}{2}}. \tag{2.50}$$

The condition for separability in Eq. (2.44) can be rewritten as

$$\tilde{d}_{-} \geq \frac{1}{2}. \tag{2.51}$$

The relation between negativity N and symplectic eignevalue $\tilde{d}_{-}$ takes the form

$$N = \frac{1}{4\tilde{d}_{-}} - \frac{1}{2}. \tag{2.52}$$

Very often instead of negativity the logarithm of the trace norm of partially transposed density matrix is used, and is called logarithmic negativity

$$E_N = \log ||\hat{\rho}^{\Gamma}||_1. \tag{2.53}$$

Or equivalently for Gaussian states in terms of symplectic eigenvalues

$$E_N = -\log 2\tilde{d}_-. \tag{2.54}$$

Apart from negativity N, logarithmic negativity E_N has an operational meaning, namely it is a special type of entanglement cost under positive partial transpose preserving operations [26].

2.5 Spontaneous Parametric Frequency Down-Conversion Process

Spontaneous parametric frequency down-conversion (SPDC) is a nonlinear optical process occuring as a result of the interaction of an intense laser beam and a medium with the second order nonlinear susceptability $\chi^{(2)}$ leading to the generation of entangled photon pairs.

From both the theoretical and the experimental points of view, the nonlinear process of parametric down-conversion, in which photon pairs are generated, has been playing an important role in quantum optics [27, 28, 29, 30]. Its individual photon pairs have been exploited in many fundamental experiments testing nonclassical behavior predicted by quantum physics [31, 32]. It has also allowed the generation of more intense fields having their electric-field amplitude quadratures squeezed below the vacuum level [33, 34, 35], exhibiting sub-shot-noise correlations [36, 37] or having sub-Poissonian photon-number statistics [38, 39, 40].

The schematical description of the process is shown in Fig. 2.1.

Here, the pump photon with the frequency ω_p is converted into two photons traditionally called signal and idler with corresponding frequences ω_s and ω_i. These two photons are generated from the vacuum of the modes $\hat{a}_s$ and $\hat{a}_i$. Moreover, the conservation law of energy and momentum gives

$$\omega_p = \omega_s + \omega_i, \quad \vec{k}_p = \vec{k}_s + \vec{k}_i, \tag{2.55}$$

where $\vec{k}$ is a wave vector.

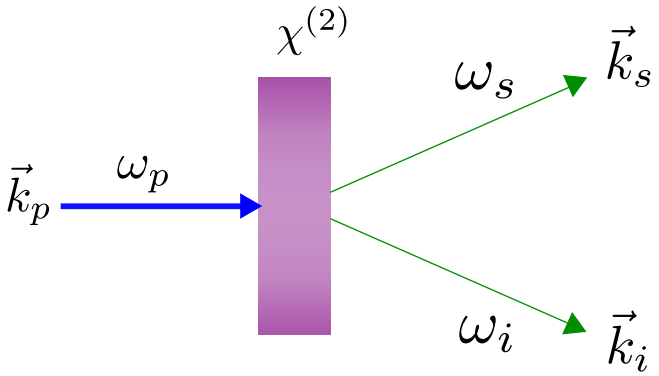

Figure 2.1: Spontaneous parametric frequency down-conversion process. The intense laser field with the wave vector $\vec{k}_p$ and frequency ω_p impinges on the nonlinear crystal with dielectric susceptability $\chi^{(2)}$ producing at the output of the crystal both a signal and idler beam with wave vectors $\vec{k}_s$, $\vec{k}_i$ and frequencies ω_s, ω_i, respectively.

Due to Eq. (2.55) the bandwidths of the frequency and momentum of the generated down-converted photons can be large. In general, the normalized quantum state of the signal and idler photons can be written as follows:

$$|\Psi\rangle = \int \Phi(\omega) \left| \frac{\omega_p}{2} + \omega; \frac{\omega_p}{2} - \omega \right\rangle \mathrm{d}\omega, \tag{2.56}$$

where $\Phi(\omega)$ is the biphoton amplitude function, the exact form of which depends on phase-matching conditions, and the properties of the pumping beam and the nonlinear medium.

There are two types of SPDC. The process is called type I (II) if the signal and idler photons have identical (orthogonal) polarizations. Additionally, the process is called collinear (noncollinear) if signal and idler photons travel in the same (different) directions.

Here below, we consider key features of the theoretical model of the frequency down-conversion process of type I, since it is of utmost importance for the present work. We also stress the importance of the phase-matching condition. The more detailed approach to describe the properties of the system based on Heisenberg equations and covariance matrix of the SPDC will be considered in the following chapters.

The interaction Hamiltonian in the interaction picture for SPDC process can be written as

$$H_I = \chi^{(2)} \int\limits_V \mathrm{d}^3 r \hat{E}_p^{(+)}(\vec{r}) \hat{E}_s^{(-)}(\vec{r}) \hat{E}_i^{(-)}(\vec{r}) + H.c., \tag{2.57}$$

where $\hat{E}_j^{(+)}$ ($\hat{E}_j^{(+)}$) is the positive (negative) frequency part of the operator of the electric field. H.c. stands for Hermitian conjugation. The integration is performed over the volume V of the crystal. For simplicity we also assumed that nonlinear susceptability $\chi^{(2)}$ is constant in the whole volume. In turn $\hat{E}_j^{(+)}$ has the form

$$\hat{E}_j^{(+)} = \sum_k \mathrm{i}\sqrt{\frac{2\pi\hbar\omega_{jk}}{n_{jk}^2 V}}\hat{a}_{jk}e^{i\vec{k}\vec{r}-i\omega_{jk}t}, \quad \hat{E}_j^{(-)} = -\sum_k \mathrm{i}\sqrt{\frac{2\pi\hbar\omega_{jk}}{n_{jk}^2 V}}\hat{a}_{jk}^\dagger e^{-i\vec{k}\vec{r}+i\omega_{jk}t}, \quad j = s, i. \quad (2.58)$$

Here n_{jk} is the refractive index of the medium at the frequency ω_{jk}, and $\hat{a}$ ($\hat{a}^\dagger$) is annihilation (creation) operator. The quantum state expressed by the Fock state can be written in the manner $|\psi\rangle \sim |n\rangle$, where n is the number of the photons in the field. In the quantum mechanics a quantum state evolves in time in the interaction picture according to the formula

$$|\Psi(t)\rangle = \exp\left(-\frac{\mathrm{i}}{\hbar}\int H_I \mathrm{d}t\right)|\Psi(0)\rangle\,. \quad (2.59)$$

Now, combining Eqs. (2.57)-(2.59) with the assumption that the pump field is very intense and thus can be treated classically $\left(\hat{E}_p^{(+)} = \varepsilon_p e^{\mathrm{i}\vec{k}_p\vec{r}+\mathrm{i}\omega_p t}\right)$, and taking the vaccum state as the initial state $|\Psi(0)\rangle = |0,0\rangle$, the first-order correction of the wave function of the spontaneous down-conversion then can read as

$$\left|\Psi^{(1)}\right\rangle \simeq \sum_{\vec{k},\vec{k}'} \hat{a}_{s\vec{k}}^\dagger \hat{a}_{i\vec{k}'}^\dagger F_{\vec{k}\vec{k}'}\,|0,0\rangle\,, \quad (2.60)$$

where

$$F_{\vec{k}\vec{k}'} = \varepsilon_p \chi^{(2)}\mathrm{i}\int_V \mathrm{d}^3 r \mathrm{e}^{\mathrm{i}\vec{k}_p\vec{r}-\mathrm{i}\vec{k}\vec{r}-\mathrm{i}\vec{k}'\vec{r}}\int \mathrm{d}t \mathrm{e}^{-\mathrm{i}\omega_p t+\mathrm{i}\omega_{sk}t+\mathrm{i}\omega_{ik'}t}\frac{2\pi\sqrt{\omega_{sk}\omega_{ik'}}}{V n_{sk} n_{ik'}}. \quad (2.61)$$

For simplicity, let us consider the case of the collinear propagation. Further, we assume that the pump field is propagating along the z direction, i.e., $\vec{k}_p = \vec{z}k_z$, and we also assume that the transverse area of the crystal (T denotes transverse components) is much larger that the transverse profile of the pump and therefore we can span the space integral in T domain to infinity. As a result, the integration over x and y axis in Eq. (2.61) would give the delta function $\delta_{\vec{k}_T+\vec{k}'_T}$. The time integration in the limit of $t \to \infty$ would also give $2\pi\delta(\omega_p - \omega_{sk} - \omega_{ik'})$. In

turn, the integral over z in the crystal with the length L becomes the phase-matching integral, namely

$$h(u) = \frac{\mathrm{e}^{\mathrm{i}u} - 1}{\mathrm{i}u}, \quad u = (k_p - k_{sz} - k_{iz})\, L \tag{2.62}$$

Thus, the function $F_{\vec{k}\vec{k}'}$ attains the form

$$F_{\vec{k}\vec{k}'} = \frac{4\pi^2 \mathrm{i}\chi^{(2)}\varepsilon_p\sqrt{\omega_{sk}\omega_{ik'}}}{n_{sk}n_{ik'}}\delta_{\vec{k}_T+\vec{k}'_T}\delta(\omega_p - \omega_{sk} - \omega_{ik'})h\left[(k_p - k_{sz} - k_{iz})\, L\right]. \tag{2.63}$$

The inspection of the form of the F function in Eq. (2.63) leads to the conslusion, that the signal and idler photons emmited from the crystal are entangled in the frequency and momentum domains. Moreover, the ideal phase-matching conditions are obtained if

$$\omega_p = \omega_{sk} + \omega_{ik'}, \quad k_p = k_{sz} + k'_{iz}. \tag{2.64}$$

Given Eqs. (2.63), (2.64), the quantum state $|\Psi\rangle$ up to the first-order correction corresponding to the spontaneous parametric frequency down-conversion can be written as follows:

$$|\Psi\rangle \simeq |0,0\rangle + F_{\vec{k}\vec{k}'}\,|1,1\rangle + \ldots \tag{2.65}$$

The Eq. (2.65) represents the two-mode quantum state of light entangled in photon numbers.

Chapter 3

Comparative study of nonclassicality, entanglement and dimensionality of multimode noisy twin beams

Text adopted from *I. I. Arkhipov, J. Peřina Jr., J. Peřina and A. Miranowicz, Phys. Rev. A* **91***, 033837 (2015)* [A1].

3.1 Introduction

In this chapter, we study nonclassicality by applying the Lee nonclassical depth [22] as well as entanglement via the negativity [41, 42] for (in general) noisy twin beams of different intensities. Such fields occur under real experimental conditions in which a nonlinear crystal generates both photon pairs and individual single photons (noise). Nevertheless, the signal and idler fields together form a bipartite quantum system. We note that entanglement and nonclassicality of twin beams generated by down-conversion seeded by thermal light have been analyzed in Refs. [43, 44, 45]. In this case, noise present in the incident thermal fields participates in the nonlinear process and generation of photon pairs. This weakens its detrimental effect on entanglement and nonclassicality of twin beams and allows us to have entangled twin beams

with a larger amount of noise.

Here we also study the problem of entanglement dimension via the negativity N for general twin beams and the Schmidt number K for noiseless twin beams in a pure state. Namely, we estimate how many degrees of freedom of two fields comprising a twin beam are entangled based on the results of Ref. [46] for axisymmetric states. On the other hand, the participation ratio R_{s} [47] determined from the reduced statistical operator $\hat{\rho}_{\mathrm{s}}$ of the signal (or idler) field gives the number of degrees of freedom in this field serving to describe both entanglement and noise. It varies from $R_{\mathrm{s}} = 1$ (for a pure state $\hat{\rho}_{\mathrm{s}}$) to $R_{\mathrm{s}} = d = \dim(\hat{\rho}_{\mathrm{s}})$ for the completely mixed state $\hat{\rho}_{\mathrm{s}} = I/d$. We note that the participation ratio R_{s} gives an effective number of states in the mixture $\hat{\rho}_{\mathrm{s}}$ implied by the property that it is a lower bound for the rank of $\hat{\rho}_{\mathrm{s}}$. Moreover, the logarithm of R is the von Neumann–Renyi entropy of second order [47]. The inverse of the participation ratio is referred to as the purity (or linear entropy). Various methods for direct measuring the Schmidt number K (even without recourse to quantum tomography) were proposed for noiseless twin beams (see, e.g., Refs. [48, 49, 50, 51, 52]). The method of Ref. [50] was recently realized experimentally [53]. We note that the negativity can also be measured without applying quantum tomography as described, e.g., for two polarization qubits using linear optical setups [54, 55].

The chapter is organized as follows. In Sec. 2.2, the model of parametric down-conversion providing an appropriate statistical operator of a twin beam is presented. Entanglement of the twin beam is addressed in Sec. 2.3 using the negativity. The nonclassical depth is introduced in Sec. 2.4 to quantify nonclassicality. The relation between the negativity and the nonclassical depth is also discussed in Sec. 2.4 The dimensionality of a twin beam described by the participation ratio together with the entanglement dimensionality described by the negativity is analyzed in Sec. 2.5. Properties of M-mode twin beams are discussed in Sec. 2.6. Section 2.7 is devoted to experimental multimode twin beams containing also noise embedded in independent spatiotemporal modes. Conclusions are drawn in Sec. 2.8.

3.2 Quantum model of a twin beam

To describe the generation of a single-mode twin beam by parametric down-conversion, we adopt the approach based on the Heisenberg equations derived from the appropriate nonlinear Hamiltonian $\hat{H}_{\rm int}$ [28],

$$\hat{H}_{\rm int} = -\hbar g \hat{A}_1 \hat{A}_2 \exp({\rm i}\omega t - {\rm i}\phi) + {\rm H.c.}, \tag{3.1}$$

where $\hat{A}_1$ ($\hat{A}_1^\dagger$) and $\hat{A}_2$ ($\hat{A}_2^\dagger$) represent the annihilation (creation) operators of the signal and idler field, respectively, and g is a real coupling constant that is linearly proportional both to the quadratic susceptibility of a nonlinear medium and to the real pump-field amplitude. The interaction time is denoted t, ω (ϕ) is the pump-field frequency (phase), and ω_1 and ω_2 stand for the signal- and idler-field frequencies, respectively. The law of energy conservation provides the relation $\omega = \omega_1 + \omega_2$. H.c. is the Hermitian conjugated term. In a real nonlinear process, also noise occurs. It can be described by the Langevin forces $\hat{L}$ belonging to a reservoir of chaotic oscillators with mean number of noise photons $\langle n_{\rm d}\rangle$.

The Heisenberg-Langevin equations corresponding to the Hamiltonian $\hat{H}_{\rm int}$ are written as

$$\begin{aligned} \frac{{\rm d}\hat{A}_1}{{\rm d}t} &= -({\rm i}\omega_1 + \gamma_1)\hat{A}_1 + {\rm i}g\hat{A}_2^\dagger \exp(-{\rm i}\omega t + {\rm i}\phi) + \hat{L}_1, \\ \frac{{\rm d}\hat{A}_2}{{\rm d}t} &= -({\rm i}\omega_2 + \gamma_2)\hat{A}_2 + {\rm i}g\hat{A}_1^\dagger \exp(-{\rm i}\omega t + {\rm i}\phi) + \hat{L}_2, \end{aligned} \tag{3.2}$$

where the constant γ_1 (γ_2) describes damping in the signal (idler) field. The Langevin operators $\hat{L}_i$ (for $i = 1, 2$) have the properties

$$\begin{aligned} \langle \hat{L}_i \rangle = \langle \hat{L}_i^\dagger \rangle = 0, \langle \hat{L}_i^\dagger \hat{L}_j \rangle = 2\gamma_j \langle n_{\rm d}\rangle \delta_{ij}, \\ \langle \hat{L}_i \hat{L}_j^\dagger \rangle = 2\gamma_j \left(\langle n_{\rm d}\rangle + 1\right) \delta_{ij}, \end{aligned} \tag{3.3}$$

where δ_{ij} stands for the Kronecker symbol.

Using the interaction representation [$\hat{A}_j(t) = a_j(t)\exp(-i\omega_j t)$] and neglecting damping together

with the Langevin forces, the solution of Eq. (3.2) attains the form

$$\begin{aligned} \hat{a}_1(t) &= \hat{a}_1(0)u(t) + i\hat{a}_2^\dagger(0)v(t)\exp(i\phi), \\ \hat{a}_2(t) &= \hat{a}_2(0)u(t) + i\hat{a}_1^\dagger(0)v(t)\exp(i\phi), \end{aligned} \tag{3.4}$$

in which $u(t) = \cosh(gt)$ and $v(t) = \sinh(gt)$.

Statistical properties of the twin beam are then described by the normal characteristic function $C_{\mathcal{N}}$ defined as

$$C_{\mathcal{N}}(\beta_1, \beta_2) = \mathrm{Tr}\left[\hat{\rho}\exp(\beta_1\hat{a}_1^\dagger + \beta_2\hat{a}_2^\dagger)\exp(-\beta_1^*\hat{a}_1 - \beta_2^*\hat{a}_2)\right], \tag{3.5}$$

where Tr denotes the trace. Using the solution given in Eq. (3.4), the normal characteristic function $C_{\mathcal{N}}$ attains the Gaussian form [56],

$$C_{\mathcal{N}}(\beta_1, \beta_2) = \exp\left[-(|\beta_1|^2 B_1 + |\beta_2|^2 B_2) + D_{12}\beta_1^*\beta_2^* + D_{12}^*\beta_1\beta_2\right], \tag{3.6}$$

in which β_1 and β_2 denote independent complex variables. For the undamped and noiseless case, we have $D_{12} = \langle \triangle\hat{a}_1 \triangle \hat{a}_2\rangle$. Also the mean number B_{p} of the generated photon pairs is determined as $B_{\mathrm{p}} = \langle \triangle\hat{a}_1^\dagger \triangle\hat{a}_1\rangle = \langle \triangle\hat{a}_2^\dagger \triangle\hat{a}_2\rangle$. When damping and noise are also considered [56], the parameters B_a (for $a = 1, 2$) contain additional noise contributions characterized by the parameters B_{s} and B_{i}, i.e., $B_1 = B_{\mathrm{p}} + B_{\mathrm{s}}$ and $B_2 = B_{\mathrm{p}} + B_{\mathrm{i}}$. Whereas the parameter B_{p} gives the mean number of photon pairs, the parameters B_{s} and B_{i} correspond to the mean number of noise photons coming from the signal- and idler-field reservoirs, respectively. On the other hand, the parameter D_{12} describing mutual correlations between the signal and idler fields is not influenced by the noise since $|D_{12}|^2 = B_{\mathrm{p}}(B_{\mathrm{p}} + 1)$.

The statistical operator $\hat{\rho}$ of the twin beam then acquires the form [28]

$$\hat{\rho} = \frac{1}{\pi^2}\int d^2\beta_1 d^2\beta_2 \mathcal{C}_{\mathcal{A}}(\beta_1, \beta_2) : \exp\left(\sum_{j=1}^{2} \hat{a}_j\beta_j^* - \hat{a}_j^\dagger\beta_j\right) : . \tag{3.7}$$

In Eq. (3.7), $C_{\mathcal{A}}(\beta_1,\beta_2)=C_{\mathcal{N}}(\beta_1,\beta_2)\exp(-|\beta_1|^2-|\beta_2|^2)$ denotes an anti-normal characteristic function and symbol : : means normal ordering of field operators.

Performing integration in Eq. (3.7) we express the statistical operator $\hat{\rho}$ in the form

$$\hat{\rho} \;=\; \frac{1}{\tilde{K}} : \exp\left[-\frac{\tilde{B}_2}{\tilde{K}}\hat{a}_1^{\dagger}\hat{a}_1-\frac{\tilde{B}_1}{\tilde{K}}\hat{a}_2^{\dagger}\hat{a}_2+\frac{|D_{12}|}{\tilde{K}}\left(\hat{a}_1\hat{a}_2+\hat{a}_1^{\dagger}\hat{a}_2^{\dagger}\right)\right] :, \tag{3.8}$$

where $\tilde{K}=\tilde{B}_1\tilde{B}_2-|D_{12}|^2$. The parameters $\tilde{B}_a$ introduced in Eq. (3.8) are related to anti-normal ordering of field operators and are given as $\tilde{B}_a=B_a+1$ with $a=1,2$. Decomposing the statistical operator $\hat{\rho}$ in the Fock-state basis we finally arrive at the formula

$$\rho_{ij,kl} \;=\; \sum_{n=0}^{\infty}\sum_{p=0}^{n}\sum_{r=0}^{p}\sum_{t=0}^{r}(-1)^{n-r}\frac{\tilde{B}_2^{n-p}\tilde{B}_1^{p-r}\tilde{K}^{-n-1}}{(n-p)!(p-r)!}\frac{|D_{12}|^r}{(r-t)!\,t!}\langle ij|\hat{a}_1^{\dagger n-p+t}\hat{a}_2^{\dagger p-r+t}\hat{a}_1^{n-p+r-t}\hat{a}_2^{p-t}|kl\rangle. \tag{3.9}$$

Direct inspection of Eq. (3.9) for the matrix elements of the statistical operator $\hat{\rho}$ written in Eq. (3.9) reveals that all nonzero elements can be parameterized by only three indices,

$$\rho_{i,j,i+d,j+d} \;=\; \frac{1}{\tilde{K}}\sqrt{\frac{(i+d)!}{i!}\frac{(j+d)!}{j!}}\sum_{m=0}^{\max(i,j)}C_m^i C_m^j\frac{m!}{(m+d)!}X_1^{j-m}X_2^{i-m}\left(\frac{|D_{12}|}{\tilde{K}}\right)^{d+2m} \tag{3.10}$$

assuming $d\geq 0$. Moreover, $\rho_{ij,i+d,j+d}=\rho_{i+d,j+d,i,j}$, $X_a=1-\tilde{B}_a/\tilde{K}$ with $a=1,2$, and C_m^i and C_m^j denote the binomial coefficients.

3.3 Negativity of the twin beam

The negativity N of a mixed bipartite system defined on the basis of the Peres-Horodecki criterion for a partially transposed statistical operator [24, 57, 42] is useful for quantifying the entanglement of the twin beam. It can be expressed as

$$N(\hat{\rho})=\frac{||\hat{\rho}^{\Gamma}||_1-1}{2} \tag{3.11}$$

using the trace norm $||\rho^{\Gamma}||_1$ of the partially transposed statistical operator ρ^{Γ}. The negativity essentially measures the degree at which ρ^{Γ} fails to be positive. As such it can be regarded as a quantitative version of the Peres-Horodecki criterion for separability [24, 57]. According to Eq. (3.11), the negativity N is given as the absolute value of the sum of the negative eigenvalues of ρ^{Γ}. It vanishes for separable states. It is worth noting that the negativity N is an entanglement monotone and so it can be used to quantify the degree of entanglement in bipartite systems. Moreover, the negativity does not reveal bound entanglement (i.e., nondistillable entanglement) in systems more complicated than two qubits or qubit-qutrit [58].

To determine the negativity N we consider the eigenvalue problem for the partially transposed statistical operator $\hat{\rho}^{\Gamma}$. The statistical operator $\hat{\rho}^{\Gamma}$ expressed in the Fock-state basis attains a characteristic block structure. The smallest block has dimension 2 and each successive block has dimension larger by 1. For a given M one has a block of dimension $M+1$. Such a block represents a matrix of $M+1$ isolated states; the sum of indices of their statistical operators equals $2M$,

$$\hat{\rho}^{\Gamma}_{M} = \begin{pmatrix} \rho_{0\,M,0\,M} & \rho_{0\,M-1,1\,M} & \cdots & \rho_{0\,0,M\,M} \\ \rho_{1\,M,0\,M-1} & \rho_{1\,M-1,1\,M-1} & \cdots & \cdots \\ \cdots & \cdots & \cdots & \cdots \\ \rho_{M\,M,0\,0} & \cdots & \cdots & \rho_{M\,0,M\,0} \end{pmatrix}. \tag{3.12}$$

It can be shown that eigenvalues of a block of dimension $M+1$ can be expressed as ν_{+}^{M}, $\nu_{+}^{M-1}\nu_{-}$,..., $\nu_{+}\nu_{-}^{M-1}$,ν_{-}^{M} using the eigenvalues ν_{+} and ν_{-} of a block with dimension 2:

$$\nu_{\pm} = 1 - \frac{1}{2\tilde{K}}\left(\tilde{B}_1 + \tilde{B}_2 \mp \sqrt{\left(\tilde{B}_2 - \tilde{B}_1\right)^2 + 4|D_{12}|^2}\right). \tag{3.13}$$

The negative eigenvalues can only be those containing odd powers of ν_{-}. They form a geometric progression whose elements can be summed to arrive at the formula for the negativity N:

$$N = \frac{1}{2}\frac{3(\tilde{B}_1 + \tilde{B}_2) + \sqrt{(\tilde{B}_1 - \tilde{B}_2)^2 + 4|D_{12}|^2} - 4\tilde{K} - 2}{4\tilde{K} - 2(\tilde{B}_1 + \tilde{B}_2) + 1}. \tag{3.14}$$

Expressing parameters $\tilde{B}_1$, $\tilde{B}_2$, and $|D_{12}|^2$ in Eq. (3.14) in terms of parameters $B_{\rm p}$, $B_{\rm s}$, and $B_{\rm i}$,

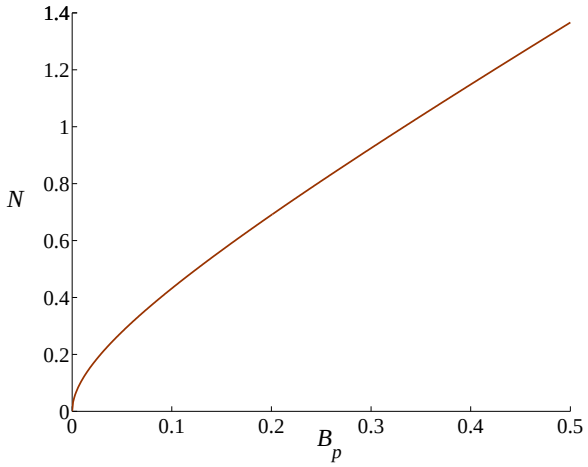

Figure 3.1: Negativity N as a function of the mean photon-pair number B_p for noiseless twin beams (i.e., $B_\mathrm{s} = B_\mathrm{i} = 0$)) according to Eq. (3.16).

we arrive at the formula

$$N = \frac{2B_\mathrm{p} - (B_\mathrm{s} + B_\mathrm{i})(4B_\mathrm{p} + 1) - 4B_\mathrm{s}B_\mathrm{i} + \sqrt{(B_\mathrm{s} - B_\mathrm{i})^2 + 4B_\mathrm{p}(B_\mathrm{p} + 1)}}{4(B_\mathrm{s} + B_\mathrm{i})(2B_\mathrm{p} + 1) + 8B_\mathrm{s}B_\mathrm{i} + 2}. \tag{3.15}$$

Equation (3.15) simplifies considerably for noiseless twin beams:

$$N = B_\mathrm{p} + \sqrt{B_\mathrm{p}(B_\mathrm{p} + 1)}. \tag{3.16}$$

According to Eq. (3.16), all noiseless twin beams are entangled. The more intense the noiseless twin beams are, the more entangled the signal and idler fields are (see Fig. 3.1). The presence of noise in a twin beam can even completely destroy entanglement, as the analysis of Eq. (3.15) shows. Indeed, the condition $N > 0$ for entanglement can be rewritten using Eq. (3.15) as follows:

$$B_\mathrm{p}[1 - (B_\mathrm{s} + B_\mathrm{i})] > B_\mathrm{s}B_\mathrm{i}. \tag{3.17}$$

Condition (3.17) cannot be fulfilled for any value of B_p provided that $B_\mathrm{s} + B_\mathrm{i} \geq 1$. Thus, the twin beam can be entangled only when

$$B_\mathrm{s} + B_\mathrm{i} < 1 \quad \text{and} \quad B_\mathrm{p} > \frac{B_\mathrm{s}B_\mathrm{i}}{1 - (B_\mathrm{s} + B_\mathrm{i})}. \tag{3.18}$$

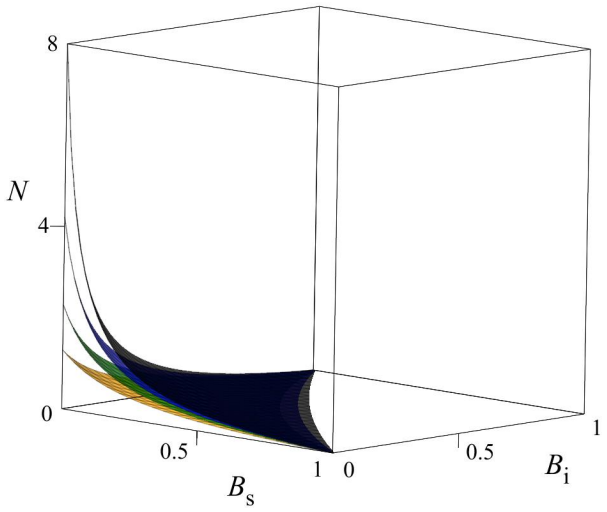

Figure 3.2: Negativity N, given in Eq. (3.15), as a function of the mean noise photon numbers B_s and B_i in the signal and idler modes, respectively, assuming the mean photon-pair number B_p equal to 0.5 [bottom light-gray (yellow) area], 1 [gray (green) area], 2 [dark-gray (blue) area] and 4 [top, black area]. The larger B_p, the larger the negativity N.

The behavior of the negativity N of noisy twin beams dependent on the noise parameters B_s and B_i is illustrated in Fig. 3.2 for several values of the mean photon-pair number B_p. It holds in general that the greater the value of the mean photon-pair number B_p, the greater the value of the negativity N. This can be explained as follows. The more intense twin beams, with their thermal statistics, are effectively spread over a larger number of the Fock states. This naturally results in the larger effectively populated Hilbert spaces used to describe the entanglement. The greater value of the negativity N means a greater effective number of the paired modes building the entanglement, i.e., a greater value of the entanglement dimensionality, as defined in Sec. 2.5. Also, the greater the value of the mean photon-pair number B_p, the larger the amount of overall noise $B_s + B_i$ acceptable in an entangled twin beam (see Fig. 3.3). The curves plotted in Fig. 3.3 indicate that entanglement is more resistent to noise when the noise is distributed in the signal and idler fields asymmetrically. We note that separable states (i.e., with $N = 0$) contain, in general, paired, signal, and idler noisy contributions. However, the noisy contributions are sufficiently strong to suppress the "entangling power" of the photon-pair contribution and so the state effectively behaves as a classical statistical mixture of the signal and idler fields.

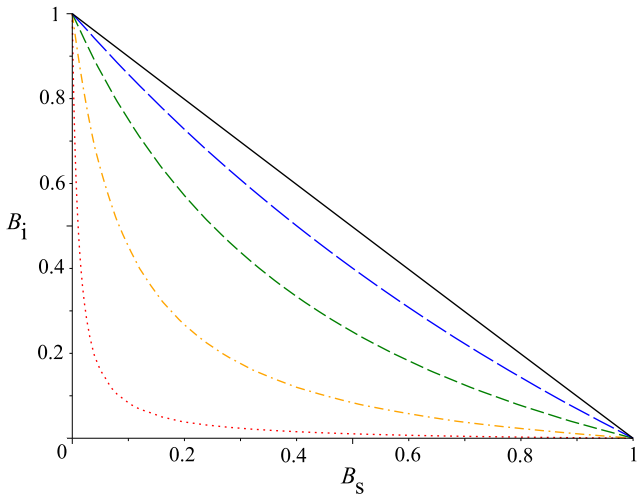

Figure 3.3: Curves giving the boundaries between entangled and separable twin beams and determined according to Eq. (3.18) plotted in the plane spanned by the mean noise photon numbers B_s and B_i assuming the mean photon-pair number B_p equal to 0.01 [dotted (red) curve], 0.1 [dash-dotted (yellow) curve], 0.5 [dashed (green) curve], 2 [long-dashed (blue) curve], and $B_p = 100$ [solid black curve]. Entangled states are localized in the lower-left corner of the plane. The larger B_p, the larger the area containing entangled states.

The decomposition of the partially transposed statistical operator $\hat{\rho}^\Gamma$ into blocks in its matrix representation and the fact that a block (subspace) with dimension $M+1$ describes only states with up to M photons in the signal (and also idler) field can be used to define the distribution d_N of the negativity N fulfilling the normalization condition

$$\sum_{M=1}^{\infty} d_N(M) = N. \tag{3.19}$$

For a given M, the element $d_N(M)$ of this distribution is given as the sum of the absolute values of the negative eigenvalues belonging to the block of dimension $M+1$. The distribution d_N of the negativity provides insight into the internal structure of entanglement. It tells us how entanglement is distributed in the Liouville space of statistical operators. Typical distributions d_N of the negativity for noiseless as well as noisy twin beams are plotted in Fig. 3.4. A teeth-like structure occurs for smaller numbers M in noiseless twin beams. Noise tends to suppress this structure, as is evident from the comparison of the distributions d_N plotted in Figs. 3.4(a) and 3.4(b). We note that the densities of the negativity have already been introduced for bipartite entangled states composed of a qubit and continuum of states [59, 60] as well as two continua of states.

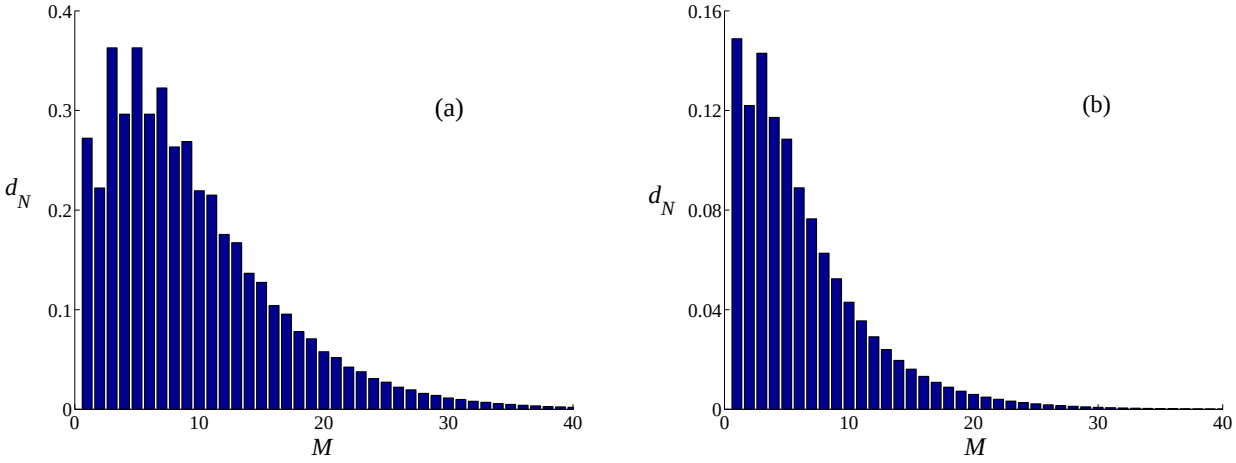

Figure 3.4: Distribution d_N of negativity N given in Eq. (3.19) assuming $B_{\rm p} = 2$ and (a) $B_{\rm s} = B_{\rm i} = 0$ and (b) $B_{\rm s} = B_{\rm i} = 0.1$. Note that $-d_N(M)$ corresponds to the sum of all the negative eigenvalues for the $(M+1)$–dimensional block of the partially transposed statistical operator $\hat{\rho}^{\Gamma}$. Thus, $d_N(M)$ shows the internal structure of entanglement in the Liouville space.

3.4 Nonclassical depth of the twin beam

To quantify nonclassicality of the twin beam we apply the nonclassical depth τ [22] derived from the threshold value $s_{\rm th}$ of the ordering parameter at which the joint signal-idler quasidistribution of integrated intensities becomes nonnegative [56, 61]. We adopt the definition $\tau = (1 - s_{\rm th})/2$. We note that the joint signal-idler quasidistribution of integrated intensities attains negative values for $1 \geq s > s_{\rm th}$ for which $\tau > 0$. The threshold value $s_{\rm th}$ can easily be obtained from the condition $\langle[\Delta(W_{\rm s} - W_{\rm i})]^2\rangle = 0$, which determines the point of the transition between quantum and classical single-mode twin beams [61]. This results in the following formula for the nonclassical depth τ:

$$\tau = \frac{1}{2}\left[\sqrt{(B_{\rm s} - B_{\rm i})^2 + 4B_{\rm p}(B_{\rm p}+1)} - 2B_{\rm p} - B_{\rm s} - B_{\rm i})\right]. \tag{3.20}$$

Assuming noiseless twin beams, Eq. (3.20) simplifies to

$$\tau = \sqrt{B_{\rm p}(B_{\rm p}+1)} - B_{\rm p}. \tag{3.21}$$

According to Eq. (3.21), all noiseless twin beams are nonclassical. The greater the mean photon-pair number $B_{\rm p}$, the greater the value of the nonclassical depth τ (see Fig. 3.5). This depth τ

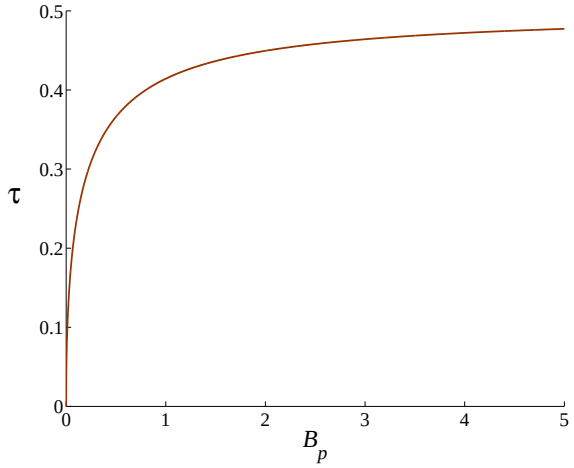

Figure 3.5: Nonclassical depth τ given in Eq. (3.21) as it depends on the mean photon-pair number $B_{\rm p}$ for noiseless twin beams, i.e., $B_{\rm s} = B_{\rm i} = 0$.

reaches its greatest value, 1/2, in the limit of an infinitely intense twin beam ($B_{\rm p} \to \infty$). We note that $\tau = 1/2$ corresponds to symmetrical ordering of the field operators.

On the other hand, and according to Eq. (3.20), noise only degrades nonclassical behavior of a twin beam, as documented in Fig. 3.6. If the noise is equally distributed in the signal and idler fields ($B_{\rm s} = B_{\rm i}$), the nonclassical depth τ determined along Eq. (3.20) gives the mean number $B_{\rm s} + B_{\rm i}$ of noise photons needed for suppressing the nonclassicality of the twin beam. So, the larger the value of the nonclassical depth τ is, the more nonclassical the field is. On the other hand, formal application of Eq. (3.20) to classical noisy twin beams results in negative values of the nonclassical depth τ. Their absolute value $|\tau|$ can be considered a measure of classicality of noisy twin beams in the sense that it quantifies the mean number of photon pairs needed to transform a classical twin beam into the classical-quantum boundary $\tau = 0$.

Condition $\tau = 0$ for the transition from quantum to classical twin beams applied to Eq. (3.20) results in the same relation among parameters $B_{\rm p}$, $B_{\rm s}$, and $B_{\rm i}$ as derived in Eq. (3.17) for the boundary between entangled and separable twin beams. Thus, entangled twin beams are nonclassical, whereas separable twin beams are classical. This means that nonclassical twin beams may contain on average only less than one noise photon ($B_{\rm s} + B_{\rm i} < 1$). We note that inequality (3.17) represents the Simon criterion for nonclassicality of Gaussian states as shown in Ref. [61].

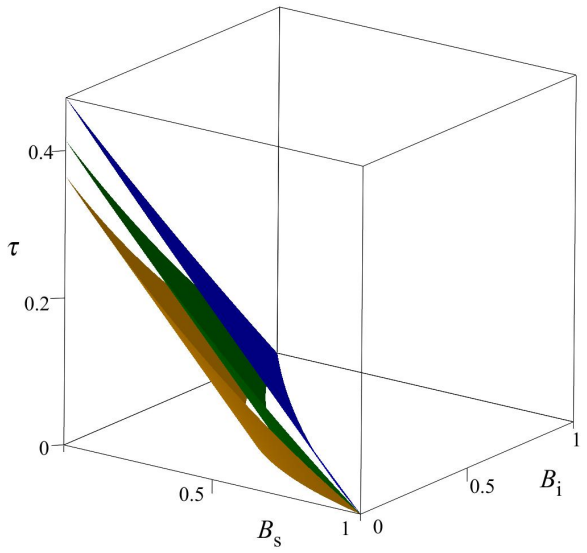

Figure 3.6: Nonclassical depth τ given in Eq. (3.20) as a function of the mean noise photon numbers B_s and B_i for the mean photon-pair number B_p equal to 0.1 [bottom, light-gray (yellow) area], 0.5 [gray (green) area], 4 [top, dark-gray (blue) area]. The greater the value of B_p, the greater the value of τ.

Comparison of Eqs. (3.16) and (3.21) made for noiseless twin beams reveals a simple relation between the negativity N and the nonclassical depth τ:

$$N = \frac{\tau}{1 - 2\tau}. \tag{3.22}$$

Direct calculation based on Eqs. (3.15) and (3.20) then confirms that relation (3.22) holds even for a general noisy twin beam. We thus have a one-to-one correspondence between the value of the negativity N and the value of the nonclassical depth τ. Moreover, according to Eq. (3.22) the negativity N is an increasing function of the nonclassical depth τ, and vice versa (see Fig. 3.7). There exists a deep physical reason for this correspondence. The nonlinear process emits photons in pairs into the signal and idler fields, which creates entanglement between these fields. It is this entanglement that gives rise to nonclassical properties of twin beams, as the classical statistical optics is unable to describe pairing of photons appropriately.

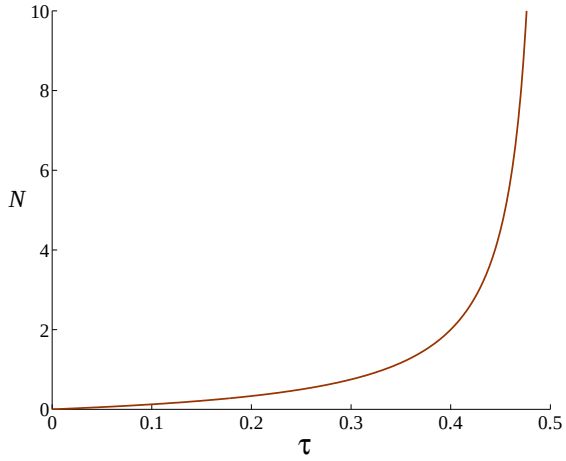

Figure 3.7: Negativity N as a function of the nonclassical depth τ, according to Eq. (3.22).

3.5 Dimensionality of the twin beam

Three different numbers are needed to determine the dimensionality of a general noisy twin beam. The dimensionality K_{ent} of entanglement gives the number of degrees of freedom constituting the entangled (paired) part of the twin beam. We also need additional degrees of freedom to characterize the noisy parts of the twin beam. As the amount of noise is, in general, different in the signal and idler fields, we have independent participation ratios R_{s} and R_{i} for both fields. The entanglement dimensionality K_{ent} for bipartite states with axisymmetric statistical operators can be given in terms of the negativity N by a simple formula [46]:

$$K_{\mathrm{ent}}(\hat{\rho}) = 2N(\hat{\rho}) + 1 = ||\hat{\rho}^{\Gamma}||_1. \tag{3.23}$$

Strictly speaking, it is the least integer $\geq K_{\mathrm{ent}}$ that gives a lower bound to the number of entangled dimensions between entangled subsystems (paired modes) of $\hat{\rho}$ [46]. According to Eq. (3.23), the entanglement dimensionality K_{ent} equals 1 for separable states ($N = 0$). It linearly increases with the negativity N. As the noise described by the mean noise photon numbers B_{s} and B_{i} decreases the values of the negativity N, it also decreases the values of the entanglement dimensionality K_{ent}. We note that, for pure states, the Schmidt number is also a good quantifier of the entanglement dimension K_{ent} [62, 63, 64]. The Schmidt decomposition of pure states accompanied by convex optimization can even be applied for quantifying the

entanglement dimension of mixed entangled states [58].

On the other hand, the noise present in the signal and idler fields requires additional degrees of freedom for its description. These degrees of freedom are, together with those reserved for describing entanglement, determined by the participation ratios R_{s} and R_{i} derived from the signal- and idler-field reduced statistical operators $\hat{\rho}_{\mathrm{s}}$ and $\hat{\rho}_{\mathrm{i}}$, respectively [63, 65]:

$$R_a = \frac{1}{\mathrm{Tr}_a[\hat{\rho}_a^2]}, \qquad a = \mathrm{s}, \mathrm{i}. \tag{3.24}$$

Equation (3.10), giving the matrix elements of the statistical operator $\hat{\rho}$, guarantees a diagonal form of the reduced statistical operators $\hat{\rho}_{\mathrm{s}}$ and $\hat{\rho}_{\mathrm{i}}$ of the signal and idler fields, respectively. In this case, Eq. (3.24) can be rewritten in the form

$$R_{\mathrm{s}} = \frac{1}{\sum_j \rho_{\mathrm{s},jj}^2}. \tag{3.25}$$

Using Eq. (3.10) the matrix elements $\rho_{\mathrm{s},jj}$ can be written as

$$\rho_{\mathrm{s},jj} = \frac{1}{\tilde{B}_{\mathrm{s}}} \left[\left(1 - \frac{\tilde{B}_{\mathrm{i}}}{\tilde{K}} \right) + \frac{|D_{12}|^2}{\tilde{K}\tilde{B}_{\mathrm{s}}} \right]^j. \tag{3.26}$$

Substituting Eq. (3.26) into Eq. (3.25) we obtain a simple formula for the participation ratio R_{s}:

$$R_{\mathrm{s}} = 2(B_{\mathrm{p}} + B_{\mathrm{s}}) + 1. \tag{3.27}$$

The same considerations made for the signal field apply also to the idler field.

To find the relation between the entanglement dimensionality K_{ent} and the participation ratios R_{s} and R_{i} we consider for a while the noiseless twin beams in pure states. In this case, the elements $\hat{\rho}_{\mathrm{s},jj}$ of the reduced statistical operator $\hat{\rho}_{\mathrm{s}}$, written in Eq. (3.26), immediately give the squared Schmidt coefficients [51]. Combining Eqs. (3.16), (3.23), and (3.27) we arrive at the formula

$$K_{\mathrm{ent}} = R_{\mathrm{s}} + \sqrt{R_{\mathrm{s}}^2 - 1}. \tag{3.28}$$

Equation (3.28) shows that, excluding weak noiseless twin beams, $K_{\mathrm{ent}} \approx 2R_{\mathrm{s}}$. This means that the definitions of the entanglement dimensionality and participation ratio set different boundaries for the Schmidt coefficients c_j included in the approximative description of a noiseless twin beam with the wave function

$$|\psi\rangle = \sum_{j=0}^{j_{\max}} c_j |j\rangle_{\mathrm{s}} |j\rangle_{\mathrm{i}}. \tag{3.29}$$

Using Eq. (3.10), the coefficients c_j in Eq. (3.29) are obtained in the form

$$c_j = \sqrt{\frac{{B_{\mathrm{p}}}^j}{(B_{\mathrm{p}}+1)^{j+1}}}, \tag{3.30}$$

which is in agreement with the thermal photon-number statistics of the signal (or idler) field. We note that the ratio $c_{K_{\mathrm{ent}}-1}/c_{R_{\mathrm{s}}-1}$ of boundary coefficients is given by the expression $[B_{\mathrm{p}}/(1+B_{\mathrm{p}})]^{B_{\mathrm{p}}+1}$. When $B_{\mathrm{p}} \to \infty$ $c_{K_{\mathrm{ent}}-1}/c_{R_{\mathrm{s}}-1} \to 1/e$.

To compare the values of entanglement dimensionality and the participation ratio for general twin beams we have to eliminate the effect of different boundaries set by different definitions, as revealed by considering the pure states. Using the formulas derived for noiseless twin beams, we introduce the modified entanglement dimensionality $\tilde{K}_{\mathrm{ent}}$ as follows:

$$\tilde{K}_{\mathrm{ent}} = \frac{2B_{\mathrm{p}}+1}{2B_{\mathrm{p}}+1+2\sqrt{B_{\mathrm{p}}^2+B_{\mathrm{p}}}}\, K_{\mathrm{ent}}. \tag{3.31}$$

Definition (3.31) of the modified entanglement dimensionality $\tilde{K}_{\mathrm{ent}}$ guarantees that the values of modified entanglement dimensionality $\tilde{K}_{\mathrm{ent}}$ and participation ratios R_{s} and R_{i} of noiseless twin beams are equal.

The values of the modified dimensionality $\tilde{K}_{\mathrm{ent}}$ of entanglement and the signal-field participation ratio R_{s} are compared in Fig. 3.8 for the mean photon-pair number $B_{\mathrm{p}} = 1$. Whereas the values of the modified entanglement dimensionality $\tilde{K}_{\mathrm{ent}}$ decrease with increasing values of the mean noise photon numbers B_{s} and B_{i}, the values of the signal-field participation ratio R_{s} increase with increasing values of the mean signal-field noise photon number B_{s}. We note that the values

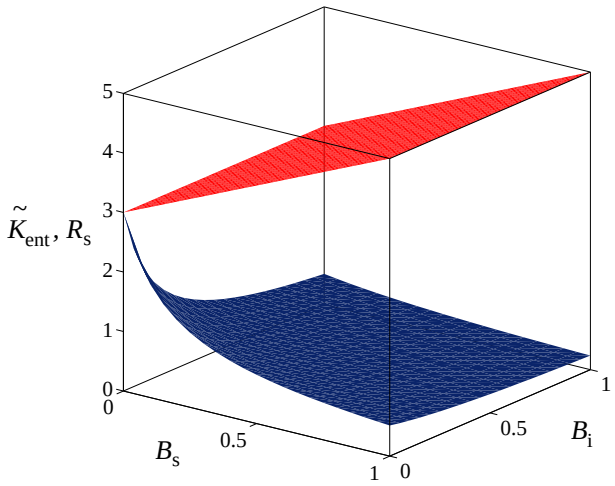

Figure 3.8: Modified entanglement dimensionality $\tilde{K}_{\rm ent}$ given in Eq. (3.31) [lower, dark-gray (blue) area] and signal-field participation ratio $R_{\rm s}$ given in Eq. (3.27) [upper, gray (red) area] as they depend on the mean noise photon numbers $B_{\rm s}$ and $B_{\rm i}$ assuming the mean photon-pair number $B_{\rm p} = 1$.

of the signal-field participation ratio $R_{\rm s}$ are greater than those of the modified entanglement dimensionality $\tilde{K}_{\rm ent}$ even for $B_{\rm s} = 0$, as the presence of noise in the idler field ($B_{\rm i} > 0$) degrades entanglement.

The relative contribution of the degrees of freedom used for describing entanglement in a twin beam is an important characteristic. This contribution can be quantified via the coefficient $r_{\rm ent}$ defined as follows:

$$r_{\rm ent} = \frac{2\tilde{K}_{\rm ent}}{R_{\rm s} + R_{\rm i}}. \tag{3.32}$$

As shown in Fig. 3.9, the greater the values of the mean noise photon numbers $B_{\rm s}$ and $B_{\rm i}$, the smaller the values of the coefficient $r_{\rm ent}$. The comparison of surfaces of the coefficient $r_{\rm ent}$ drawn for the mean photon-pair numbers $B_{\rm p} = 1$ and $B_{\rm p} = 10$ in Fig. 3.9 reveals seemingly paradoxical behavior. The values of the coefficient $r_{\rm ent}$ decrease with increasing values of the mean photon-pair number $B_{\rm p}$. This behavior, however, naturally originates in fragility of entanglement with respect to the noise. More intense twin beams (with greater values of $B_{\rm p}$) are less resistant to a given amount of noise compared to low-intensity twin beams. This is explained by the larger dimensions of the effectively populated Hilbert spaces of more intense twin beams and, thus, the more complex structures of their entanglement. As a consequence, relatively higher numbers of degrees of freedom serving to describe entanglement in more intense noiseless twin

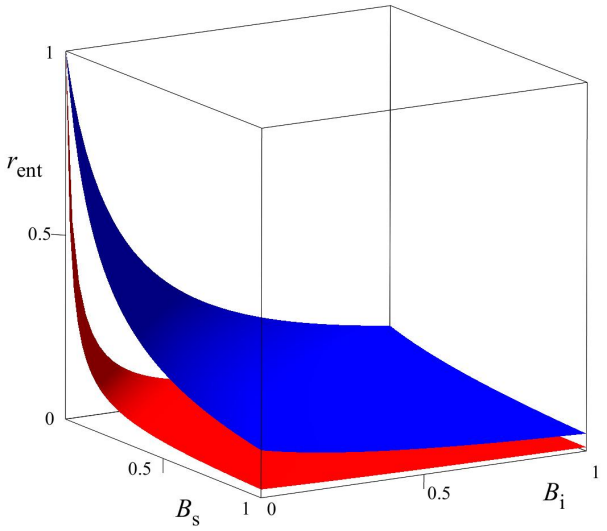

Figure 3.9: Coefficient r_{ent} given in Eq. (3.32) versus the mean noise photon numbers B_{s} and B_{i} for the mean photon-pair number B_{p} equal to 1 [upper, dark-gray (blue) area], and 10 [lower, gray (red) area].

beams are "released" by the noise and enlarge the noise parts of twin beams.

Alternatively to the participation ratio R, we may apply the von Neumann entropy S of a reduced statistical operator. Taking into account the diagonal form of the signal-field reduced statistical operator $\hat{\rho}_{\mathrm{s}}$ with the elements written in Eq. (3.26), the signal-field entropy S_{s} is in general determined along the formula

$$S_{\mathrm{s}} = -\mathrm{Tr}(\hat{\rho}_{\mathrm{s}} \ln \hat{\rho}_{\mathrm{s}}) = -\sum_{j} \rho_{\mathrm{s},jj} \ln(\rho_{\mathrm{s},jj}). \tag{3.33}$$

Considering the specific form of matrix elements $\rho_{\mathrm{s},jj}$ given in Eq. (3.26), the formula for entropy S_{s} attains the form

$$\begin{aligned} S_{\mathrm{s}} &= (1 + B_{\mathrm{p}} + B_{\mathrm{s}}) \ln(1 + B_{\mathrm{p}} + B_{\mathrm{s}}) \\ &\quad - (B_{\mathrm{p}} + B_{\mathrm{s}}) \ln(B_{\mathrm{p}} + B_{\mathrm{s}}); \end{aligned} \tag{3.34}$$

ln stands for natural logarithm. Combining Eqs. (3.25) and (3.34), the entropy S_{s} is revealed

as an increasing function of the participation ratio R_{s}:

$$S_{\mathrm{s}} = \frac{1}{2}\left[(R_{\mathrm{s}}+1)\ln(R_{\mathrm{s}}+1) - (R_{\mathrm{s}}-1)\ln(R_{\mathrm{s}}-1)\right] - 1. \tag{3.35}$$

Analogous formulas for the idler-field entropy S_{i} can easily be derived. The general dependence of entropy S_{s} on the participation ratio R_{s} is plotted in Fig. 3.10. We would like to note that the entropy S serves as a good measure of the entanglement for pure states.

3.6 Twin beam composed of M modes

In real experiments, twin beams are rarely composed of only one paired spatiotemporal mode [61, 66]. We note that a twin beam composed of one paired mode represents an ideal field from the experimental point of view [67]. For this reason, we consider a multimode twin beam containing M independent identical single-mode twin beams. Its statistical operator $\hat{\rho}_M$ is given as $\hat{\rho}_M = \otimes_M \hat{\rho}$ using the statistical operator $\hat{\rho}$ written in Eq. (3.8). There are four parameters characterizing the twin beam: number M of modes, mean photon-pair number B_{p}, mean signal-field noise photon number B_{s}, and mean idler-field noise photon number B_{i}. We note that such an M-mode twin beam represents a good approximation of a real twin beam when all spatiotemporal modes participating in the nonlinear interaction are detected.

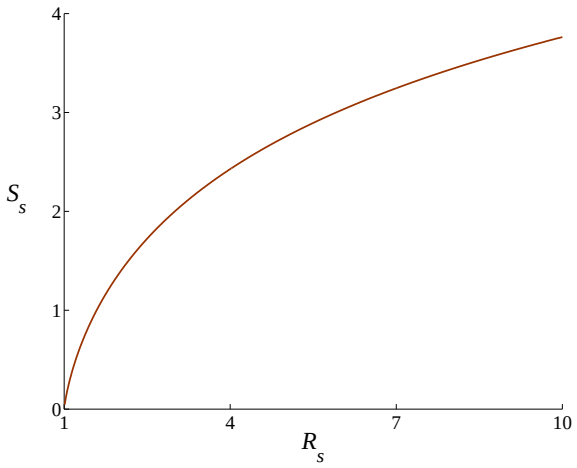

Figure 3.10: von Neumann entropy S_{s} as a function of the participation ratio R_{s} according to Eq. (3.35).

The considered physical quantities behave differently with respect to the number M of modes. It has been shown in Refs. [56] and [61] that the nonclassical depth τ does not depend on the number M of modes. On the other hand, the multimode negativity N_M, $N_M = (1+2N)^M$, as well as the participation ratios $R_{M,a}$, $R_{M,a} = R_a^M$ for $a = s, i$, are multiplicative. We note that the form of the multimode negativity originates in the multiplicative property of the trace norm and its relation to the negativity expressed in Eq. (3.11) [42]. In fact, the multimode negativity N_M coincides with the entanglement dimensionality $K_{\rm ent}$ defined in Eq. (3.23) for a single-mode twin beam. The multimode entropies $S_{M,a}$, $a = \mathrm{s}, \mathrm{i}$, are then additive. To reveal similar relations among the studied quantities as has been done for single-mode twin beams, we have to define suitable quantities derived from those considered above. Defining the logarithmic negativity $N_M^{\log} \equiv \ln(N_M)$ and the logarithmic participation ratios $R_{M,a}^{\log} \equiv \ln(R_{M,a})$, $a = \mathrm{s}, \mathrm{i}$, we replace the multiplicative quantities with the additive ones. Introducing the logarithmic negativity $\mathcal{N}$, logarithmic participation ratios $\mathcal{R}_a^{\log}$, and entropies $\mathcal{S}_a$ related per one mode,

$$\begin{aligned} \mathcal{N} &= \frac{N_M^{\log}}{M} = \ln(1+2N), \\ \mathcal{R}_a &= \frac{R_{M,a}^{\log}}{M} = \ln(R_a), \\ \mathcal{S}_a &= \frac{S_{M,a}}{M} = S_a, \end{aligned} \tag{3.36}$$

with $a = \mathrm{s}, \mathrm{i}$, we reveal the suitable quantities. The quantities defined in Eq. (3.36) together with the nonclassical depth τ behave qualitatively in the same way as those defined for single-mode twin beams discussed above. Especially, the logarithmic negativity $\mathcal{N}$ per mode is an increasing function of the nonclassical depth τ. Also, the entropy $\mathcal{S}_a$ per mode is an increasing function of the logarithmic participation ratio $\mathcal{R}_a$ per mode, $a = \mathrm{s}, \mathrm{i}$.

3.7 Experimental multimode twin beams

Real experimental multimode twin beams have a more complex structure than that discussed in Sec. 2.6 [68, 61, 66]. The reason is that the spatiotemporal modes of twin beams are shared by the signal and idler fields and so they can be broken before or during the detection owing to

spectral and/or spatial filtering. As a consequence, real multimode twin beams are composed of three components [61, 69]. A paired component describes photons embedded in spatiospectral modes detected by both signal- and idler-field detectors. A noise signal (idler) component then describes photons occurring in signal (idler) spatiotemporal modes that originate in filtering of the idler (signal) field. If we assume for simplicity that the paired component is ideal, i.e., without noise, we need six parameters to describe a real twin beam. Each component is characterized by the number M of modes and mean photon-pair (or noise photon) number B. The statistical operator $\hat{\rho}_E$ of the experimental twin beam can be expressed as

$$\hat{\rho}_E = \bigotimes_{M_\mathrm{p}} \hat{\rho}_\mathrm{p} \bigotimes_{M_\mathrm{s}} \hat{\rho}_{n,s} \bigotimes_{M_\mathrm{i}} \hat{\rho}_{n,\mathrm{i}} \tag{3.37}$$

using single-mode statistical operators $\hat{\rho}_\mathrm{p}$, $\hat{\rho}_{n,s}$, and $\hat{\rho}_{n,i}$ of the photon-pair, noise signal, and noise idler components. In Eq. (3.37), M_p, M_s, and M_i give the numbers of equally populated modes with the mean numbers B_p, B_s, and B_i of photon pairs per mode, respectively.

Entanglement in the experimental twin beam is created only by its paired component and as such it can be quantified by the logarithmic negativity $N^{\log}_{M_\mathrm{p}}$ introduced in Sec. 2.6. The noise components do not contribute to entanglement on one side, and they do not degrade entanglement on the other side. This is qualitatively different from the case of multimode twin beams discussed in Sec. 2.6 and containing noise in paired spatiotemporal modes.

Nonclassicality can be quantified by a multimode generalization of nonclassical depth τ_E introduced in Ref. [22] for a single-mode field. In a multimode twin beam, we may first determine the standard nonclassical depths τ_n for each single-mode field, included either in the paired part of the twin beam or in the noisy signal and idler parts of the twin beam. Then we can take either $\max_n(\tau_n)$ or $\sum_n \tau_n$ to quantify the multimode nonclassical depth τ_E. In the first case, the nonclassical depth τ_E of the experimental multimode twin beam is just given by the nonclassical depth τ of a paired mode. The second case is physically more interesting, as the value of τ_E is linearly proportional to the minimum amount of additional noise needed to conceal nonclassicality of the multimode state. In this case, we have, for the experimental multimode

twin beams,

$$\tau_E = M_{\rm p}\tau. \tag{3.38}$$

Using the logarithmic negativity $N_{M_p}^{\log}$ defined in Sec. 2.6 and the nonclassical depth τ_E, one-to-one correspondence between the entanglement and the nonclassicality is obtained also for M-mode twin beams.

On the other hand, the concept of weak nonclassicality [70, 71, 72] is also useful for the experimental multimode twin beams considered to be composed of one effective paired (macro)mode. The joint quasidistribution P_W of the integrated intensities W_s and W_i of the signal and idler fields, respectively, describes the properties of this effective paired mode [28]. As no information about the phase is encoded in this simplified effective description, we may only determine the nonclassical intensity depth τ_W quantifying nonclassicality, which demonstrates itself by negative values of the marginal quasidistribution of integrated intensities. We have to emphasize that the nonclassical intensity depth τ_W is only a nonclassicality witness or parameter, which reveals nonclassicality solely in photon-number statistics. Contrary to this, the nonclassical depth τ is a genuine and commonly used nonclassicality measure. We note that te standard nonclassicality quantified by τ reveals both strongly and weakly nonclassical states [70, 71]. From this point of view τ is a *strong* tool or criterion. On the other hand, τ_W detects only strongly nonclassical states; i.e., it is a *weak* tool.

The nonclassical intensity depth τ_W has been determined for the experimental multimode twin beams in Ref. [61],

$$\tau_W \;=\; \sqrt{\beta^2-\gamma}-\beta, \tag{3.39}$$

where

$$\begin{aligned}\beta &= \frac{M_{\rm s}B_{\rm s}+M_{\rm i}B_{\rm i}+2M_{\rm p}B_{\rm p}}{M_{\rm s}+M_{\rm i}+2M_{\rm p}},\\ \gamma &= \frac{M_{\rm s}B_{\rm s}^2+M_{\rm i}B_{\rm i}^2-2M_{\rm p}B_{\rm p}}{M_{\rm s}+M_{\rm i}+2M_{\rm p}}.\end{aligned} \tag{3.40}$$

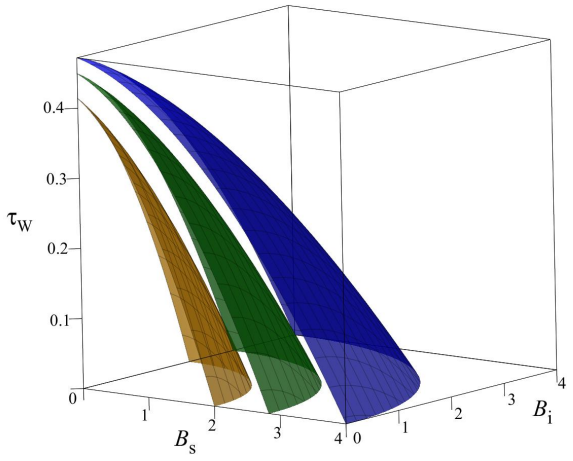

Figure 3.11: Nonclassical intensity depth τ_W as a function of the mean noise photon numbers B_s and B_i for the mean photon-pair number B_p equal to 2 [bottom, light-gray (yellow) area], 4 [gray (green) area], and 8 [top, dark-gray (blue) area], assuming $M_\mathrm{p} = M_\mathrm{s} = M_\mathrm{i} = 1$. The greater the value of B_p, the greater the value of τ_W.

The analysis of Eq. (3.39) shows that the experimental multimode twin beam is strongly nonclassical ($\tau_W > 0$) provided that

$$M_\mathrm{s} B_\mathrm{s}^2 + M_\mathrm{i} B_\mathrm{i}^2 < 2 M_\mathrm{p} B_\mathrm{p}. \tag{3.41}$$

Inequality (3.41) means that the multimode strong nonclassicality of the twin beam is lost if the noise is sufficiently strong. For example, if $M_\mathrm{p} = M_\mathrm{s} = M_\mathrm{i}$, strongly nonclassical multimode twin beams are observed for $B_\mathrm{s}^2 + B_\mathrm{i}^2 < 2B_\mathrm{p}$ (see Fig. 3.11). This behavior is similar to that discussed in Sec. 2.4, though the boundary given by $\tau_W = 0$ is quantitatively different (compare Figs. 3.6 and 3.11). We also have here that the greater the value of the mean photon-pair number B_p, the greater the value of the nonclassical intensity depth τ_W. Also, the greater the values of mean noise photon numbers B_s and B_i, the smaller the value of the nonclassical intensity depth τ_W.

Similarly as in Sec. 2.6, the logarithmic participation ratio $R^{\log}$ can be defined for each component of the twin beam to quantify its dimensionality. The logarithmic participation ratio $R^{\log}$ of the whole twin beam is then naturally given as the sum of the logarithmic participation ratio $R^{\log}_{M_\mathrm{p},\mathrm{p}}$ of the paired component and the logarithmic participation ratio $R^{\log}_{M_\mathrm{s},\mathrm{s}} + R^{\log}_{M_\mathrm{i},\mathrm{i}}$ of the noise signal and idler components. We note that Eq. (3.25) is appropriate for determining

the participation ratio of both the single-mode noise signal (or idler) field and the single-mode paired field. Alternatively we may consider entropies of the components instead of participation ratios. Entropies of the single-mode noise fields are given by Eq. (3.33). Equation (3.33) is applicable also for determination of the entropy of entanglement of a single-mode paired field in a pure state for which $\hat{\rho}_{\mathrm{s},jj} \leftarrow c_j^2$. As a consequence, the entropies $S_{M_a,a}$ for $a = \mathrm{p}, \mathrm{s}, \mathrm{i}$, of each component are increasing functions of the corresponding participation ratios $R_{M_a,a}$. In single-mode cases, these functions are determined by Eq. (3.35), plotted in Fig. 3.10. Similarly to the overall logarithmic participation ratio $R^{\log}$, the overall entropy S can be naturally split into its entangled part $S_{M_\mathrm{p},\mathrm{p}}$ and noisy part $S_{M_\mathrm{s},\mathrm{s}} + S_{M_\mathrm{i},\mathrm{i}}$, originating in the noise signal and idler components.

Finally, we briefly address the issue of the experimental determination of the quantities discussed above. As these quantities characterize the "internal" structure of a twin beam, only their indirect determination is possible. It is based upon the measurement of the joint signal-idler photocount histogram using photon-number-resolving detectors. Knowing these detector parameters [73], reconstruction of the joint signal-idler photon-number distribution [69, 61] provides the applied mean photon(-pair) numbers B and numbers M of modes. The above-derived formulas then give the discussed quantities.

3.8 Conclusions

The entanglement and nonclassicality of a single-mode noisy twin beam have been quantified using the negativity and the nonclassical depth, respectively. Universal mapping between the nonclassical depth and the negativity has been revealed for noisy twin beams. The mapping reflects the fact that nonclassicality of a twin beam is caused by the entanglement of its two parts originating in pairing of photons. Limitations to the amount of noise have been found to preserve entanglement together with nonclassicality. the degrees of freedom of a twin beam quantified by the signal- and idler-field participation numbers have been divided into those needed to describe entanglement and the remaining ones forming the noisy signal and idler

parts of the twin beam. The entanglement dimensionality derived from the negativity has been applied here. Entropy as an increasing function of the participation number has been discussed. Properties of multimode twin beams have been analyzed using appropriate quantities related per one mode. Also, experimental multimode twin beams containing additional noise in independent spatiotemporal modes have been investigated from the point of view of their entanglement and multimode nonclassicality including weak nonclassicality and dimensionality.

Chapter 4

Interplay of nonclassicality and entanglement of two-mode Gaussian fields generated in optical parametric processes

Text adopted from *I. I. Arkhipov, J. Peřina Jr., J. Peřina and A. Miranowicz, Phys. Rev. A.* **94**, *013807 (2016)* [A3].

4.1 Introduction

Entanglement between two optical fields is one of the most frequently studied forms of nonclassical light. Such light emerges in various two-mode or multimode nonlinear optical processes, e.g., in spontaneous parametric down-conversion. In this process, pairs of photons composed of the signal and idler modes are created at the expense of the annihilated pump photons. This pairwise character of emitted light lies in the heart of entanglement here. The process of spontaneous parametric down-conversion has its degenerate variant called second-subharmonic generation, where both photons in a pair are emitted into the same optical mode. This gives

raise to phase squeezing of the second-subharmonic field composed of, in general, many photon pairs. The squeezed light is also considered nonclassical as it has its phase fluctuations suppressed below the classical limit. The nonclassicality in both cases has the same origin which is pairing of photons. On the other side, the emitted photon pairs can be manipulated by linear optics. In detail, two photons from one pair present in the same mode of a squeezed state of light can be split (on a beam splitter) and contribute to the entanglement of the output fields. Also, two photons from a pair incident on different input ports of a beam splitter can "stick together" (bunch) and leave the beam splitter in the same output port (as testified in the Hong-Ou-Mandel interferometer [74]). The interconnection of these two types of fields by the means of linear optics has already been shown by Braunstein [75] and later elaborated by Adesso [76] for arbitrarily strong Gaussian states. This behavior poses a natural question whether it is possible to introduce a physical quantity that quantifies "a nonclassicality resource" present during the creation of both types of fields and later conserved during linear-optical transformations.

The answer to this question is intimately related to the quantifiers of *entanglement* and *local nonclassicality*. Several measures were proposed to quantify the entanglement in both discrete and continuous domains [42, 77, 58, 24, 57, 78]. The negativity (or its logarithmic variant) is considered, probably, as the most useful at present. On the other hand, the Lee nonclassicality depth [20] is conventionally used to quantify the nonclassicality of optical fields. Alternatively, the nonclassicality of an optical field can be transcribed to entanglement using a beam splitter and quantified via an entanglement measure [79, 80]. For a comparative study of these two nonclassicality measures see, e.g., recent Refs. [81, 82].

We note that, apart from the local nonclassicalities of two parts of a bipartite state, also *global nonclassicality* can naturally be defined. All these three quantities have been analyzed in Ref. [A1] for intense multi-mode twin beams with the following result: whenever a twin beam is entangled it is globally nonclassical. On the other hand, its signal and idler constituents are multi-thermal and so locally classical. A general approach for describing the relation between the entanglement and global nonclassicality of two-mode states has been proposed in Ref. [83].

Returning back to our question, we look for an invariant with respect to linear-unitary trans-

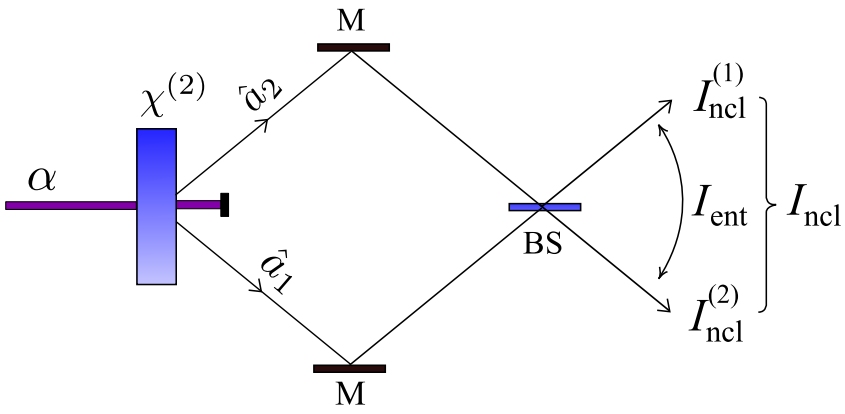

Figure 4.1: Diagram showing the main goal of this chapter: The local ($I_{\rm ncl}^{(1)}$ and $I_{\rm ncl}^{(2)}$) and global ($I_{\rm ncl}$) nonclassicality invariants are analyzed in relation with the entanglement, described by the invariant $I_{\rm ent}$, for the light generated by the optical parametric process (described by the second-order susceptibility $\chi^{(2)}$) and then combined at a beam splitter BS with varying transmissivity T. Here, α is the amplitude of a classical pump field, $\hat{a}_1$ and $\hat{a}_2$ are the annihilation operators of the generated light, and M denotes a mirror.

formations (conserving the overall number of photons) that comprises both the entanglement and local nonclassicalities. This question has recently been addressed in Ref. [84] considering beam-splitter transformations and a quantity composed of the logarithmic negativity and the logarithm of nonclassicality depth. However, the introduced quantity has been found useful only under very specific conditions [A2].

In this chapter we construct such an invariant for general two-mode Gaussian states arising in nonlinear processes described by the second order susceptibility $\chi^{(2)}$. The processes of spontaneous parametric down-conversion and second-subharmonic generation represent their most important examples. As schematically shown in Fig. 4.1, the found invariant is decomposable into three parts characterizing in turn entanglement and two local nonclassicalities. The entanglement indicator is shown to be a monotone of the logarithmic negativity similarly to the newly defined nonclassicality measure that is a monotone of the Lee nonclassicality depth under any linear unitary transformation.

The obtained results are potentially interesting for manipulations with nonclassicality in quantum engineering that have become substantial ingredients of a growing number of applications of quantum technologies [14, 58, 85, 86, 87].

The chapter is organized as follows. In Sec. 4.2, a model comprising parametric down-conversion

and second-subharmonic generation is developed. A suitable nonclassicality invariant is suggested using local and global invariants of two-mode Gaussian fields. Its decomposition into an entanglement quantifier and local nonclassicality quantifiers is also discussed. Twin beams as they behave on a beam splitter are discussed in Sec. 4.3. In Sec. 4.4, a single-mode squeezed state on a beam splitter is analyzed. Section 4.5 is devoted to the behavior of two single-mode squeezed states interfering on a beam splitter. States having both 'twin-beam' and squeezed components are investigated in Sec. 4.6. Conclusions are drawn in Sec. 4.7.

4.2 Gaussian states generated in $\chi^{(2)}$ interactions and their invariants

We consider a nonlinear interaction Hamiltonian $\hat{H}_{\rm int}$ describing both parametric down-conversion and second-subharmonic generation that provide photon pairs [28] (for the scheme, see Fig. 4.2):

$$\hat{H}_{\rm int} = -\hbar g_{12}^{*} \hat{a}_1 \hat{a}_2 - \hbar g_{11}^{*} \hat{a}_1^2 - \hbar g_{22}^{*} \hat{a}_2^2 + \text{h.c.} \tag{4.1}$$

In Eq. (4.1), the symbols $\hat{a}_1$ ($\hat{a}_1^{\dagger}$) and $\hat{a}_2$ ($\hat{a}_2^{\dagger}$) represent the annihilation (creation) operators of the fields 1 and 2, g_{12} is a nonlinear coupling constant characterizing parametric down-conversion and g_{ii} stands for a nonlinear coupling constant of the second-subharmonic generation in the ith mode described by the second-order susceptibility $\chi^{(2)}$ of a medium. Symbol h.c. represents the Hermitian conjugated terms. Due to the presence of noise in real nonlinear processes we also consider the Langevin forces $\hat{L}_j$ arising in the interaction with the reservoir chaotic oscillators characterized by means of noise photon numbers $\langle n_d \rangle$. This leads to damping processes described by the damping constants γ_j.

The Heisenberg-Langevin operator equations corresponding to the Hamiltonian $\hat{H}_{\rm int}$ are derived in the following matrix form:

$$\frac{d\hat{\mathbf{a}}}{dt} = \mathbf{M}\hat{\mathbf{a}} + \hat{\mathbf{L}} \tag{4.2}$$

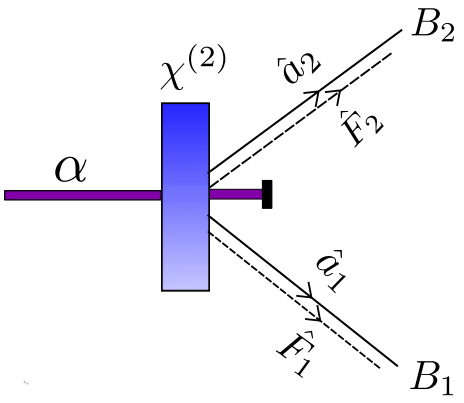

Figure 4.2: Diagram of the optical parametric process described by Eq. (4.1): the classical pump field, with complex amplitude α, generates the signal and idler modes described by the annihilation operators $\hat{a}_j$ and affected by the noise stochastic operators $\hat{F}_j$, $j = 1, 2$. For simplicity, the pump-field amplitude α is incorporated into the coupling constants g_{ij}. The mean photon number in the signal (idler) mode influenced by the noise is denoted by B_1 (B_2). In Sec. 3.3, $B_1 = B_\mathrm{p} + B_\mathrm{s}$ and $B_2 = B_\mathrm{p} + B_\mathrm{i}$, where $B_\mathrm{p} = \sinh^2(g_{12}t)$ is the mean number of generated photon pairs and $B_\mathrm{s} = \langle \hat{F}_1^\dagger \hat{F}_1 \rangle$ ($B_\mathrm{i} = \langle \hat{F}_2^\dagger \hat{F}_2 \rangle$) is the mean number of signal (idler) noise photons. In Secs. 3.4 and 3.5, $B_1 = \tilde{B}_\mathrm{p}^\mathrm{s} + B_\mathrm{s}$ and $B_2 = \tilde{B}_\mathrm{p}^\mathrm{i} + B_\mathrm{i}$, where $\tilde{B}_\mathrm{p}^\mathrm{s}$ ($\tilde{B}_\mathrm{p}^\mathrm{i}$) is the mean number of squeezed photons in the signal (idler) mode.

using the vectors $\hat{\mathbf{a}} = \left(\hat{a}_1, \hat{a}_1^\dagger, \hat{a}_2, \hat{a}_2^\dagger\right)^T$ and $\hat{\mathbf{L}} = \left(\hat{L}_1, \hat{L}_1^\dagger, \hat{L}_2, \hat{L}_2^\dagger\right)^T$, and the matrix

$$\mathbf{M} = \begin{bmatrix} -\gamma_1/2 & 2ig_{11} & 0 & ig_{12} \\ -2ig_{11} & -\gamma_1/2 & -ig_{12} & 0 \\ 0 & ig_{12} & -\gamma_2/2 & 2ig_{22} \\ -ig_{12} & 0 & -2ig_{22} & -\gamma_2/2 \end{bmatrix}. \tag{4.3}$$

The Langevin operators $\hat{L}_1$ and $\hat{L}_2$ introduced in Eq. (4.2) obey the following relations:

$$\begin{aligned} \langle \hat{L}_i(t) \rangle &= \langle \hat{L}_i^\dagger(t) \rangle = 0, \\ \langle \hat{L}_i^\dagger(t) \hat{L}_j(t') \rangle &= \delta_{ij} \langle n_d \rangle \delta(t - t'), \\ \langle \hat{L}_i(t) \hat{L}_j^\dagger(t') \rangle &= \delta_{ij} \big(\langle n_d \rangle + 1 \big) \delta(t - t'), \end{aligned} \tag{4.4}$$

where δ_{ij} stands for the Kronecker symbol and δ denotes the Dirac delta function.

The solution of Eq. (4.2) for the operators $\hat{a}_1$ and $\hat{a}_2$ is conveniently written in the following matrix form using suitable evolution matrices $\mathbf{U}$ and $\mathbf{V}$ and a stochastic operator vector $\hat{\mathbf{F}}$ (for

details, see, e.g. [88]):

$$\begin{bmatrix} \hat{a}_1(t) \\ \hat{a}_2(t) \end{bmatrix} = \mathbf{U}(t) \begin{bmatrix} \hat{a}_1(0) \\ \hat{a}_2(0) \end{bmatrix} + \mathbf{V}(t) \begin{bmatrix} \hat{a}_1^\dagger(0) \\ \hat{a}_2^\dagger(0) \end{bmatrix} + \hat{\mathbf{F}}(t). \tag{4.5}$$

Specific forms of the general evolution matrices $\mathbf{U}$ and $\mathbf{V}$ are discussed in the sections below. The elements of the stochastic operator vector $\hat{\mathbf{F}} \equiv (\hat{F}_1, \hat{F}_2)$ are derived as linear combinations of the Langevin forces $\hat{L}_j$ and $\hat{L}_j^\dagger$ that reflect the 'deterministic' solution described by the matrices $\mathbf{U}$ and $\mathbf{V}$ [88].

Statistical properties of the emitted fields, in a given state $\hat{\rho}$, are described by the Glauber-Sudarshan P function, or, equivalently, by the normal quantum characteristic function $C_{\mathcal{N}}$ defined as

$$C_{\mathcal{N}}(\beta_1, \beta_2) = \left\langle \exp(\beta_1 \hat{a}_1^\dagger + \beta_2 \hat{a}_2^\dagger) \exp(-\beta_1^* \hat{a}_1 - \beta_2^* \hat{a}_2) \right\rangle, \tag{4.6}$$

where symbol $\langle \dots \rangle$ denotes quantum averaging including both system and reservoir. Using the solution given in Eq. (4.5) and the initial vacuum states in both fields, the normal characteristic function $C_{\mathcal{N}}$ attains the following form:

$$\begin{aligned} C_{\mathcal{N}}(\beta_1, \beta_2) &= \exp\left[-B_1 |\beta_1|^2 - B_2 |\beta_2|^2 + \left(\frac{C_1}{2} \beta_1^{*2} \right.\right. \\ &\quad \left.\left. + \frac{C_2}{2} \beta_2^{*2} + D_{12} \beta_1^* \beta_2^* + \bar{D}_{12} \beta_1 \beta_2^* + \text{c.c.} \right) \right], \end{aligned} \tag{4.7}$$

where the auxiliary functions are defined as follows:

$$\begin{aligned} B_j &= \langle \Delta \hat{a}_j^\dagger \Delta \hat{a}_j \rangle = \sum_{k=1,2} |V_{jk}|^2 + \langle \hat{F}_j^\dagger \hat{F}_j \rangle, \\ C_j &= \langle (\Delta \hat{a}_j)^2 \rangle = \sum_{k=1,2} U_{jk} V_{jk} + \langle \hat{F}_j^2 \rangle, \\ D_{12} &= \langle \Delta \hat{a}_1 \Delta \hat{a}_2 \rangle = \sum_{k=1,2} U_{1k} V_{2k} + \langle \hat{F}_1 \hat{F}_2 \rangle, \\ \bar{D}_{12} &= -\langle \Delta \hat{a}_1^\dagger \Delta \hat{a}_2 \rangle = -\sum_{k=1,2} V_{1k}^* V_{2k} - \langle \hat{F}_1^\dagger \hat{F}_2 \rangle. \end{aligned} \tag{4.8}$$

Ordering	Quasidistribution		Characteristic function		Covariance matrix of a Gaussian state
Normal	$P(\alpha_1,\alpha_2)\equiv W^{(s=1)}(\alpha_1,\alpha_2)$	$\Longleftrightarrow$	$C_{\mathcal{N}}(\beta_1,\beta_2)$	$\longleftrightarrow$	$A_{\mathcal{N}}$
	$\Downarrow\uparrow$		$\Downarrow\Uparrow$		$\Downarrow\Uparrow$
Symmetric	$W(\alpha_1,\alpha_2)\equiv W^{(s=0)}(\alpha_1,\alpha_2)$	$\Longleftrightarrow$	$C_{\mathcal{S}}(\beta_1,\beta_2)$	$\longleftrightarrow$	$A_{\mathcal{S}}$

Table 4.1: Schematic diagram for the relations between (a) two quasiprobability distributions (quasidistributions), i.e., the Glauber-Sudarshan P and Wigner W functions for a given two-mode state $\hat{\rho}$, (b) characteristic functions $C_{\mathcal{N}}$ and $C_{\mathcal{S}}$, and (c) covariance matrices $A_{\mathcal{N}}$ and $A_{\mathcal{S}}$ assuming here that $\hat{\rho}$ is a Gaussian state for normal and symmetric orderings, respectively. Their interrelations (as marked by left-right arrows) are given in Appendix A. The single arrow indicates that the calculation of the P function from the Wigner function is more complicated (it can be done via the relation between $C_{\mathcal{S}}$ and $C_{\mathcal{N}}$) than the trivial calculation of the Wigner function from the P function (as marked by double arrow).

The normal characteristic function given in Eq. (4.7) can conveniently be rewritten into its matrix form $C_{\mathcal{N}}(\boldsymbol{\beta})=\exp(\boldsymbol{\beta}^{\dagger}\mathbf{A}_{\mathcal{N}}\boldsymbol{\beta}/2)$ using the covariance matrix $\mathbf{A}_{\mathcal{N}}$ related to the normal ordering [89] (for different possibilities in describing the generated fields, see Table 4.1):

$$\mathbf{A}_{\mathcal{N}}=\begin{bmatrix} -B_1 & C_1 & \bar{D}_{12}^{*} & D_{12} \\ C_1^{*} & -B_1 & D_{12}^{*} & \bar{D}_{12} \\ \bar{D}_{12} & D_{12} & -B_2 & C_2 \\ D_{12}^{*} & \bar{D}_{12}^{*} & C_2^{*} & -B_2 \end{bmatrix}, \tag{4.9}$$

and the column vector $\boldsymbol{\beta}=(\beta_1,\beta_1^{*},\beta_2,\beta_2^{*})^{T}$.

The covariance matrix $\mathbf{A}_{\mathcal{N}}$ related to the normal ordering determines the *global nonclassicality* of a two-mode Gaussian state via the Lee nonclassicality depth τ. The nonclassicality depth τ is defined with the help of the maximal positive eigenvalue $\lambda_{+}(\mathbf{A}_{\mathcal{N}})$ of the matrix $\mathbf{A}_{\mathcal{N}}$ as follows:

$$\tau=\max[0,\lambda_{+}(\mathbf{A}_{\mathcal{N}})]. \tag{4.10}$$

We note that the nonclassicality depth τ, according to its definition [20], gives the amount of noise photons present equally in both modes and needed to conceal the nonclassical character of the state.

The covariance matrix $\mathbf{A}_{\mathcal{N}}$ of the two-mode field can be written in the following block form:

$$\begin{aligned} \mathbf{A}_{\mathcal{N}} &= \begin{bmatrix} \mathbf{B}_1 & \mathbf{D}_{12} \\ \mathbf{D}_{21} & \mathbf{B}_2 \end{bmatrix}, \quad \mathbf{B}_j = \begin{bmatrix} -B_j & C_j \\ C_j^* & -B_j \end{bmatrix}, \quad j = 1, 2, \\ \mathbf{D}_{12} &= \begin{bmatrix} \bar{D}_{12}^* & D_{12} \\ D_{12}^* & \bar{D}_{12} \end{bmatrix}, \quad \mathbf{D}_{21} = \begin{bmatrix} \bar{D}_{12} & D_{12} \\ D_{12}^* & \bar{D}_{12}^* \end{bmatrix}. \end{aligned} \tag{4.11}$$

This form points out at the existence of three local invariants I_j, $j = 1, 2, 3$, that do not change under any local linear unitary transformation applied in mode 1 or 2. The local invariants I_j are expressed as:

$$I_1 = \det(\mathbf{B}_1), \quad I_2 = \det(\mathbf{B}_2), \quad I_3 = \det(\mathbf{D}_{12}). \tag{4.12}$$

Moreover, there exist two global invariants I and Δ preserved under arbitrary linear unitary transformations and applied to both modes:

$$I = \det(\mathbf{A}_{\mathcal{N}}), \quad \Delta = I_1 + I_2 + 2I_3. \tag{4.13}$$

Whereas the global invariant I encompasses the whole complex structure of the matrix $\mathbf{A}_{\mathcal{N}}$ and, as such, is not useful in our considerations, the global invariant Δ reflects the block structure of the matrix $\mathbf{A}_{\mathcal{N}}$ and lies in the center of our attention.

Moreover, the global invariant Δ includes the additive local invariants I_1 and I_2 that indicate the nonclassical behavior of the reduced states of modes 1 and 2, respectively. Indeed, the determinants defining these invariants occur in the Fourier transform of the normal characteristic functions of the reduced states directly related to their local Glauber-Sudarshan P functions. If a determinant fails to be positive then the corresponding Glauber-Sudarshan P function does not exist as a nonnegative function. Thus, the value of determinant I_j can be used to quantify the *local nonclassicality* of the reduced state in mode j as it is a monotone of the local Lee nonclassicality depth τ_j. The local Lee nonclassicality depth τ_j is defined along the formula

(4.10) that provides the relation:

$$\tau_j = \max(0, |C_j| - B_j), \quad j = 1, 2. \tag{4.14}$$

Using Eq. (4.14) we arrive at the monotonic relation between the local nonclassicality depth τ_j and local nonclassicality invariant (NI) I_j if we assume τ_j to be continuous:

$$I_j = -\tau_j \left(\tau_j + 2B_j\right). \tag{4.15}$$

We can redefine the local symplectic invariant in Eq. (4.15) as $I_{\mathrm{ncl}}^{(j)} = -I_j$ in order to deal with positive values when quantifying the local nonclassicality. We note that not only the positive values of this local NI $I_{\mathrm{ncl}}^{(1)}$ are useful for quantifying the local nonclassicality, also the negative values of this invariant are important as they quantify the "robustness" of the classicality of a local state.

Returning back to the last term I_3 in the global invariant Δ, this term describes solely the mutual quantum correlations between the fields 1 and 2. As such, it has to play a crucial role in the description of the entanglement between two fields. To reveal and quantify this entanglement and the role of local invariant I_3 here, we apply for a while the phase space (x, p) approach for describing the fields in the symmetric ordering of field operators corresponding to the Wigner formalism (see Table 1 and then the Appendix). The reason is technical and is given by the fact that we know how to derive the covariance matrix of a Gaussian state obtained by the partial transposition of the original state. According to Simon [90], the partial transposition means to replace p by $-p$. The covariance matrix of the partially transposed state then provides us the logarithmic negativity E_N that is a commonly used measure for the entanglement. Moreover, it provides as an entanglement measure useful in our considerations.

In detail, the covariance matrix $\mathbf{A}_{\mathcal{S}}$ expressed in the symmetric ordering is obtained in its block

structure as follows:

$$\begin{aligned}
\mathbf{A}_{\mathcal{S}} &= \begin{bmatrix} \mathbf{B}_{\mathcal{S}1} & \mathbf{D}_{\mathcal{S}} \\ \mathbf{D}_{\mathcal{S}}^{T} & \mathbf{B}_{\mathcal{S}2} \end{bmatrix}, \\
\mathbf{B}_{\mathcal{S}j} &= \begin{bmatrix} B_j + \mathrm{Re}(C_j) + 1/2 & \mathrm{Im}(C_j) \\ \mathrm{Im}(C_j) & B_j - \mathrm{Re}(C_j) + 1/2 \end{bmatrix}, \\
& \qquad j = 1, 2, \\
\mathbf{D}_{\mathcal{S}} &= \begin{bmatrix} \mathrm{Re}(D_{12} - \bar{D}_{12}) & \mathrm{Im}(D_{12} + \bar{D}_{12}) \\ \mathrm{Im}(D_{12} - \bar{D}_{12}) & -\mathrm{Re}(D_{12} + \bar{D}_{12}) \end{bmatrix}.
\end{aligned} \tag{4.16}$$

The covariance matrix $\mathbf{A}_{\mathcal{S}}$, similarly as its normally-ordered counterpart, has three local invariants $I_{\mathcal{S}j}$, $j = 1, 2, 3$, and two global ones denoted as $I_{\mathcal{S}}$ and $\Delta_{\mathcal{S}}$:

$$\begin{aligned}
I_{\mathcal{S}1} = \det(\mathbf{B}_{\mathcal{S}1}), \quad I_{\mathcal{S}2} = \det(\mathbf{B}_{\mathcal{S}2}), \quad I_{\mathcal{S}3} = \det(\mathbf{D}_{\mathcal{S}}), \\
I_{\mathcal{S}} = \det(\mathbf{A}_{\mathcal{S}}), \quad \Delta_{\mathcal{S}} = I_{\mathcal{S}1} + I_{\mathcal{S}2} + 2I_{\mathcal{S}3}.
\end{aligned} \tag{4.17}$$

Moreover, the comparison of the formulas for the invariants I_3 and $I_{\mathcal{S}3}$ shows that $I_3 = I_{\mathcal{S}3}$.

Following Refs. [91, 90, 78], the entanglement criterion can be expressed through the positivity of the entanglement indicator (EI) I_{ent} defined in terms of the invariants in Eq. (4.17) as follows:

$$I_{\mathrm{ent}} = \frac{1}{4}(I_{\mathcal{S}1} + I_{\mathcal{S}2} - 2I_{\mathcal{S}3}) - I_{\mathcal{S}} - \frac{1}{16}. \tag{4.18}$$

As we show below the EI I_{ent} is a monotonous function of logarithmic negativity E_N, which can be derived from the symplectic eigenvalue $\tilde{d}_-$ of the partially transposed (PT) matrix $\mathbf{A}_{\mathcal{S}}^{\mathrm{PT}}$ along the formula [92] (see Fig. 4.3)

$$E_N = \max[0, -\ln(2\tilde{d}_-)]. \tag{4.19}$$

According to Eq. (4.19), a state is entangled if $\tilde{d}_- < 1/2$. In turn, the symplectic eigenvalue

$\tilde{d}_-$ is found as:

$$\tilde{d}_- = \frac{1}{\sqrt{2}}\sqrt{\tilde{\Delta}_{\mathcal{S}} - \sqrt{\tilde{\Delta}_{\mathcal{S}}^2 - 4I_{\mathcal{S}}}}\,, \tag{4.20}$$

where $\tilde{\Delta}_{\mathcal{S}} = I_{\mathcal{S}1} + I_{\mathcal{S}2} - 2I_{\mathcal{S}3}$. Combining Eqs. (4.18) and (4.20) we arrive at the relation between the symplectic eigenvalue $\tilde{d}_-$ and entanglement indicator I_{ent}:

$$\tilde{d}_- = \frac{1}{\sqrt{2}}\sqrt{I' - \sqrt{I'^2 - 4I_{\mathcal{S}}}}\,, \tag{4.21}$$

where $I' = 4I_{\mathcal{S}} + 4I_{\text{ent}} + \frac{1}{4}$.

Assuming the global invariant $I_{\mathcal{S}}$ is fixed, the relation (4.21) shows that the larger is the entanglement indicator I_{ent}, the smaller is the symplectic eigenvalue $\tilde{d}_-$ and, according to formula (4.19), also the larger is the logarithmic negativity E_N. As a consequence, the entanglement indicator I_{ent} represents an alternative to the logarithmic negativity E_N in quantifying entanglement. We illustrate the monotonous dependence of the logarithmic negativity E_N on the entanglement indicator I_{ent} in Fig. 4.2. We note that a simple analytical formula between the logarithmic negativity E_N and entanglement indicator I_{ent} is derived for pure states ($I_{\mathcal{S}} = 1/16$) assuming $I_{\text{ent}} > 0$:

$$E_N = \ln(2\sqrt{I_{\text{ent}}} + \sqrt{1 + 4I_{\text{ent}}}). \tag{4.22}$$

As we look for a relation among the local invariants $I_{\text{ncl}}^{(1)}$ and $I_{\text{ncl}}^{(2)}$ and the entanglement indicator I_{ent} (see Fig. 4.1), we eliminate the invariants $I_3 = I_{\mathcal{S}3}$ from Eqs. (4.13) and (4.18) by their comparing. This leaves us with the relation:

$$I_{\text{ncl}}^{(1)} + I_{\text{ncl}}^{(2)} + 2I_{\text{ent}} = \frac{1}{2}\Delta_{\mathcal{S}} - \Delta - 2I_{\mathcal{S}} - \frac{1}{8}. \tag{4.23}$$

As only the global invariants occur at the r.h.s. of Eq. (4.23), the relation $I_{\text{ncl}}^{(1)} + I_{\text{ncl}}^{(2)} + 2I_{\text{ent}}$ is invariant under any global linear unitary transformation.

Equation (4.23) can be transformed into the central result of this chapter, if we define a new

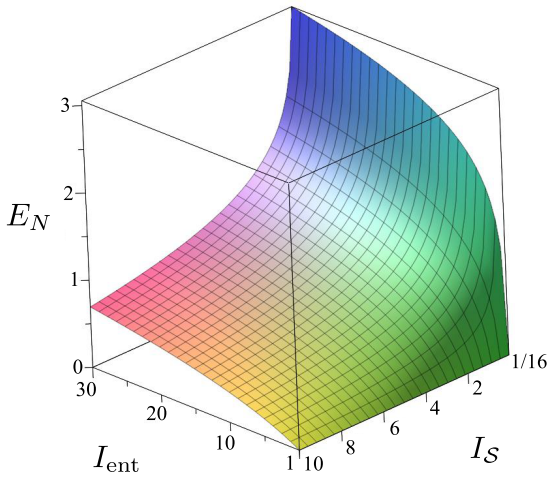

Figure 4.3: Logarithmic negativity E_N as a function of entanglement indicator I_{ent}, given by Eq. (4.18), and global nonclassicality invariant $I_{\mathcal{S}}$, given by Eq. (4.17).

quantity I_{ncl}, which is a global nonclassicality invariant:

$$I_{\text{ncl}} = I_{\text{ncl}}^{(1)} + I_{\text{ncl}}^{(2)} + 2I_{\text{ent}}, \tag{4.24}$$

In the derivation of this equation, it is useful to recall the property that the local determinants for the normally-ordered CF, I_3, and the symmetrically-ordered CF, $I_{\mathcal{S}3}$, are equal $I_3 = I_{\mathcal{S}3}$, and given by Eqs. (4.13) and (4.17). Thus, we have

$$\begin{aligned} I_{\text{ncl}} &= I_{\text{ncl}}^{(1)} + I_{\text{ncl}}^{(2)} + 2I_{\text{ent}} \\ &= -I_1 - I_2 + \frac{1}{2}(I_{\mathcal{S}1} + I_{\mathcal{S}2} - 2I_{\mathcal{S}3}) - 2I_{\mathcal{S}} - \frac{1}{8} \\ &= -I_1 - I_2 - 2I_{\mathcal{S}3} + \frac{1}{2}(I_{\mathcal{S}1} + I_{\mathcal{S}2} + 2I_{\mathcal{S}3}) - 2I_{\mathcal{S}} - \frac{1}{8} \\ &= -\Delta + \frac{1}{2}\Delta_{\mathcal{S}} - 2I_{\mathcal{S}} - \frac{1}{8}. \end{aligned} \tag{4.25}$$

Equation (4.24) means that the local nonclassicality invariants $I_{\text{ncl}}^{(1)}$ and $I_{\text{ncl}}^{(2)}$ together with the entanglement indicator I_{ent} form the global NI I_{ncl}. Any linear unitary transformation in general modifies both the local NIs $I_{\text{ncl}}^{(1)}$ and $I_{\text{ncl}}^{(2)}$ and the entanglement invariant I_{ent} only in such a way that it preserves the value of the global NI I_{ncl}. Whenever I_{ncl} is positive, the analyzed state is nonclassical due to the local nonclassicality of the reduced states or its entanglement. The

Table 4.2: Regions of different entanglement and local nonclassicalities observed in the figures of Secs. 3.3—3.6.

case/region	Entanglement	Nonclassicality of one mode	Nonclassicality of another mode	Figures
I	Yes	Yes	Yes	6, 10
II	Yes	Yes	No	6(b)
III	Yes	No	No	6, 10
IV	No	Yes	Yes	6, 10
V	No	Yes	No	6(b)
VI	No	No	No	6, 10

negative values of the global NI $I_{\rm ncl}$ do not necessarily mean that a given state is classical, as we will see below.

In the next sections, we analyze the nonclassicality and entanglement of several kinds of important quantum states from the point of view of their transformation by a beam splitter. The division of the global NI into the EI and the local NIs is in the center of our attention. In general, six regions differing in the occurrence of entanglement and local nonclassicalities can be defined (see Table 4.2). All these regions are found in the examples analyzed in the next sections, as indicated in Table 4.2.

We note that an invariant based on the second-order intensity moments and, as such, describing intensity auto- and cross-correlations has been suggested in Ref. [93] for two-mode fields with specific mode correlations and unitary transformations. Later, this invariant was experimentally analyzed in Ref. [94]. Here, we describe the propagation of fields through the beam splitter (see Fig. 4.1) described by the real transmissivity T and the phase ϕ through the unitary transformation characterized by the matrix $\mathbf{U}$,

$$\mathbf{U} = \begin{pmatrix} \sqrt{T} & 0 & -\sqrt{R}e^{i\phi} & 0 \\ 0 & \sqrt{T} & 0 & -\sqrt{R}e^{-i\phi} \\ \sqrt{R}e^{-i\phi} & 0 & \sqrt{T} & 0 \\ 0 & \sqrt{R}e^{i\phi} & 0 & \sqrt{T} \end{pmatrix}; \tag{4.26}$$

$R = 1 - T$ is the reflectivity of the beam splitter. The covariance matrix $\mathbf{A}^{\rm out}$ at the output of the beam splitter is obtained as $\mathbf{A}^{\rm out} = \mathbf{U}^\dagger \mathbf{A} \mathbf{U}$.

4.3 Twin beam

These beams are generated by parametric down-conversion from the vacuum into which photon pairs are ideally emitted. For this reason, only the terms B_1, B_2, and D_{12} in the normal characteristic function $C_{\mathcal{N}}$ are nonzero. The evolution matrices $\mathbf{U}$ and $\mathbf{V}$ in Eq. (4.5) have the following nonzero elements:

$$\begin{aligned} U_{11}(t) &= U_{22}(t) = \cosh(gt), \\ V_{12}(t) &= V_{21}(t) = i\exp(i\theta)\sinh(gt). \end{aligned} \tag{4.27}$$

The coefficients B_1 and B_2 can be expressed as $B_1 = B_\mathrm{p} + B_\mathrm{s}$ and $B_2 = B_\mathrm{p} + B_\mathrm{i}$, where $B_\mathrm{p} = \sinh^2(g_{12}t)$ gives the mean number of generated photon pairs and $B_\mathrm{s} = \langle \hat{F}_1^\dagger \hat{F}_1 \rangle$ ($B_\mathrm{i} = \langle \hat{F}_2^\dagger \hat{F}_2 \rangle$) denotes the mean number of signal (idler) noise photons coming from the reservoir (see Fig. 4.2). On the other hand, the parameter D_{12} characterizing mutual correlations depends only on the mean number B_p of photon pairs as $D_{12} = i\sqrt{B_\mathrm{p}(B_\mathrm{p}+1)}$ ($\theta = 0$ is assumed without the loss of generality).

The general formulas for the local NIs $I_\mathrm{ncl}^{(j)}$, entanglement invariant I_ent, and the global NI I_ncl attain the following forms for twin beams:

$$\begin{aligned} I_\mathrm{ncl}^{(1)} &= 4TR(B_\mathrm{p}^2 + B_\mathrm{p}) - \left[B_\mathrm{p} + TB_\mathrm{s} + RB_\mathrm{i}\right]^2, \\ I_\mathrm{ncl}^{(2)} &= 4TR(B_\mathrm{p}^2 + B_\mathrm{p}) - \left[B_\mathrm{p} + TB_\mathrm{i} + RB_\mathrm{s}\right]^2, \\ I_\mathrm{ent} &= -\left[(B_\mathrm{s}+B_\mathrm{i})^2 - (T-R)^2\right](B_\mathrm{p}^2 + B_\mathrm{p}) - 2B_\mathrm{p}B_\mathrm{s}B_\mathrm{i}(B_\mathrm{s}+B_\mathrm{i}) - (B_\mathrm{s}^2+B_\mathrm{s})(B_\mathrm{i}^2+B_\mathrm{i}) \\ &\quad - TR(B_\mathrm{s}+B_\mathrm{i})^2, \end{aligned} \tag{4.28}$$

$$I_\mathrm{ncl} = 2B_\mathrm{p} - (B_\mathrm{s}+B_\mathrm{i})^2[2(B_\mathrm{p}^2+B_\mathrm{p})+1] - 2B_\mathrm{p}(1+2B_\mathrm{s}B_\mathrm{i})(B_\mathrm{s}+B_\mathrm{i}) - 2B_\mathrm{s}B_\mathrm{i}(B_\mathrm{s}+B_\mathrm{i}+B_\mathrm{s}B_\mathrm{i}). \tag{4.29}$$

We first discuss the behavior of noiseless twin beams for which $B_\mathrm{s} = B_\mathrm{i} = 0$. In this case, the

global NI I_{ncl} equals $2B_{\mathrm{p}}$ and

$$\begin{aligned} I_{\mathrm{ncl}}^{(j)} &= 4TR(B_{\mathrm{p}}^2 + B_{\mathrm{p}}) - B_{\mathrm{p}}^2, \quad j = 1, 2, \\ I_{\mathrm{ent}} &= (T - R)^2(B_{\mathrm{p}}^2 + B_{\mathrm{p}}). \end{aligned} \tag{4.30}$$

As suggested by the formula in Eq. (4.30), the local NIs $I_{\mathrm{ncl}}^{(j)}$ can be decomposed into two terms. The negative term reflects classical thermal statistics of photon pairs in a twin beam with its photon bunching effect and as such suppresses the nonclassical behavior of the twin beam. On the other hand, the positive term refers to squeezing appearing at the individual output ports of the beam splitter. The squeezing effect originates in pairing of photons in individual output ports caused by "sticking of two photons from a pair together" (photon bunching) at the beam splitter [27]. Photon pairs with both photons in one output port contribute to the local nonclassicality of the field in this port. On the other hand, when two photons from one photon-pair occur in different output ports, they contribute to the entanglement. "A given individual photon pair" is, thus, responsible either for the local nonclassicality in one of the output ports or for their entanglement. Never for both. Propagation through the beam splitter can, thus, be viewed as the process of breaking photon pairs (antibunching) arriving at the same input port and gluing (bunching) of photons from a given pair coming from different input ports. Whereas the first process disturbs local squeezing and supports entanglement, the second process strengthens squeezing at the expense of entanglement. The global NI I_{ncl} is equal twice the number B_{p} of photon pairs and, as such, indicates an appropriate choice of this nonclassicality resource quantifier.

Detailed analysis of the formulas in Eq. (4.30) shows that the local marginal states are nonclassical only if the transmissivity T lies in certain interval around $\frac{1}{2}$:

$$T \in \left(\frac{1}{2} - \frac{1}{2\sqrt{B_{\mathrm{p}} + 1}}, \frac{1}{2} + \frac{1}{2\sqrt{B_{\mathrm{p}} + 1}} \right). \tag{4.31}$$

It holds that the larger is the mean photon-pair number B_{p}, the narrower is the interval. The optimal transmissivity T maximizing the local NIs $I_{\mathrm{ncl}}^{(j)}$ equals $\frac{1}{2}$. In this case, the entanglement

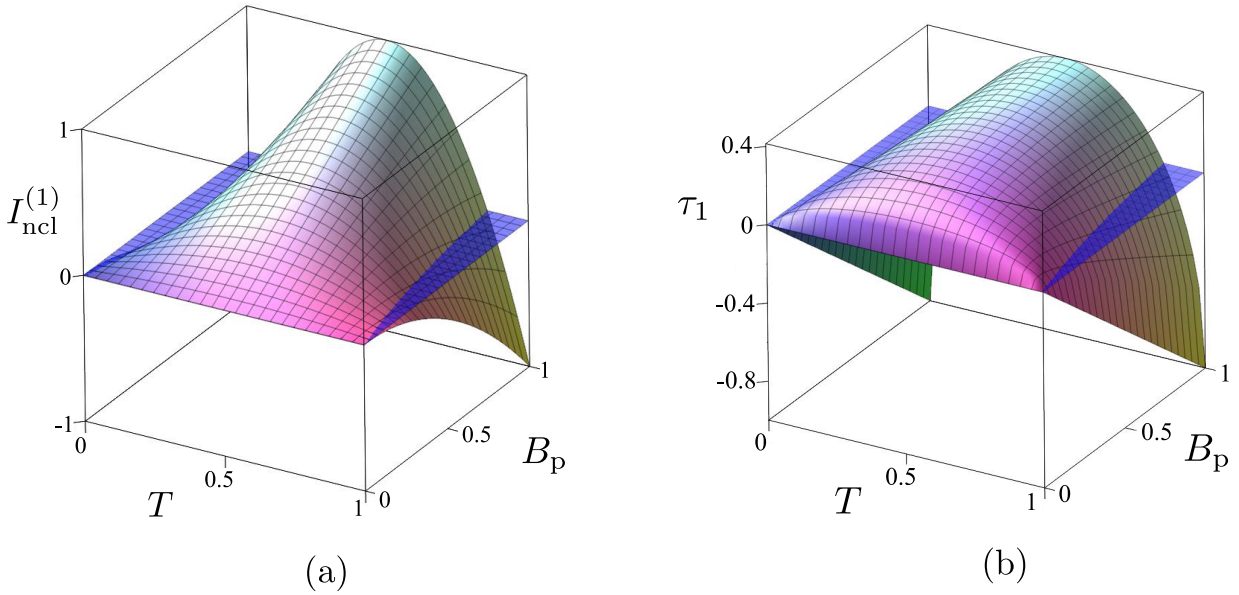

Figure 4.4: (a) Local nonclassicality invariant $I_{\mathrm{ncl}}^{(1)}$ and (b) continuous Lee nonclassicality depth τ_1 (including negative values) at the output port 1 of the beam splitter as a function of the mean photon-pair number B_{p} and the beam-splitter transmissivity T for pure twin beam states. In panel (a) and (b), the blue dark grey plain surface at $I_{\mathrm{ncl}}^{(1)} = 0$ and $\tau_1 = 0$ shows the boundary between the classical and nonclassical domains.

of the incident twin beam is completely and equally transferred into the local nonclassicalities of the two output modes. On the other hand, the twin beam loses its entanglement only when $T = \frac{1}{2}$. In this case, all the incident photon pairs stick together (bunch) at the beam splitter suppressing completely their entanglement. Hand in hand, the local NIs $I_{\mathrm{ncl}}^{(1)} = I_{\mathrm{ncl}}^{(2)}$ attain their maximal values. This can be interpreted such that the initial entanglement is transferred into the squeezing of the marginal output fields [95]. These effects are shown in Figs. 4.4(a) and 4.5(a) for the dependencies of the local NI $I_{\mathrm{ncl}}^{(1)}$ and EI I_{ent} on the transmissivity T and mean photon-pair number B_{p}. The commonly used the Lee nonclassicality depth τ_1 and the logarithmic negativity E_N are shown for comparison in Figs. 4.4(b) and 4.5(b). We note, that whereas the values of the Lee nonclassicality depth τ_1 cannot exceed $\frac{1}{2}$, the values of the local NI $I_{\mathrm{ncl}}^{(1)}$ can be arbitrarily large depending on the intensity of the twin beam.

Now we consider general noisy twin beams. It has been shown in Ref. [A1] that whenever the overall noise $B_{\mathrm{s}} + B_{\mathrm{i}}$ exceeds one, the twin beam is unentangled and, thus, it cannot generate any nonclassical feature. Even if $B_{\mathrm{s}} + B_{\mathrm{i}} < 1$, the mean photon-pair number B_{p} has to be

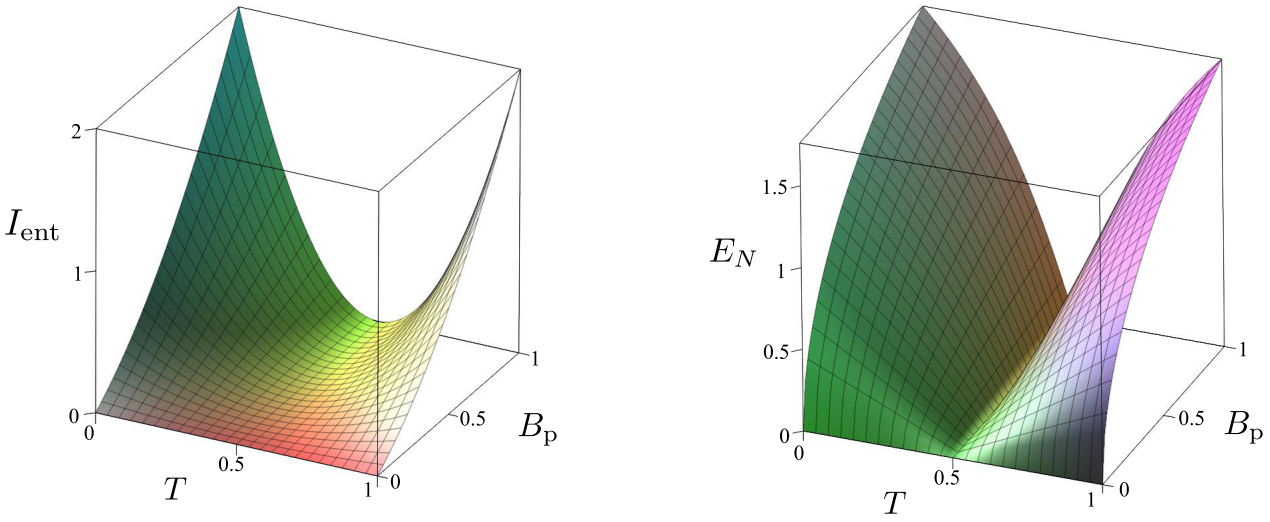

Figure 4.5: (a) Entanglement invariant E_I and (b) logarithmic negativity E_N after the beam splitter transformation considered as functions of the mean photon-pair number B_{p} and the beam-splitter transmissivity T for pure twin beams states.

sufficiently large, as given by

$$B_{\mathrm{p}} > \frac{B_{\mathrm{s}} B_{\mathrm{i}}}{1 - (B_{\mathrm{s}} + B_{\mathrm{i}})}. \tag{4.32}$$

Then, the incident noisy twin beam is entangled and is capable to provide its entanglement and local nonclassicality after the beam splitter. However, the general analysis of Eqs. (4.28) and (4.29) leads to the conclusion that the noise only degrades the non-classical behavior independently whether it is manifested by local nonclassicality or entanglement. The stronger the noise, the weaker the non-classical features.

To provide a deeper insight into the role of noise, we analyze two special cases: in the first one, the noise is equally divided into both modes of the incident twin beam; while noise occurs only in one mode of the incident twin beam in the second case.

When noise occurs in both modes of the incident twin beam ($B_{\mathrm{n}} \equiv B_{\mathrm{s}} = B_{\mathrm{i}}$), the globally nonclassical output states can be divided into three groups. They are displayed in the "phase diagram" in Fig. 4.6. In this diagram, the surfaces $I^{(1)}_{\mathrm{ncl}}(B_{\mathrm{n}}, B_{\mathrm{p}}, T) = 0$ and $I_{\mathrm{ent}}(B_{\mathrm{n}}, B_{\mathrm{p}}, T) = 0$ are shown. They identify four different regions belonging to different groups of states (see Table 4.2 for details). The states exhibiting both entanglement and local nonclassicality occur

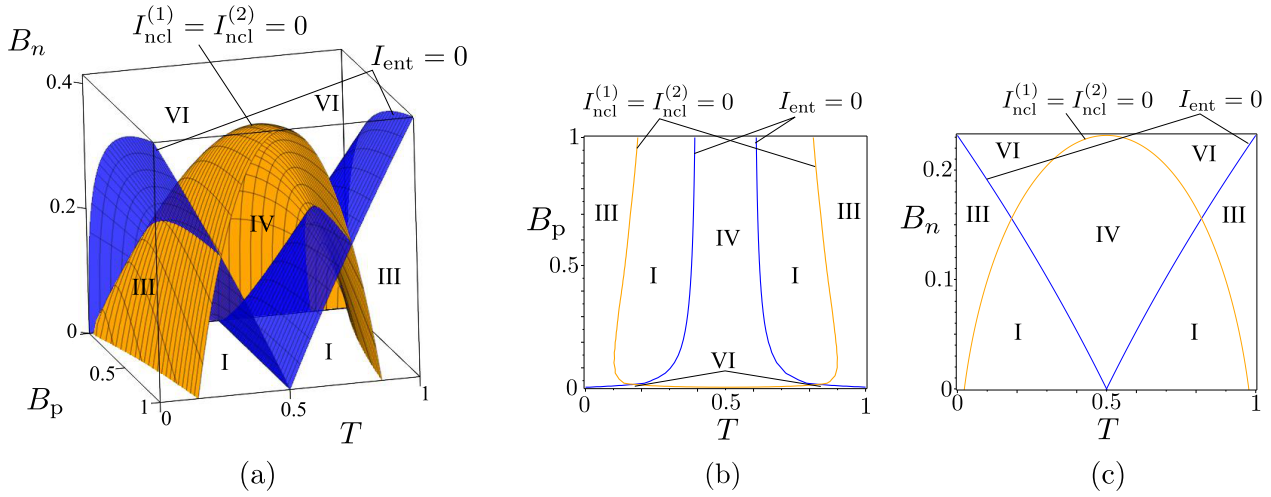

Figure 4.6: Diagram (a) shows the nonclassicality and entanglement invariants for the twin beams states occurring at the output ports of a beam splitter depending on the mean noise photon number $B_{\rm n}$, mean photon-pair number $B_{\rm p}$, and transmissivity T according to Eq. (4.28) for $B_{\rm n} \equiv B_{\rm s} = B_{\rm i}$. The surfaces are plotted at $I^{(1)}_{\rm ncl}(B_{\rm n}, B_{\rm p}, T) = 0$ [orange light gray surface], $I^{(2)}_{\rm ncl}(B_{\rm n}, B_{\rm p}, T) = 0$ [orange light gray] and $E_I(B_{\rm n}, B_{\rm p}, T) = 0$ [blue dark surface] indicating six different regions specified in the text and Tab. 4.2. Diagrams (b) and (c) show the perpendicular cross-sections of diagram (a) taken at chosen values of $B_{\rm n} = 0.1$ and $B_{\rm p} = 0.1$, respectively.

in region I. In region III, the states are entangled but locally classical. The locally nonclassical and unentangled states are found in region IV. In region VI, the unentangled and locally classical states exist.

The presence of noise in only one mode of the incident twin beam ($B_{\rm s} = 0$, $B_{\rm i} \equiv B_{\rm n} \neq 0$) leads to asymmetry between the output modes. This is shown in Fig. 4.7, where the surfaces $I^{(1)}_{\rm ncl}(B_{\rm n}, B_{\rm p}, T) = 0$ and $I^{(2)}_{\rm ncl}(B_{\rm n}, B_{\rm p}, T) = 0$ behave differently. The symmetry, with respect to the plane for $T = \frac{1}{2}$, which is clearly visible in Fig. 4.6, does not exist in Fig. 4.7. As a consequence, two additional groups of states are found in the diagram. In region V, there are unentangled states with only one marginal field exhibiting local nonclassicality. The entangled states with only one locally nonclassical field are found in region II. In detail, mode 1 (2) is locally nonclassical for $T < \frac{1}{2}$ ($T > \frac{1}{2}$). We note that the EI $I_{\rm ent}$ is not sensitive to the noise asymmetry, as shown by the surface $I_{\rm ent}(B_{\rm n}, B_{\rm p}, T) = 0$ in Fig. 4.7. It is worth noting that positive values of the GNI $I_{\rm ncl}$ are exhibited when either entanglement or local nonclassicality or even both are found. The negative values of the global NI $I_{\rm ncl}$ do not necessarily mean classicality. The state with the negative GNI $I_{\rm ncl}$ can still be globally nonclassical due to

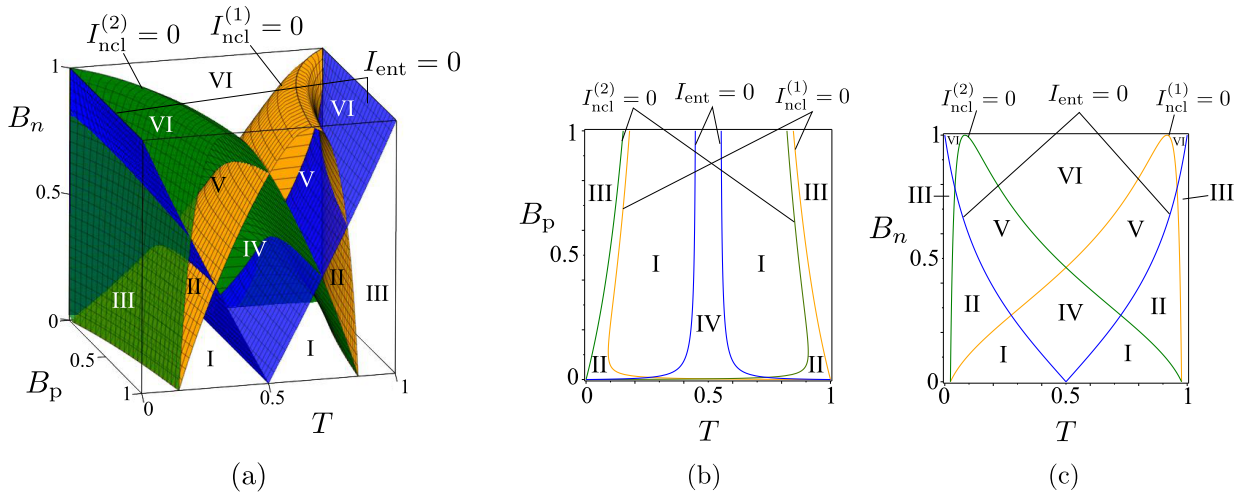

Figure 4.7: Diagram (a) shows the nonclassicality and entanglement invariants for the twin beams states occurring at the output ports of a beam splitter depending on the mean noise photon number $B_{\rm n}$, mean photon-pair number $B_{\rm p}$, and transmissivity T according to Eq. (4.28) for $B_{\rm s}=0$ and $B_{\rm n}=B_{\rm i}$. The surfaces are plotted at $I_{\rm ncl}^{(1)}(B_{\rm n},B_{\rm p},T)=0$ [orange light gray surface], $I_{\rm ncl}^{(2)}(B_{\rm n},B_{\rm p},T)=0$ [green dark gray surfaces] and $E_I(B_{\rm n},B_{\rm p},T)=0$ [blue dark surface] indicating six different regions specified in the text and Tab. 4.2. Diagrams (b) and (c) show the perpendicular cross-sections of diagram (a) taken at fixed values of $B_{\rm n}=0.1$ and $B_{\rm p}=0.1$, respectively. These cross-sections are analogous to those in Figs. 4.6(b) and 4.6(c).

either its entanglement or local nonclassicality, but not both. The diagram in Fig. 4.6(a) can serve as an example. The surface $I_{\rm ncl}(B_{\rm n},B_{\rm p},T)=0$ lies naturally in between the surfaces $I_{\rm ncl}^{(1)}(B_{\rm n},B_{\rm p},T)=0$, and $I_{\rm ent}(B_{\rm n},B_{\rm p},T)=0$ and its position identifies the globally nonclassical states with $I_{\rm ncl}<0$.

4.4 Squeezed vacuum state with noise

Here, we consider a squeezed vacuum state [27] mixed with the noise incident on one input port of the beam splitter, whereas the second input port is left in the vacuum state. In this case, the nonzero elements of evolution matrices $\mathbf{U}$ and $\mathbf{V}$ in Eq. (4.5) are given as ($\theta=0$ is assumed):

$$U_{11}(t)=\cosh(gt),\quad U_{22}(t)=1,\quad V_{11}(t)=i\exp(i\theta)\sinh(gt). \tag{4.33}$$

The non-zero parameters of the normal characteristic function $C_{\mathcal{N}}$ in Eq. (4.9) are B_1 and C_1 as given by: $B_1 = \tilde{B}_{\rm p}^{\rm sq} + B_{\rm s}$ and $C_1 = i\sqrt{\tilde{B}_{\rm p}^{\rm sq}(\tilde{B}_{\rm p}^{\rm sq}+1)}$. The symbol $\tilde{B}_{\rm p}^{\rm sq}$ denotes the mean number of squeezed photons and the symbol $B_{\rm s}$ stands for the mean number of the signal noise photons (see also Fig. 4.2). The local NIs $I_{\rm ncl}^{(j)}$ and EI $I_{\rm ent}$ are easily expressed in terms of the global NI $I_{\rm ncl}$ as follows

$$I_{\rm ncl}^{(1)} = T^2 I_{\rm ncl}, \quad I_{\rm ncl}^{(2)} = R^2 I_{\rm ncl}, \quad I_{\rm ent} = TRI_{\rm ncl}, \quad I_{\rm ncl} = \tilde{B}_{\rm p}^{\rm sq}(1-2B_{\rm s}) - B_{\rm s}^2. \tag{4.34}$$

As the local NIs $I_{\rm ncl}^{(1)}$ and $I_{\rm ncl}^{(2)}$, as well as the EI $I_{\rm ent}$ are linearly proportional to the global NI $I_{\rm ncl}$, the global nonclassicality of the output states immediately guarantees both local nonclassicalities and entanglement. This occurs only for the positive values of the global NI $I_{\rm ncl}$. According to Eq. (4.34), $I_{\rm ncl} > 0$ provided that the mean noise photon number $B_{\rm s}$ in the signal mode is sufficiently small:

$$B_{\rm s} < \sqrt{\tilde{B}_{\rm p}^{\rm sq}(\tilde{B}_{\rm p}^{\rm sq}+1)} - \tilde{B}_{\rm p}^{\rm sq}. \tag{4.35}$$

Following Eq. (4.34), the mean noise photon number $B_{\rm s}$ in the signal mode has to be smaller than 1. Also, the more intense is the squeezed state, the smaller is the number $B_{\rm s}$ of accepted noise photons. We note that the condition, given in Eq. (4.34), can immediately be revealed when the global Lee nonclassicality depth τ is analyzed. As an illustration, the dependencies of the local NIs $I_{\rm ncl}^{(1)}$ and $I_{\rm ncl}^{(2)}$ and the EI $I_{\rm ent}$ on the beam-splitter transmissivity T are plotted in Fig. 4.8 for the incident noiseless squeezed states. The greatest values of EI $I_{\rm ent}$ are reached for the balanced beam splitter ($T = \frac{1}{2}$). However, some incident photon pairs are not broken (i.e., split) by the beam splitter and give raise to nonzero local nonclassicalities $I_{\rm ncl}^{(1)}$ and $I_{\rm ncl}^{(2)}$ even in this case.

The strength of squeezing in a given mode is commonly characterized by a principal squeeze variance λ [33], which is here given by

$$\lambda_j = 1/2 + B_j - |C_j|. \tag{4.36}$$

When a given output mode $j = 1, 2$ is locally nonclassical, it is also squeezed, which corresponds

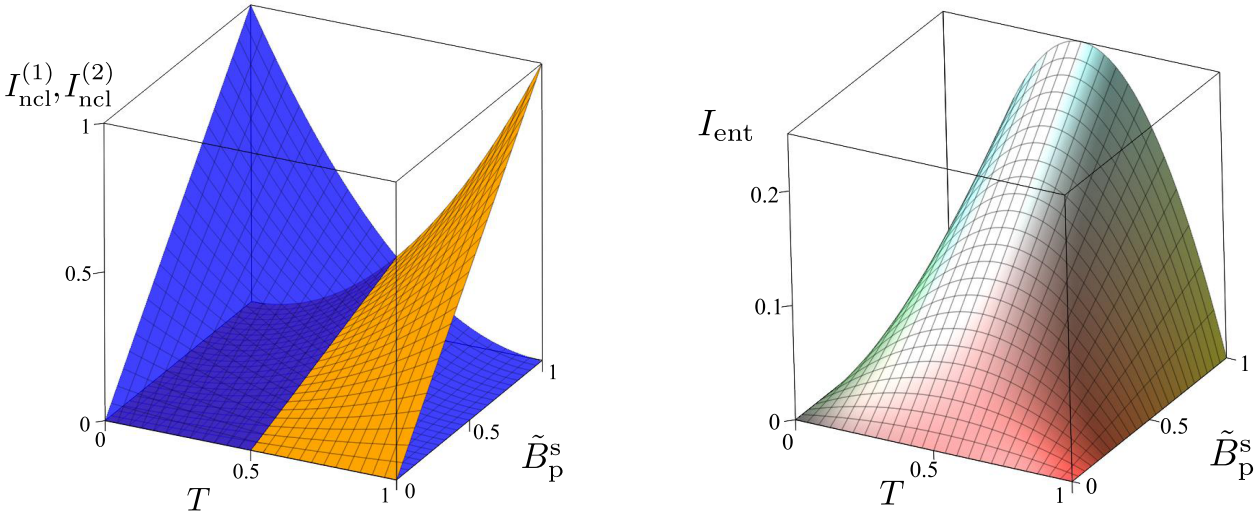

Figure 4.8: Invariant nonclassicality parameters: (a) the local nonclassicality invariants $I_{\rm ncl}^{(1)}$ (orange light gray surface) and $I_{\rm ncl}^{(2)}$ (blue dark gray surface), and (b) the entanglement invariant $I_{\rm ent}$ versus the mean number $\tilde{B}_{\rm p}^{\rm s}$ of squeezed photons and the beam-splitter transmissivity T according to Eq. (4.34) assuming $B_{\rm s} = 0$.

to $\lambda_j < \frac{1}{2}$. According to the relation between the local NI $I_{\rm ncl}^{(j)}$ and the principal squeeze variance λ_j derived by combining Eqs. (4.15) and (4.36),

$$I_{\rm ncl}^{(j)} = (\frac{1}{2} - \lambda_j)(2B_j + \frac{1}{2} - \lambda_j), \tag{4.37}$$

the smaller is the value of the principal squeeze variance λ_j below $\frac{1}{2}$, the greater is the value of the local NI $I_{\rm ncl}^{(j)}$.

4.5 Two squeezed vacua

Two independent squeezed states are generated by the Hamiltonian given in Eq. (4.1) provided that the process of parametric down-conversion does not occur in the nonlinear medium ($g_{12} = 0$). The solution of the evolution governed by the Hamiltonian (4.1) gives us the following

nonzero elements of the evolution matrices $\mathbf{U}$ and $\mathbf{V}$:

$$\begin{aligned} U_{11} &= \cosh(2g_{11}t), \quad V_{11} = i\exp(i\kappa_1)\sinh(2g_{11}t), \\ U_{22} &= \cosh(2g_{22}t), \quad V_{22} = i\exp(i\kappa_2)\sinh(2g_{11}t), \end{aligned} \tag{4.38}$$

where κ_1 and κ_2 are arbitrary phases. The nonzero coefficients of the incident covariance matrix $\mathbf{A}_{\mathcal{N}}$ are given as $B_{1,2} = \tilde{B}_{\rm p}^{\rm s,i} + B_{\rm s,i}$ and $C_{1,2} = \exp(i\theta_{1,2})\sqrt{\tilde{B}_{\rm p}^{\rm s,i}(\tilde{B}_{\rm p}^{\rm s,i}+1)}$, $\theta_j = \kappa_j + \pi/2$ for $j = 1, 2$, where $\tilde{B}_{\rm p}^{\rm s}$ ($\tilde{B}_{\rm p}^{\rm i}$) stands for the mean number of squeezed photons in the signal (idler) mode, whereas the corresponding mean signal (idler) noise photon number is denoted as $B_{\rm s}$ ($B_{\rm i}$).

After the beam splitter, the local NIs $I_{\rm ncl}^{(j)}$, EI $I_{\rm ent}$ and global NI $I_{\rm ncl}$ acquire the form:

$$\begin{aligned} I_{\rm ncl}^{(1)} &= T^2\tilde{B}_{\rm p}^{\rm s}(\tilde{B}_{\rm p}^{\rm s}+1) + R^2\tilde{B}_{\rm p}^{\rm i}(\tilde{B}_{\rm p}^{\rm i}+1) + TR\bar{D}'_{12}\cos(\theta_1-\theta_2) - \Big[T\tilde{B}_{\rm p}^{\rm s} + R\tilde{B}_{\rm p}^{\rm i} + TB_{\rm s} + RB_{\rm i}\Big]^2, \\ I_{\rm ncl} &= B_1 + B_2 - 2B_{\rm s}B_{\rm i}\Big[2B_1(1+\tilde{B}_{\rm p}^{\rm i}) + 2\tilde{B}_{\rm p}^{\rm i}(1+B_1) + B_{\rm i}(1+2B_1) + B_{\rm s}(1+2B_2)\Big] \\ &\quad - 2(B_{\rm s}B_1 + B_{\rm i}B_2) - (B_{\rm s}+B_{\rm i})^2, \\ I_{\rm ent} &= TR\Big[-\bar{D}'_{12}\cos(\theta_1-\theta_2) + (\tilde{B}_{\rm p}^{\rm s} + \tilde{B}_{\rm p}^{\rm i} + 2\tilde{B}_{\rm p}^{\rm s}\tilde{B}_{\rm p}^{\rm i}) - (B_{\rm s}+B_{\rm i})^2 - 2(\tilde{B}_{\rm p}^{\rm s} - \tilde{B}_{\rm p}^{\rm i})(B_{\rm s}-B_{\rm i})\Big] \\ &\quad + B_{\rm s}B_{\rm i}\Big[2\tilde{B}_{\rm p}^{\rm s}(1+B_{\rm i}) + 2\tilde{B}_{\rm p}^{2}(1+B_{\rm s}) + 4\tilde{B}_{\rm p}^{\rm s}\tilde{B}_{\rm p}^{\rm i} + (1+B_{\rm s})(1+B_{\rm i})\Big], \end{aligned} \tag{4.39}$$

where $\bar{D}'_{12} = 2\sqrt{\tilde{B}_{\rm p}^{\rm s}(\tilde{B}_{\rm p}^{\rm s}+1)\tilde{B}_{\rm p}^{\rm i}(\tilde{B}_{\rm p}^{\rm i}+1)}$, $B_1 = \tilde{B}_{\rm p}^{\rm s} + B_{\rm s}$, $B_2 = B_{\rm p}^{\rm i} + B_{\rm i}$, and, for simplicity, we assumed $\phi = 0$ in Eq. (4.26). The formula for $I_{\rm ncl}^{(2)}$ is obtained from that for $I_{\rm ncl}^{(1)}$ in Eq. (4.39) with the substitution s $\leftrightarrow$ i.

The global NI $I_{\rm ncl}$ does not depend on the relative phase $\Delta\theta = \theta_1 - \theta_2$ of two incident squeezed states, while the local NIs $I_{\rm ncl}^{(j)}$ and EI $I_{\rm ent}$ change with the relative phase $\Delta\theta$. The case of two equally intense incident noiseless squeezed states, as graphically analyzed in Fig. 4.9, shows that the phase difference $\Delta\theta$ plays a crucial role in distributing the nonclassicality between the output entanglement and local nonclassicalities. If the phases θ_1 and θ_2 are equal, the incident photon pairs stick (bunch) ideally together due to the interference at the beam splitter and the

incident locally-nonclassical squeezed states are moved into the output ports. No photon pair is broken and so no entanglement is observed. On the other hand, if $\Delta\theta = \pi$, then some incident photon pairs are broken and, thus, the output squeezing (as well as local nonclassicalities) is weaker. The broken photon pairs give rise to the entanglement. The value of EI I_{ent} is maximal for the transmissivity $T = \frac{1}{2}$. In this case, all the photon pairs are broken, their signal and idler photons occur in different output ports and, as a consequence, the ideal conditions for entanglement generation are met. Hand in hand, the vanishing local NIs $I_{\mathrm{ncl}}^{(j)}$ are found (see Fig. 4.9).

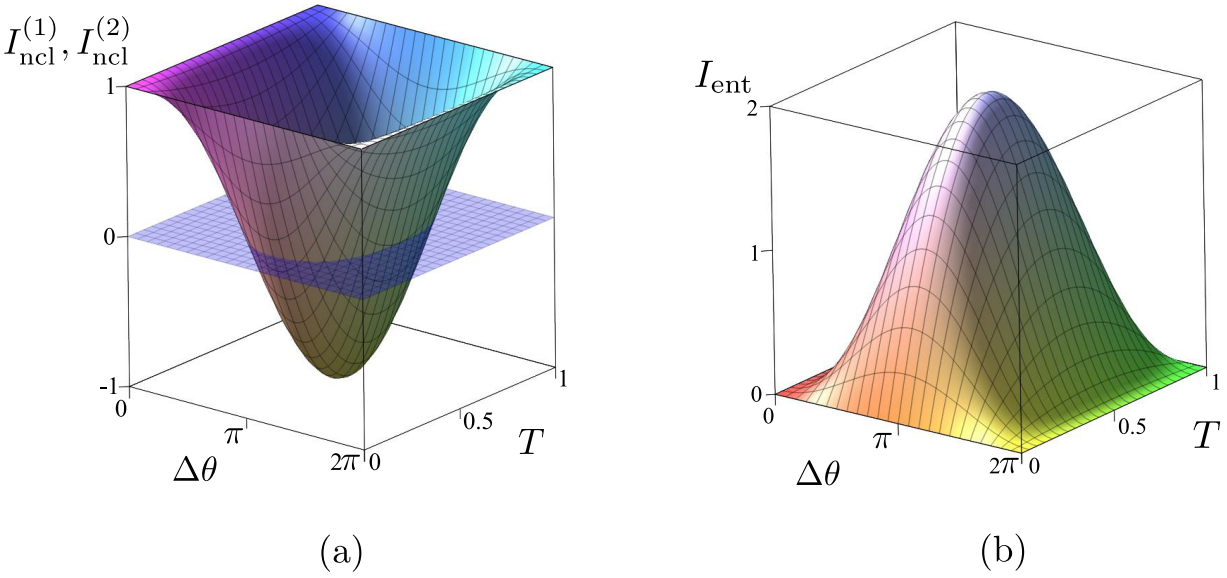

Figure 4.9: (a) Local nonclassicality invariants $I_{\mathrm{ncl}}^{(1)} = I_{\mathrm{ncl}}^{(2)}$ and (b) entanglement invariant I_{ent} versus the phase difference $\Delta\theta$ and beam-splitter transmissivity T for two noiseless squeezed states according to Eq. (4.39); $\tilde{B}_{\mathrm{p}}^{\mathrm{s}} = \tilde{B}_{\mathrm{p}}^{\mathrm{i}} = 1$. In panel (a), the blue surface at $I_{\mathrm{ncl}}^{(1)} = I_{\mathrm{ncl}}^{(2)} = 0$ shows the boundary between classical and nonclassical states.

It is remarkable that the global NI I_{ncl} for the equally intense noiseless squeezed states is given formally by the same formula as that valid for the noiseless twin beams considering the mean photon-pair number B_{p} instead of $\tilde{B}_{\mathrm{p}}^{\mathrm{s}} = \tilde{B}_{\mathrm{p}}^{\mathrm{i}} \equiv \tilde{B}_{\mathrm{p}}$. However, the incident twin beam serves as a source of locally-nonclassical (squeezed) states, whereas the incident squeezed states provide entangled states at the output of the beam splitter. The comparison of graphs in Figs. 4.4(a) and 4.5(a) with those in Figs. 4.10(a) and 4.10(b) reveals that the incident noiseless squeezed states generate entangled states for an arbitrary value of the transmissivity T, but the incident

noiseless twin beams are capable of the generation of the output squeezed states only in a certain interval of the transmissivity T depending on the intensity.

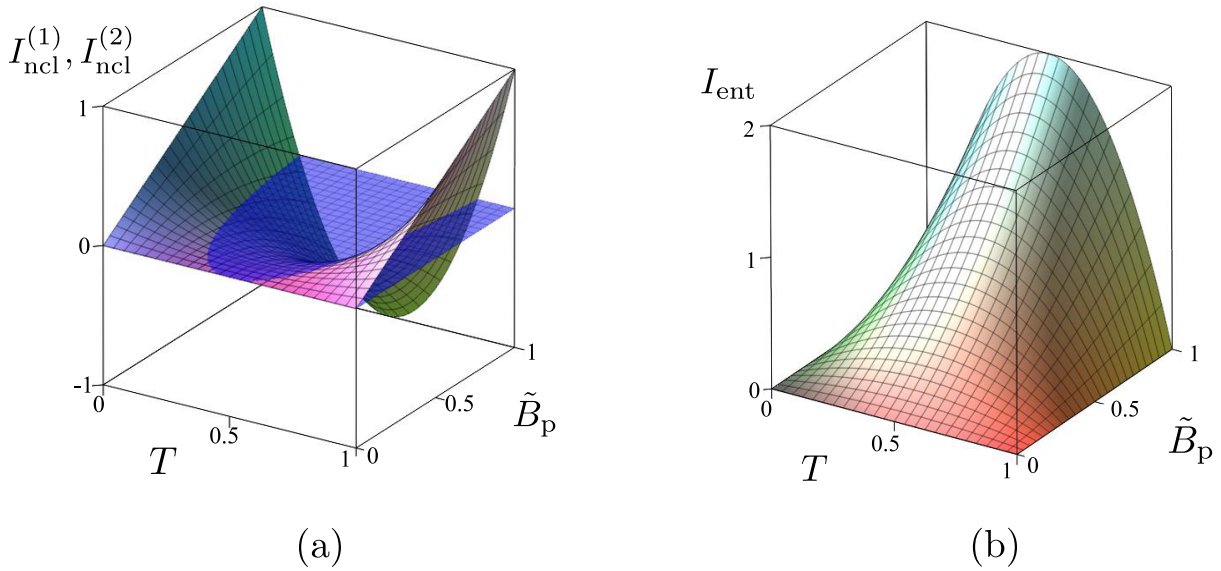

Figure 4.10: (a) Local nonclassicality invariant $I_{\rm ncl}^{(1)}$ and (b) entanglement invariant $I_{\rm ent}$ versus the beam-splitter transmissivity T and mean number $\tilde{B}_{\rm p}$ of squeezed photons for two noiseless squeezed states according to Eq. (4.39); $\tilde{B}_{\rm p} \equiv \tilde{B}_{\rm p}^{\rm s} = \tilde{B}_{\rm p}^{\rm i}$; $\Delta\theta = \pi$. In panel (a) the blue surface at $I_{\rm ncl}^{(1)} = I_{\rm ncl}^{(2)} = 0$ shows the boundary between classical and nonclassical states.

Similarly as for the twin beams, the noise diminishes the global NI $I_{\rm ncl}$ [see the formula for $I_{\rm ncl}$ in Eq. (4.39)]. Considering the incident states with $\tilde{B}_{\rm p}^{\rm s} = \tilde{B}_{\rm p}^{\rm i}$ and $B_{\rm s} = B_{\rm i}$, the presence of noise leads to the occurrence of the three different types of globally nonclassical states already discussed in the connection with the noisy twin beams with symmetric noise. Regions corresponding to different types of the output states are shown in the diagram in Fig. 4.11(a) that can be compared with that of Fig. 4.6(a).

4.6 Twin beam mixed with squeezed states

Finally, we analyze an interplay of noiseless twin beams and equally populated noiseless squeezed states ($\Delta\theta = 0$) in forming the output state at the beam splitter with phase ϕ. Such state is generated by the Hamiltonian (4.1) assuming $g_{11} = g_{22} = g$ and described by the following

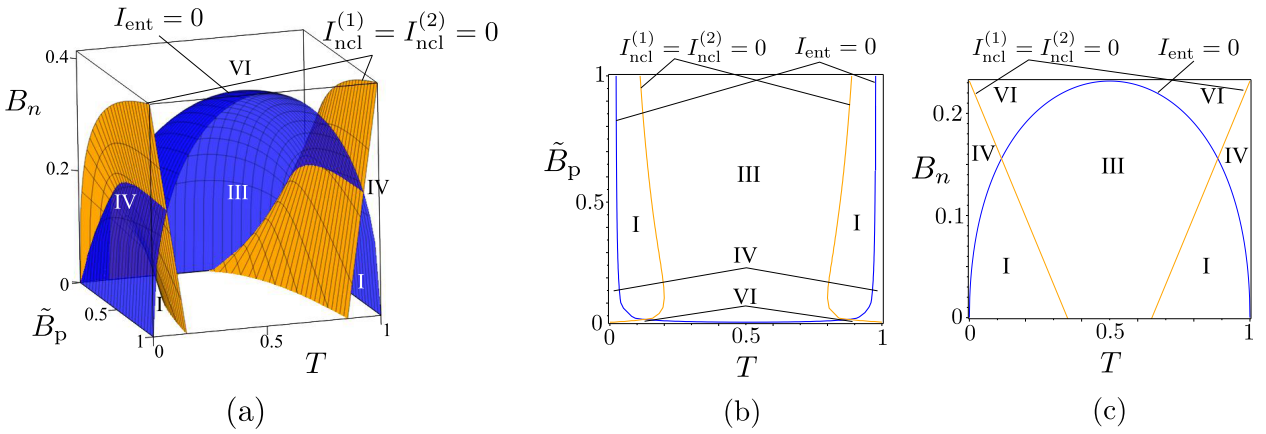

Figure 4.11: Diagram (a) shows the nonclassicality and entanglement invariants for the two squeezed vacua occurring at the output ports of the beam splitter versus the mean noise photon number $B_{\rm n}$, mean number $\tilde{B}_{\rm p}$ of squeezed photons and transmissivity T assuming $B_{\rm n} \equiv B_{\rm s} = B_{\rm i}$ and $\tilde{B}_{\rm p} \equiv \tilde{B}^{\rm s}_{\rm p} = \tilde{B}^{\rm i}_{\rm p}$ and $\Delta\theta = \pi$. Surfaces at $I^{(j)}_{\rm ncl}(B_{\rm n}, \tilde{B}_{\rm p}, T) = 0$ $(j = 1, 2)$ (orange light gray) and $I_{\rm ent}(B_{\rm n}, \tilde{B}_{\rm p}, T) = 0$ (blue dark gray) are shown surrounding different regions specified in Tab. 4.2. Diagrams (b) and (c) show the perpendicular cross-sections of diagram (a) taken at given values of $B_{\rm n} = 0.1$ and $\tilde{B}_{\rm p} = 0.1$, respectively. These cross-sections can be compared with those in panels (b) and (c) in Figs. 4.6 and 4.7.

elements of the evolution matrices $\mathbf{U}$ and $\mathbf{V}$:

$$\begin{aligned} U_{11} &= U_{22} = \cosh(g_{12}t)\cosh(2gt), \\ V_{11} &= V_{22} = i\cosh(g_{12}t)\sinh(2gt), \\ U_{12} &= U_{21} = \sinh(g_{12}t)\sinh(2gt), \\ V_{12} &= V_{21} = i\sinh(g_{12}t)\cosh(2gt). \end{aligned} \tag{4.40}$$

Introducing the mean photon-pair number $B_{\rm p}$ as $B_{\rm p} = \sinh^2(g_{12}t)$ and mean number $\tilde{B}_{\rm p}$ of squeezed photons per mode, $\tilde{B}_{\rm p} = \sinh^2(2gt)$, the coefficients of the covariance matrix $\mathbf{A}_{\mathcal{N}}$ are found in the form:

$$\begin{aligned} B_1 &= B_2 = B_{\rm p} + \tilde{B}_{\rm p} + 2B_{\rm p}\tilde{B}_{\rm p}, \\ C_1 &= C_2 = i\sqrt{\tilde{B}_{\rm p}(\tilde{B}_{\rm p}+1)}(2B_{\rm p}+1), \\ D_{12} &= i\sqrt{B_{\rm p}(B_{\rm p}+1)}(2\tilde{B}_{\rm p}+1), \\ \bar{D}_{12} &= -2\sqrt{B_{\rm p}(B_{\rm p}+1)\tilde{B}_{\rm p}(\tilde{B}_{\rm p}+1)}. \end{aligned} \tag{4.41}$$

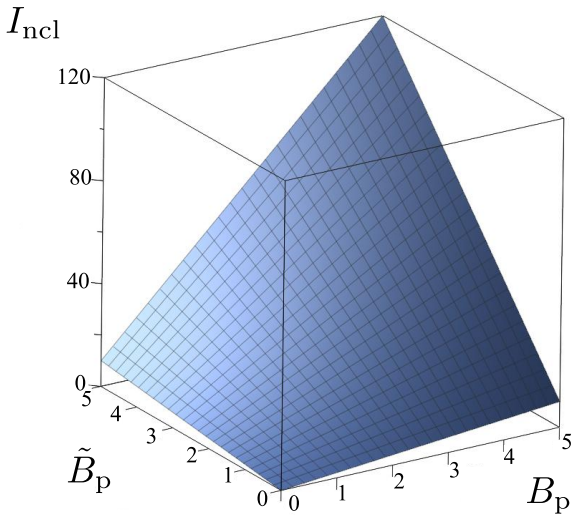

Figure 4.12: Global nonclassicality invariant I_{ncl} as a function of the mean photon-pair number B_{p} and mean number $\tilde{B}_{\mathrm{p}}$ of squeezed photons considering the noiseless twin beams and squeezed states.

The local NIs $I_{\mathrm{ncl}}^{(j)}$, EI I_{ent}, and global NI I_{ncl} are then derived as follows:

$$\begin{aligned} I_{\mathrm{ncl}}^{(1,2)} &= [1-4TR\sin^2(\phi)]\tilde{B}_{\mathrm{p}}(\tilde{B}_{\mathrm{p}}+1)+4TRB_{\mathrm{p}}(B_{\mathrm{p}}+1)-(\tilde{B}_{\mathrm{p}}-B_{\mathrm{p}})^2 \pm K, \\ K &= 4\sqrt{TR}\cos(\phi)\sqrt{B_{\mathrm{p}}(B_{\mathrm{p}}+1)\tilde{B}_{\mathrm{p}}(\tilde{B}_{\mathrm{p}}+1)}, \\ I_{\mathrm{ent}} &= (T-R)^2 B_{\mathrm{p}}(B_{\mathrm{p}}+1)+4TR\sin^2(\phi)\tilde{B}_{\mathrm{p}}(\tilde{B}_{\mathrm{p}}+1), \\ I_{\mathrm{ncl}} &= 2(B_{\mathrm{p}}+\tilde{B}_{\mathrm{p}}+2B_{\mathrm{p}}\tilde{B}_{\mathrm{p}}). \end{aligned} \tag{4.42}$$

The formula for the global NI I_{ncl}, given in Eq. (4.42), shows that both parametric down-conversion and second subharmonic generation contribute to the global NI making I_{ncl} always positive. Moreover, both processes enhance each other in producing larger values of the global NI. The greater is the mean photon-pair number B_{p} and also the greater is the mean number $\tilde{B}_{\mathrm{p}}$ of squeezed photons, the greater is the global NI I_{ncl} (see Fig. 4.12). Additionally, both LNI $I_{\mathrm{ncl}}^{(j)}$ and EI I_{ent} become dependent on the phase ϕ of the beam splitter.

Provided that the phases of the incident squeezed states equal ($\phi = n\pi$, $n \in Z$), photons in pairs stick together (bunch) completely when propagating through the beam splitter and so they cannot contribute to the entanglement in the output state. In this case, the entanglement originates only in photon pairs of the incident twin beam. When $T = 1/2$ all photons in pairs from the twin beam are glued and so the output state is separable. Contrary to this, the

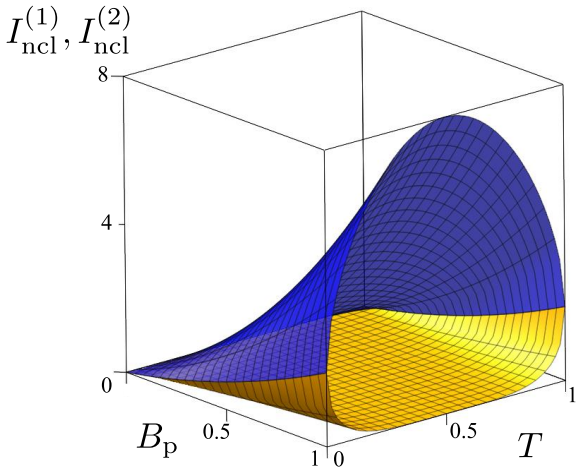

Figure 4.13: Local nonclassicality invariants $I_{\mathrm{ncl}}^{(1)}$ (blue dark upper surface) and $I_{\mathrm{ncl}}^{(2)}$ (orange light coloured lower surface) versus the beam-splitter transmissivity T and mean photon-pair number B_{p} assuming $B_{\mathrm{p}} = \tilde{B}_{\mathrm{p}}$ appropriate for the noiseless twin beams and squeezed states according to Eq. (4.42) assuming $\phi = 0$.

local NIs $I_{\mathrm{ncl}}^{(j)}$ depend on both mean photon-pair number B_{p} and mean number $\tilde{B}_{\mathrm{p}}$ of squeezed photons. The fields characterizing photon pairs in individual output ports and originating in the incident squeezed states and the incident twin beam interfere causing the asymmetry between the output ports. Depending on the parity of n one obtains the maximal local NI $I_{\mathrm{ncl}}^{(1)}$ ($I_{\mathrm{ncl}}^{(2)}$) if $n = 2k$ ($n = 2k + 1$), $k \in \mathbb{Z}$. This asymmetry is the largest for $T = 1/2$. In this case, the bunched photon pairs are completely missing in one output port due to completely destructive interference. On the other hand, constructive interference provides the greatest number of the bunched photon pairs in the other output port guaranteeing the largest attainable value of its local NI $I_{\mathrm{ncl}}^{(j)}$. This behavior is quantified in the graph in Fig. 4.13.

If $\phi = \frac{\pi}{2} + n\pi$, the local NIs are equal ($I_{\mathrm{ncl}}^{(1)} = I_{\mathrm{ncl}}^{(2)}$) and the state at the beam-splitter output ports acquires a symmetry. Under these phase relations, also the incident squeezed photon pairs contribute, together with the twin-beam photon pairs, to the entanglement. It is worth noting that for $B_{\mathrm{p}} = \tilde{B}_{\mathrm{p}}$ all the state quantifiers are the same: $I_{\mathrm{ncl}}^{(1)} = I_{\mathrm{ncl}}^{(2)} = I_{\mathrm{ent}} = B_{\mathrm{p}}(B_{\mathrm{p}} + 1)$.

4.7 Conclusions

Local and global invariants of the general two-mode Gaussian states have been used to construct a specific local nonclassicality quantifier and entanglement quantifier. These quantifiers applied, respectively, to the single-mode marginal states and the whole two-mode state add together to give a quantity that is invariant under global linear unitary transformations. This invariant then quantifies the nonclassicality resources of Gaussian states. Remarkably, this invariant is linearly proportional to the number of photon pairs in the noiseless Gaussian states. The general results have been used to study the beam-splitter transformations of fields composed of photon pairs and additional noisy photons. Twin beams, squeezed states as well as their combinations have been considered as important examples. The behavior of photon pairs at the beam splitter causing their breaking or gluing (i.e., antibinching or bunching) has been used to explain the flow of nonclassical resources between local nonclassicalities (implying squeezing) and entanglement. A complete transfer of the entanglement of incident twin beams into the squeezing of the output modes has been observed. Also the complete transfer of the incident squeezing into the entanglement of the output fields can be reached. The role of noise in the transfer of the nonclassicality invariant via the beam splitter has been elucidated on several examples.

Chapter 5

Experimental detection of nonclassicality of single-mode fields via intensity moments

Text adopted from *I. I. Arkhipov, J. Peřina Jr., O. Haderka and V. Michálek, Opt. Express.* **24**, *29496 (2016)* [A6].

5.1 Introduction

Inequalities containing only moments of intensities are frequently used to reveal the nonclassicality of experimentally investigated states, contrary to those written for amplitude moments. This is natural, as the measurement of amplitude moments requires the homodyne scheme [27] whose complexity of implementation is comparable to the homodyne tomography. On the other hand, intensity moments can be obtained with the usual 'quadratic' optical detectors or, for low intensities, with their modern variants resolving individual photon numbers [96]. In this contribution, we compare the nonclassicality inequalities derived from the matrix approach with those provided by the majorization theory using a set of sub-Poissonian states with increasing mean photon numbers [38]. These states are generated from a twin beam [A1] by postselection

[97, 39] that is based on the detection of a given photocount number in one arm of the twin beam by an intensified charge-coupled-device (iCCD) camera [98]. The iCCD camera is also used to experimentally analyze the sub-Poissonian states with mean photon numbers ranging from 7 to 14.

The chapter is organized as follows. In Sec. 5.2, systematic approach for the derivation of nonclassicality inequalties is given using both the matrix approach and the majorization theory. Inequalities derived in Sec. 5.2 are tested on the experimental data in Sec. 5.3. Sec. 5.4 brings conclusions.

5.2 Derivation of nonclassicality inequalities

For the moments of classical integrated intensity I [28], a general nonnegative quadratic form for the classical field is constructed via the function $g(I)$ that is an arbitrary linear superposition of the terms I^j for $j = 0, 1, \ldots$:

$$g(I) = \sum_{j=0}^{N} g_j I^j, \tag{5.1}$$

and N is an arbitrary integer number giving the number of terms in the sum. The condition $\int_0^\infty dI\, P(I)|g(I)|^2 \geq 0$ for a classical state with non-negative probability function P, when transformed into the operator form written for the powers of photon-number operator $\hat{n}$ ($I^j \propto :\hat{n}^j:$), suggests the following nonclassicality condition [99, 100, 101, 102]:

$$\sum_{j,j'=0}^{N} g_j g_{j'} \langle :\hat{n}^{j+j'}: \rangle < 0; \tag{5.2}$$

symbol : : denotes normal ordering of field operators. Inequality (5.2) can be equivalently expressed as the condition for negativity of a matrix M of dimension $(N+1) \times (N+1)$ with the elements $M_{jj'} = \langle :\hat{n}^{j+j'}: \rangle$. The Hurwitz criterion then guarantees negativity of the matrix M whenever any of its principal minors is negative.

The simplest 2×2 minors of the matrix M written as

$$\det \begin{bmatrix} \langle :\hat{n}^{2k}: \rangle & \langle :\hat{n}^{k+l}: \rangle \\ \langle :\hat{n}^{k+l}: \rangle & \langle :\hat{n}^{2l}: \rangle \end{bmatrix} \tag{5.3}$$

provide the nonclassicality inequalities containing the products of two moments of in general different orders:

$$\langle :\hat{n}^{2k}: \rangle \langle :\hat{n}^{2l}: \rangle < \langle :\hat{n}^{k+l}: \rangle^2, \quad 0 \leq k \leq l. \tag{5.4}$$

The 3×3 minors of matrix M parameterized by integer numbers k, l and m already give more complex nonclassicality inequalities involving in general 6 terms in the sum, each formed by three moments in the product:

$$\det \begin{bmatrix} \langle :\hat{n}^{2k}: \rangle & \langle :\hat{n}^{k+l}: \rangle & \langle :\hat{n}^{k+m}: \rangle \\ \langle :\hat{n}^{k+l}: \rangle & \langle :\hat{n}^{2l}: \rangle & \langle :\hat{n}^{l+m}: \rangle \\ \langle :\hat{n}^{k+m}: \rangle & \langle :\hat{n}^{l+m}: \rangle & \langle :\hat{n}^{2m}: \rangle \end{bmatrix} < 0, \quad 0 \leq k \leq l \leq m. \tag{5.5}$$

The form of nonclassicality inequalities originating in $k \times k$ minors for $k > 3$ is similar to that derived for the 3×3 minors.

On the other hand, the majorization theory [103] gives us the nonclassicality inequalities involving two moments in the product and having the following form [20]:

$$\tilde{R}_{u,v}^{u+m,v-m} \equiv \langle :\hat{n}^{u+m}: \rangle \langle :\hat{n}^{v-m}: \rangle - \langle :\hat{n}^{u}: \rangle \langle :\hat{n}^{v}: \rangle < 0, \quad u \geq v \geq 0,\ v \geq m \geq 0. \tag{5.6}$$

The inequalities written in Eq. (5.4) are a subset of those given in Eq. (5.6) with the mapping $u = v = k + l$ and $m = l - k$.

The following nonclassicality inequalities of the majorization theory represent the counterpart of inequalities in Eq. (5.6) derived from the 3×3 minors:

$$\tilde{R}_{u,v,w}^{u+k+l,v-k+m,w-l-m} \equiv \langle :\hat{n}^{u+k+l}: \rangle \langle :\hat{n}^{v-k+m}: \rangle \langle :\hat{n}^{w-l-m}: \rangle - \langle :\hat{n}^{u}: \rangle \langle :\hat{n}^{v}: \rangle \langle :\hat{n}^{w}: \rangle < 0,$$
$$u \geq v \geq w \geq 0; \qquad k, l, m \geq 0. \tag{5.7}$$

Inequalities in Eq. (5.7) formed by two additive terms differ from those of Eq. (5.5) that contain six additive terms. There does not seem to exist any simple relation between inequalities written in Eqs. (5.7) and (5.5).

In general, the majorization theory provides a larger number of nonclassicality inequalities compared to the matrix approach. Moreover these inequalities attain a simpler form [compare Eqs. (5.5) and (5.7)]. To get a more detailed comparison of the two methods, we write down explicitly the inequalities involving the moments with the overall power up to five, that are useful for the experimental analysis below. The explicit formulas of Eq. (5.6) written in their normalized (dimensionless) form are expressed as follows:

$$\begin{aligned}
R^{2,0}_{1,1} &\equiv \frac{\langle :\hat{n}^2: \rangle}{\langle :\hat{n}: \rangle^2} - 1 < 0, \\
R^{3,0}_{2,1} &\equiv \frac{\langle :\hat{n}^3: \rangle}{\langle :\hat{n}: \rangle^3} - \frac{\langle :\hat{n}^2: \rangle}{\langle :\hat{n}: \rangle^2} < 0, \\
R^{3,1}_{2,2} &\equiv \frac{\langle :\hat{n}^3: \rangle}{\langle :\hat{n}: \rangle^3} - \frac{\langle :\hat{n}^2: \rangle^2}{\langle :\hat{n}: \rangle^4} < 0, \\
R^{4,0}_{2,2} &\equiv \frac{\langle :\hat{n}^4: \rangle}{\langle :\hat{n}: \rangle^4} - \frac{\langle :\hat{n}^2: \rangle^2}{\langle :\hat{n}: \rangle^4} < 0, \\
R^{4,0}_{3,1} &\equiv \frac{\langle :\hat{n}^4: \rangle}{\langle :\hat{n}: \rangle^4} - \frac{\langle :\hat{n}^3: \rangle}{\langle :\hat{n}: \rangle^3} < 0, \\
R^{5,0}_{4,1} &\equiv \frac{\langle :\hat{n}^5: \rangle}{\langle :\hat{n}: \rangle^5} - \frac{\langle :\hat{n}^4: \rangle}{\langle :\hat{n}: \rangle^4} < 0, \\
R^{4,1}_{3,2} &\equiv \frac{\langle :\hat{n}^4: \rangle}{\langle :\hat{n}: \rangle^4} - \frac{\langle :\hat{n}^2: \rangle \langle :\hat{n}^3: \rangle}{\langle :\hat{n}: \rangle^5} < 0, \\
R^{5,0}_{3,2} &\equiv \frac{\langle :\hat{n}^5: \rangle}{\langle :\hat{n}: \rangle^5} - \frac{\langle :\hat{n}^2: \rangle \langle :\hat{n}^3: \rangle}{\langle :\hat{n}: \rangle^5} < 0.
\end{aligned} \tag{5.8}$$

Only the first and the fourth inequalities in Eq. (5.8) stem from the matrix approach providing Eq. (5.4). Similarly, the general formula in Eq. (5.7) leaves us with the following four normalized

inequalities, which cannot be obtained from the matrix approach:

$$\begin{aligned} R^{3,0,0}_{1,1,1} &\equiv \frac{\langle{:}\hat{n}^3{:}\rangle}{\langle{:}\hat{n}{:}\rangle^3} - 1 < 0, \\ R^{4,0,0}_{2,1,1} &\equiv \frac{\langle{:}\hat{n}^4{:}\rangle}{\langle{:}\hat{n}{:}\rangle^4} - \frac{\langle{:}\hat{n}^2{:}\rangle}{\langle{:}\hat{n}{:}\rangle^2} < 0, \\ R^{5,0,0}_{2,2,1} &\equiv \frac{\langle{:}\hat{n}^5{:}\rangle}{\langle{:}\hat{n}{:}\rangle^5} - \frac{\langle{:}\hat{n}^2{:}\rangle^2}{\langle{:}\hat{n}{:}\rangle^4} < 0, \\ R^{5,0,0}_{3,1,1} &\equiv \frac{\langle{:}\hat{n}^5{:}\rangle}{\langle{:}\hat{n}{:}\rangle^5} - \frac{\langle{:}\hat{n}^3{:}\rangle}{\langle{:}\hat{n}{:}\rangle^3} < 0. \end{aligned} \tag{5.9}$$

The majorization theory gives us also inequalities containing four (five) moments in the product, which encompass the following two (one) inequalities useful in our experimental analysis:

$$\begin{aligned} R^{4,0,0,0}_{1,1,1,1} &\equiv \frac{\langle{:}\hat{n}^4{:}\rangle}{\langle{:}\hat{n}{:}\rangle^4} - 1 < 0, \\ R^{5,0,0,0}_{2,1,1,1} &\equiv \frac{\langle{:}\hat{n}^5{:}\rangle}{\langle{:}\hat{n}{:}\rangle^5} - \frac{\langle{:}\hat{n}^2{:}\rangle}{\langle{:}\hat{n}{:}\rangle^2} < 0, \\ R^{5,0,0,0,0}_{1,1,1,1,1} &\equiv \frac{\langle{:}\hat{n}^5{:}\rangle}{\langle{:}\hat{n}{:}\rangle^5} - 1 < 0. \end{aligned} \tag{5.10}$$

The above inequalities can be applied both to photon-number distributions as well as to photocount distributions that are directly measured. Whereas the normally-ordered moments of photon number $\hat{n}$ are suitable for characterizing intensity distributions, the usual moments are immediately derived from the experimental photocount distributions. They are mutually related by the following formula [28]:

$$\langle{:}\hat{n}^k{:}\rangle = \left\langle \frac{\hat{n}!}{(\hat{n}-k)!} \right\rangle . \tag{5.11}$$

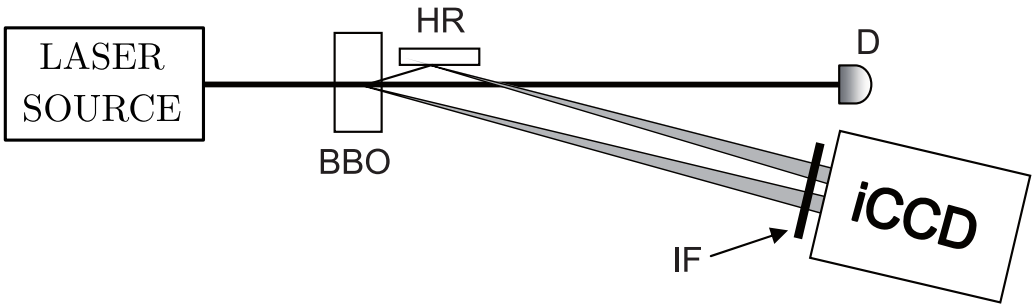

Figure 5.1: Scheme of the experiment generating sub-Poissonian states. A twin beam is generated in noncollinear geometry in a 5-mm-long type-I barium-borate crystal (BaB_2O_4, BBO) pumped by the third harmonics (280 nm) of a femtosecond cavity dumped Ti:sapphire laser (pulse duration 150 fs, central wavelength 840 nm). The signal field as well as the idler field (after reflection on a highly-reflecting mirror HR) are detected by $N_\mathrm{s} = 6528$ and $N_\mathrm{i} = 6784$ pixels of the photocathode of iCCD camera Andor DH3345-18U-63 with dark-count rate $d = 0.04$ ($D_a = d/N_a$, $a = \mathrm{s}, \mathrm{i}$). The nearly-frequency-degenerate signal and idler photons at the wavelength of 560 nm are filtered by a 14-nm-wide bandpass interference filter IF. Intensity of the pump beam that is actively stabilized via a motorized half-wave plate followed by a polarizer is monitored by detector D.

5.3 Experimental testing of nonclassicality inequalities

The above nonclassicality inequalities have been applied to a set of states with different 'degree' of sub-Poissonian photon-number statistics that were generated from a twin beam using postselection based on the detection of a given number c_s of photocounts in the signal field [38]. For an ideal photon-number-resolving detector, detection of a given number c_s of signal photocounts leaves the idler field in the Fock state with c_s photons. For a real photon-number-resolving detector, an idler field with reduced photon-number fluctuations and potentially sub-Poissonian photon-number statistics is obtained. As the mean number of idler photons in a postselected field increases with the increasing signal photocount number c_s, the set of generated states is appealing for testing the power of the nonclassicality inequalities.

In the reported experiment, the twin beam was generated in a nonlinear crystal and both its signal and idler fields were detected by an iCCD camera [73]. Whereas the signal photocounts were used for the postselection process, the histograms of idler photocounts provided the information about the postselected potentially sub-Poissonian idler fields. Experimental details are written in the caption to Fig. 5.1. The experiment was repeated 1.2×10^6 times. The obtained

2D histogram of the signal and idler photocounts was used both to determine the photocount moments occurring in the nonclassicality inequalities and to reconstruct the photon-number distributions of the postselected idler fields by the method of maximum likelihood [104]. In the reconstruction method, the idler-field conditional photon-number distribution $p_{\mathrm{c,i}}(n_{\mathrm{i}}; c_{\mathrm{s}})$ left after detecting c_{s} signal photocounts is reached as a steady state found in the following iteration procedure (with iteration index n) [73]

$$p_{\mathrm{c,i}}^{(n+1)}(n_{\mathrm{i}}; c_{\mathrm{s}}) = p_{\mathrm{c,i}}^{(n)}(n_{\mathrm{i}}; c_{\mathrm{s}}) \sum_{c_{\mathrm{i}}} \frac{f_{\mathrm{i}}(c_{\mathrm{i}}; c_{\mathrm{s}}) T_{\mathrm{i}}(c_{\mathrm{i}}, n_{\mathrm{i}})}{\sum_{n_i'} T_{\mathrm{i}}(c_{\mathrm{i}}, n_{\mathrm{i}}') p_{\mathrm{c,i}}^{(n)}(n_{\mathrm{i}}'; c_{\mathrm{s}})} \tag{5.12}$$

that uses the normalized idler-field 1D photocount histogram $f_{\mathrm{i}}(c_{\mathrm{i}}; c_{\mathrm{s}}) \equiv \frac{f(c_{\mathrm{s}}, c_{\mathrm{i}})}{\sum\limits_{c_{\mathrm{i}}} f(c_{\mathrm{s}}, c_{\mathrm{i}})}$ built from the detections with c_{s} detected signal photocounts and contained in the joint signal-idler photocount histogram $f(c_{\mathrm{s}}, c_{\mathrm{i}})$. In Eq. (5.12), the functions $T(c_{\mathrm{i}}, n_{\mathrm{i}})$ give the probabilities of having c_{i} photocounts when detecting a field with n_{i} photons. The folowing formula was derived for an iCCD camera with N_a active pixels, detection efficiency η_a and dark-count rate per pixel D_a [73]:

$$\begin{aligned} T_a(c_a, n_a) \;=\; & \begin{pmatrix} N_a \\ c_a \end{pmatrix} (1 - D_a)^{N_a} (1 - \eta_a)^{n_a} (-1)^{c_a} \sum_{l=0}^{c_a} \begin{pmatrix} c_a \\ l \end{pmatrix} \frac{(-1)^l}{(1 - D_a)^l} \\ & \times \left(1 + \frac{l}{N_a} \frac{\eta_a}{1 - \eta_a} \right)^{n_a}; \qquad a = \mathrm{s}, \mathrm{i}. \end{aligned} \tag{5.13}$$

The 2D histogram $f(c_{\mathrm{s}}, c_{\mathrm{i}})$ with $\langle c_{\mathrm{s}} \rangle = 2.20$ and $\langle c_{\mathrm{i}} \rangle = 2.18$ signal and idler mean photocounts, respectively, also allowed to reconstruct the whole original twin beam in the form of multimode Gaussian fields composed of the independent multimode paired, signal and idler parts characterized by mean photon(-pair) numbers B_a per mode and numbers M_a of independent modes, $a = \mathrm{p}, \mathrm{s}, \mathrm{i}$ [61]. The photon-nunber distribution $p_{\mathrm{si}}(n_{\mathrm{s}}, n_{\mathrm{i}})$ of the whole twin beam was expressed in the form of a two-fold convolution of three Mandel-Rice photon-number distributions [28] in this case [69, 61, 56]:

$$p_{\mathrm{si}}(n_{\mathrm{s}}, n_{\mathrm{i}}) = \sum_{n=0}^{\min[n_{\mathrm{s}}, n_{\mathrm{i}}]} p(n_{\mathrm{s}} - n; M_{\mathrm{s}}, B_{\mathrm{s}}) p(n_{\mathrm{i}} - n; M_{\mathrm{i}}, B_{\mathrm{i}}) p(n; M_{\mathrm{p}}, B_{\mathrm{p}}); \tag{5.14}$$

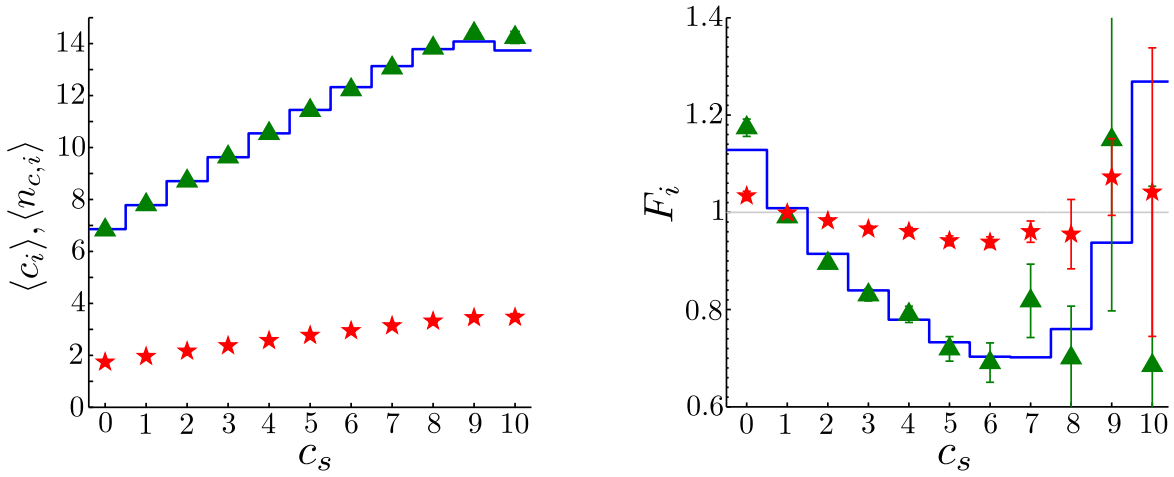

Figure 5.2: (a) Mean idler photocount number $\langle c_\mathrm{i}\rangle$ and photon number $\langle n_\mathrm{c,i}\rangle$ and (b) Fano factor F_i [$F_\mathrm{i} \equiv (\langle \hat{n}_\mathrm{i}^2\rangle - \langle \hat{n}_\mathrm{i}\rangle^2)/\langle \hat{n}_\mathrm{i}\rangle$] as they depend on the signal photocount number c_s. The values appropriate for the distributions of experimental photocounts are plotted with red asterisks whereas those characterizing the reconstructed photon-number distributions arising from the maximum-likelihood method (from the best fit of the twin beam) are plotted with green triangles (blue solid curves). Error bars in (a) are smaller than the used symbols.

$p(n; M, B) = \Gamma(n+M)/[n!\,\Gamma(M)]b^n/(1+B)^{n+M}$ and symbol Γ stands for the Γ-function. This reconstruction revealed the following values of mean photon(-pair) numbers B_a and numbers M_a of modes: $M_\mathrm{p} = 270$, $B_\mathrm{p} = 0.032$, $M_\mathrm{s} = 0.01$, $B_\mathrm{s} = 7.6$, $M_\mathrm{i} = 0.026$, and $B_\mathrm{i} = 5.3$. The method also provided the signal ($\eta_\mathrm{s} = 0.23$) and idler ($\eta_\mathrm{i} = 0.22$) detection efficiencies and the theoretical prediction for the conditional idler-field photon-number distributions $p^\mathrm{t}_\mathrm{c,i}(n_\mathrm{i}; c_\mathrm{s})$ arising in the postselection process with c_s detected signal photounts (for details, see [38]):

$$p^\mathrm{t}_\mathrm{c,i}(n_\mathrm{i}; c_\mathrm{s}) = \frac{\sum_{n_\mathrm{s}} T_\mathrm{s}(c_\mathrm{s}, n_\mathrm{s}) p_\mathrm{si}(n_\mathrm{s}, n_\mathrm{i})}{f^\mathrm{t}_\mathrm{s}(c_\mathrm{s})} \tag{5.15}$$

where $f^\mathrm{t}_\mathrm{s}(c_\mathrm{s}) \equiv \sum_{n_\mathrm{s},n_\mathrm{i}} T_\mathrm{s}(c_\mathrm{s}, n_\mathrm{s}) p_\mathrm{si}(n_\mathrm{s}, n_\mathrm{i})$ is the theoretical prediction for the signal-field photocount distribution.

In the experiment, eleven conditional idler fields generated after detection of a given number c_s of signal photocounts in the range $< 0, 10 >$ were analyzed. Their mean photocount numbers $\langle c_\mathrm{i}\rangle$ and photon numbers $\langle n_\mathrm{c,i}\rangle$ plotted in Fig. 5.2(a) show that the conditional idler fields contained from 7 to 14 photons on average. The corresponding Fano factors F_i determined from the first- and second-order moments and drawn in Fig. 5.2(b) identify, within the experimental

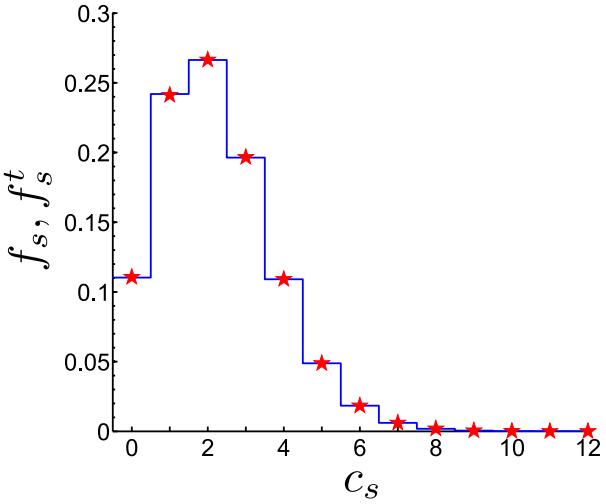

Figure 5.3: Marginal signal-field photocount distribution $f_{\rm s}(c_{\rm s}) = \sum_{c_{\rm i}} f(c_{\rm s}, c_{\rm i})$ (red asterisks) and its theoretical prediction $f^{\rm t}_{\rm s}$ defined below Eq. (5.15) (blue solid curve). Error bars of $f_{\rm s}$ are smaller than the used symbols.

errors, the conditional fields with $c_{\rm s} \in < 2, 7 >$ as sub-Poissonian. They also suggest that the nonclassicality of the conditional idler fields increases as $c_{\rm s}$ increases from 2 to 6, but then the nonclassicality decreases and it is lost for $c_{\rm s} = 9$. This behavior originates in the noise present both in the experimental twin beam and the iCCD camera (that makes the postselection, smaller $c_{\rm s}$) as well as the relatively low detection efficiency of the iCCD camera (greater $c_{\rm s}$) [38].

Fano factors $F_{\rm i}$ for $c_{\rm s} > 4$ plotted in Fig. 5.2(b) are determined with larger errors that increase with the increasing signal photocount number $c_{\rm s}$. This originates in relatively small numbers of measurements appropriate for the mentioned numbers $c_{\rm s}$. Mean numbers of these measurements are described by the signal-field photocount distribution $f_{\rm s}$ plotted in Fig. 5.3. According to this distribution, the probability of detecting the signal photocount numbers $c_{\rm s}$ greater than 7 is less than 1 %. Despite the large number $N = 1.2 \times 10^6$ of experimental repetitions, the determined quantities suffer from relatively large experimental errors in these cases. The experimental errors (for photocounts) are quantified by the mean squared fluctuation σ_x ($\sigma_x = \sqrt{\langle x^2 \rangle - \langle x \rangle^2}$) multiplied by factor $1/\sqrt{N_{\rm r}}$ that depends on the number $N_{\rm r}$ of actual experimental realizations. This approach was also applied to the determination of error bars of the quantities characterizing the photon-number distributions reached by the maximum-likelihood reconstruction. In this method that gives the most-probable photon-number distribution the

experimental errors are naturally smoothed [also due to the form of T_a given in Eq. (5.13) that includes D_a]. We note that the extended approach based on the Fischer information matrix [105] allows to quantify their contribution to the uncertainty characterizing the reconstructed photon-number distribution. The reconstruction based on the best fit of the 2D experimental histogram $f(c_{\rm s}, c_{\rm i})$ exploits the whole ensemble of the measured data with $N = 1.2 \times 10^6$ entries and so the corresponding relative errors are negligible.

The nonclassicality identifiers R belonging to the experimental photocounts and plotted in Fig. 5.4 identify the conditional idler fields with $c_{\rm s} \in < 2, 7 >$ as nonclassical, in agreement with the predictions made by the Fano factors. According to the graphs in Fig. 5.4, nonclassical conditional idler fields can be divided into two groups. The conditional idler fields with $c_{\rm s} \in < 5, 7 >$ have all fifteen nonclassicality identifiers R negative, determined both for photocounts and photon numbers. Such fields can thus be considered as firmly nonclassical. This accords with the lowest attained values of the Fano factor $F_{\rm i}(c_{\rm s})$ shown in Fig. 5.2(b). On the other hand, the conditional idler fields with $c_{\rm s} \in < 2, 4 >$ have negative only the nonclassicality identifiers R of the 'order', given as the sum of their upper (or equivalently lower) indices, lower than four. The nonclassicality identifiers R of 'order' four and five are positive for the experimental photocounts. The maximum-likelihood reconstruction, that relies on the whole 1D experimental histograms, additionally provides negative nonclassicality identifiers R of 'order' four for $c_{\rm s} \in < 3, 4 >$ and five for $c_{\rm s} = 4$. This corresponds to the decreasing values of Fano factor $F_{\rm i}(c_{\rm s})$ drawn in Fig. 5.2(b). Detailed inspection of the graphs in Fig. 5.4 reveals that the behavior of nonclassicality identifiers R reached by the maximum-likelihood reconstruction qualitatively agrees (up to $c_{\rm s} = 7$) with the behavior predicted by the reconstruction based on the best fit of the 2D experimental histogram and quantified by blue solid curves in the graphs of Figs. 5.2 and 5.4.

Compared to the Fano factor $F_{\rm i}$, the nonclassicality identifiers R of 'order' three or higher are endowed with weaker capability to reveal the nonclassicality of the analyzed states obtained by the post-selection method. The greater the 'order' of nonclassicality identifier R the weaker the capability. On the other hand, if the nonclassicality is observed in the nonclassicality identifiers R of higher 'order' it can be considered in certain sense as firm. This is the case of the conditional

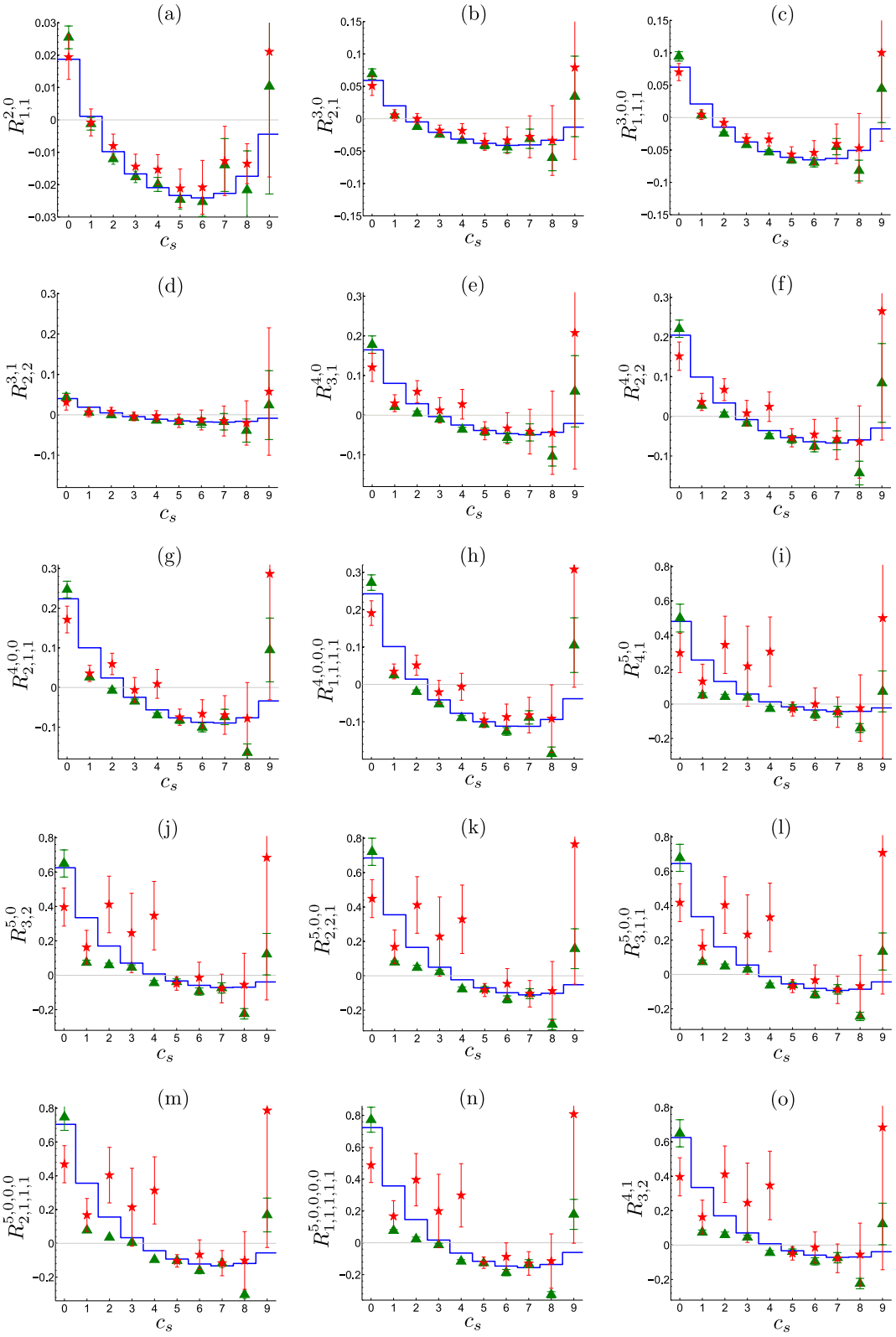

Figure 5.4: Nonclassicality identifiers R given in Eqs. (5.8)—(5.10) and determined for distributions of experimental photocounts (red asterisks with error bars), photon-number distributions reached by the maximum-likelihood reconstruction method (green triangles with error bars) and photon-number distributions derived from the best fit of the twin beam (blue solid curves) as they depend on the signal photocount number c_s. Some error bars are smaller than the plotted symbols.

idler fields obtained after postselecting by the detection of 5, 6 and 7 signal photocounts. These fields, containing on average about 12-14 idler photons, exhibit their nonclassicality in all observed nonclassicality identifiers.

5.4 Conclusions

We have shown that the majorization theory provides a greater number and more suitable nonclassicality identifiers based on intensity moments compared to the commonly used matrix method. Considering the products of moments up to the fifth order, we identified fifteen independent identifiers and tested them on the experimental states with different 'degree' of sub-Poissonian photon-number statistics. Identifiers based on lower intensity moments were identified as more powerful compared to those containing greater intensity moments. The latter ones have been found useful for identifying states being firmly nonclassical.

Chapter 6

Entanglement and nonclassicality in four-mode Gaussian states generated via parametric down-conversion and frequency up-conversion

Text adopted from *I. I. Arkhipov, J. Peřina Jr., O. Haderka, A. Allevi and M. Bondani, Sci. Rep.* **6**, *33802 (2016)* [A5].

6.1 Introduction

In this chapter, we consider a four-mode system composed of two down-converted modes and two up-converted modes. In the system, parametric down-conversion and frequency up-conversion involving both down-converted modes simultaneously occur in the same nonlinear medium [106]. While parametric down-conversion serves as the primary source of entanglement [27], frequency up-conversion is responsible for the transfer of the entanglement to the up-converted modes.

This transfer operation is interesting from the fundamental point of view, as it generalizes the well-known property of 'one-mode' frequency up-conversion pumped by a strong coherent field, in which the statistical properties of the incident field are transferred to the frequency up-converted counterpart, also including the nonclassical ones (e.g., squeezing, [28]). We note that such properties are important for the applications of the up-conversion process: For instance, it has been used many times for 'shifting' an optical 'one-mode' field to an appropriate frequency where its detection could be easily achieved [107, 108].

In the general analysis of the four-mode system, we quantify its global nonclassicality via the Lee nonclassicality depth [22]. Since the four-mode system under consideration cannot exhibit nonclassicality of individual single modes, the global nonclassicality automatically implies the presence of entanglement among the modes (for a two-mode Gaussian system involving parametric down-conversion, see [A2]). The analysis of 'the structure of entanglement' further simplifies by applying the Van Loock and Furusawa inseparability criterion [109] that excludes the presence of genuine three- and four-partite entangled states. This means that in the system discussed here there are only bipartite entangled states. It is thus sufficient to divide the analyzed four-mode state into different bipartitions to monitor the structure of entanglement. Then, the well-known entanglement criterion based on the positive partial transposition of the statistical operator [24, 57], which gives the logarithmic negativity as an entanglement quantifier, is straightforwardly applied [110, 42].

The experimental detection of two-mode (-partite) entanglement is in general quite challenging, as it requires measurements in complementary bases. Here, we theoretically show that, for the considered system with the assumed initial vacuum state, any two-mode partition exhibiting sub-shot-noise intensity correlations is also entangled. As a consequence, the measurement of intensity auto- and cross-correlations in this system is sufficient to give the evidence of the presence of two-mode entangled states through the commonly used noise reduction factor.

Finally, we note that the Hamiltonian of the analyzed four-mode system formally resembles that describing a twin beam with signal and idler fields divided at two beam splitters. This analogy results in similar properties of the four-mode states obtained in the two cases, though

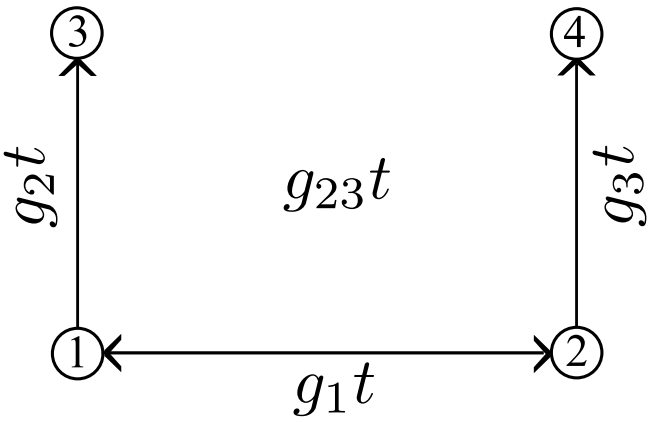

Figure 6.1: Optical fields in modes 1 and 2 interact via parametric down-conversion described by the nonlinear coupling constant g_1. Photons from mode 1 (2) are converted into photons of mode 3 (4) thanks to the frequency up-conversion characterized by the coupling constant g_2 (g_3); t stands for the interaction time. In the symmetric case we have $g_{23} = g_2 = g_3$.

the processes of down-conversion and up-conversion occur simultaneously in our system, at variance with the system with two beam splitters, which modify the already emitted twin beam. We note that the system with two beam splitters has been frequently addressed in the literature as a prototype of more complex devices based on two multiports that are used to have access to intensity correlation functions for the detailed characterization of the measured fields [101], also including their photon-number statistics [111, 68, 112, 73, 113, 114]. The chapter is organized as follows. In Section 6.2 the model of four-mode nonlinear interaction including parametric down-conversion and frequency up-conversion is analyzed. Nonclassicality of the overall system is addressed in Section 6.3. In Section 6.4, the entanglement of the overall system is investigated considering the partitioning of the state into different bipartitions. Two-mode entangled states obtained after state reduction are analyzed in Section 6.5, together with two-mode sub-shot-noise intensity correlations. Suitable parameters of the corresponding experimental setup can be found in Section 6.6. Section 6.7 summarizes the obtained results.

6.2 Four-mode nonlinear interaction

We consider a system of four nonlinearly interacting optical modes (for the scheme, see Fig. 6.1). Photons in modes 1 and 2 are generated by parametric down-conversion with strong pumping (coupling constant g_1). Photons in mode 1 (2) can then be annihilated with the simultaneous

creation of photons in mode 3 (4). The two up-conversion processes are possible thanks to the presence of two additional strong pump fields with coupling constants g_2 and g_3. The overall interaction Hamiltonian for the considered four-mode system is written as [106]:

$$\hat{H}_{\rm int} = \hbar g_1 \hat{a}_1^\dagger \hat{a}_2^\dagger + \hbar g_2 \hat{a}_1 \hat{a}_3^\dagger + \hbar g_3 \hat{a}_2 \hat{a}_4^\dagger + \text{H.c.}, \tag{6.1}$$

where the operators $\hat{a}_1^\dagger$ and $\hat{a}_2^\dagger$ create an entangled photon pair in modes 1 and 2 and the creation operators $\hat{a}_3\dagger$ and $\hat{a}_4^\dagger$ put the up-converted photons into modes 3 and 4, respectively. Symbol H.c. replaces the Hermitian conjugated terms.

The Heisenberg-Langevin equations corresponding to the Hamiltonian $\hat{H}_{\rm int}$ in Eq. (6.1) are written in their matrix form as follows:

$$\frac{d\hat{\mathbf{a}}}{dt} = \mathbf{U}\hat{\mathbf{a}} + \hat{\mathbf{L}}, \tag{6.2}$$

where $\hat{\mathbf{a}} = (\hat{a}_1^\dagger, \hat{a}_2, \hat{a}_3^\dagger, \hat{a}_4)^T$ and $\hat{\mathbf{L}} = (\hat{L}_1^\dagger, \hat{L}_2, \hat{L}_3^\dagger, \hat{L}_2)^T$. The matrix $\mathbf{U}$ introduced in Eq. (6.2) is expressed as

$$\mathbf{U} = \begin{pmatrix} -\gamma_1/2 & -ig_1 & -ig_2 & 0 \\ ig_1 & -\gamma_2/2 & 0 & ig_3 \\ -ig_2 & 0 & -\gamma_3/2 & 0 \\ 0 & ig_3 & 0 & -\gamma_4/2, \end{pmatrix} \tag{6.3}$$

in which γ_j stands for the damping coefficient of mode j, $j = 1, \ldots, 4$. The Langevin operators $\hat{L}_j$, $j = 1, \ldots, 4$, obey the following relations:

$$\begin{aligned} \langle \hat{L}_j(t) \rangle = \langle \hat{L}_j^\dagger(t) \rangle = 0, \quad \langle \hat{L}_j^\dagger(t) \hat{L}_k(t') \rangle = \delta_{jk} \gamma_j \langle n_{dj} \rangle \delta(t - t'), \\ \langle \hat{L}_j(t) \hat{L}_k^\dagger(t') \rangle = \delta_{jk} \gamma_j (\langle n_{dj} \rangle + 1) \delta(t - t'). \end{aligned} \tag{6.4}$$

The Kronecker symbol is denoted as δ_{ij} and the symbol $\delta(t)$ means the Dirac function. The mean numbers n_{dj} corresponding to noise reservoir photons have been used in Eqs. (6.4). We note that for the noiseless system the following quantity $\langle \hat{a}_1^\dagger \hat{a}_1 \rangle + \langle \hat{a}_4^\dagger \hat{a}_4 \rangle - \langle \hat{a}_2^\dagger \hat{a}_2 \rangle - \langle \hat{a}_3^\dagger \hat{a}_3 \rangle$ is conserved in the interaction.

Introducing frequencies ω_j and wave vectors $\vec{k}_j$ of the mutually interacting modes, we formulate the assumed ideal frequency and phase-matching conditions of the considered nonlinear interactions in the form:

$$\begin{aligned} &\omega_{p12} = \omega_1 + \omega_2, \quad \omega_{p13} = \omega_1 + \omega_3, \quad \omega_{p24} = \omega_2 + \omega_4, \\ &\vec{k}_{p12} = \vec{k}_1 + \vec{k}_2, \quad \vec{k}_{p13} = \vec{k}_1 + \vec{k}_3, \quad \vec{k}_{p24} = \vec{k}_2 + \vec{k}_4. \end{aligned} \tag{6.5}$$

In Eqs. (6.5), ω_{p12} ($\vec{k}_{p12}$) stands for the pump-field frequency (wave vector) of parametric down-conversion, whereas ω_{p13} [ω_{p24}] ($\vec{k}_{p13}$ [$\vec{k}_{p24}$]) means the frequency (wave vector) of the field pumping the up-conversion process between modes 1 [2] and 3 [4].

The solution of the system of first-order linear operator stochastic equations (6.2) can be conveniently expressed in the following matrix form:

$$\hat{\mathbf{a}}(t) = \mathbf{M}\hat{\mathbf{a}}(0) + \hat{\mathbf{F}}(t), \tag{6.6}$$

where the evolution matrix $\mathbf{M}$ is written in Eq. (6.18) of Appendix for the noiseless case and vector $\hat{F}$ arises from the presence of the stochastic Langevin forces. More details can be found in Ref. [88]. When applying the solution (6.6), we consider the appropriate phases of the three pump fields such that the coupling constants g_j, $j = 1, 2, 3$, are real.

The statistical properties of the optical fields generated both by parametric down-conversion and up-conversion are described by the normal characteristic function $C_{\mathcal{N}}$ defined as

$$C_{\mathcal{N}}(\boldsymbol{\beta}) = \mathrm{Tr}\left[\hat{\rho}(0)\exp\left(\sum_{i=1}^{4}\beta_i\hat{a}_i^{\dagger}\right)\exp\left(-\sum_{i=1}^{4}\beta_i^{*}\hat{a}_i\right)\right], \tag{6.7}$$

where Tr denotes the trace and $\boldsymbol{\beta} \equiv (\beta_1, \beta_2, \beta_3, \beta_4)^T$. Using the solution given in Eq. (6.6), the normal characteristic function $C_{\mathcal{N}}$ attains the Gaussian form:

$$\begin{aligned} C_{\mathcal{N}}(\boldsymbol{\beta}) = \exp\Big\{ -\sum_{i=1}^{4} B_i|\beta_i|^2 + \Big[& D_{12}^{*}\beta_1\beta_2 + \bar{D}_{13}^{*}\beta_1\beta_3^{*} + D_{14}^{*}\beta_1\beta_4 + D_{23}^{*}\beta_2\beta_3 \\ & + \bar{D}_{24}^{*}\beta_2\beta_4^{*} + D_{34}^{*}\beta_3\beta_4 + \mathrm{c.c.}\Big]\Big\} \end{aligned} \tag{6.8}$$

and c.c. replaces the complex conjugated terms. The coefficients occurring in Eq. (6.8) are derived in the form:

$$\begin{aligned}
B_1 &= \langle \Delta\hat{a}_1^\dagger \Delta\hat{a}_1 \rangle = |M_{12}|^2 + |M_{14}|^2 + \langle \hat{F}_1^\dagger \hat{F}_1 \rangle, \\
B_2 &= \langle \Delta\hat{a}_2^\dagger \Delta\hat{a}_2 \rangle = |M_{21}|^2 + |M_{23}|^2 + \langle \hat{F}_2^\dagger \hat{F}_2 \rangle, \\
B_3 &= \langle \Delta\hat{a}_3^\dagger \Delta\hat{a}_3 \rangle = |M_{32}|^2 + |M_{34}|^2 + \langle \hat{F}_3^\dagger \hat{F}_3 \rangle, \\
B_4 &= \langle \Delta\hat{a}_4^\dagger \Delta\hat{a}_4 \rangle = |M_{41}|^2 + |M_{43}|^2 + \langle \hat{F}_4^\dagger \hat{F}_4 \rangle, \\
D_{12} &= \langle \Delta\hat{a}_1 \Delta\hat{a}_2 \rangle = M_{11}^* M_{21} + M_{13}^* M_{23} + \langle \hat{F}_1 \hat{F}_2 \rangle, \\
\bar{D}_{13} &= -\langle \Delta\hat{a}_1^\dagger \Delta\hat{a}_3 \rangle = -M_{11}^* M_{31} - M_{13}^* M_{33} - \langle \hat{F}_1^\dagger \hat{F}_3 \rangle, \\
D_{14} &= \langle \Delta\hat{a}_1 \Delta\hat{a}_4 \rangle = M_{11}^* M_{41} + M_{13}^* M_{43} + \langle \hat{F}_1 \hat{F}_4 \rangle, \\
D_{23} &= \langle \Delta\hat{a}_2 \Delta\hat{a}_3 \rangle = M_{32}^* M_{22} + M_{34}^* M_{24} + \langle \hat{F}_2 \hat{F}_3 \rangle, \\
\bar{D}_{24} &= -\langle \Delta\hat{a}_2^\dagger \Delta\hat{a}_4 \rangle = -M_{42}^* M_{22} - M_{44}^* M_{24} - \langle \hat{F}_2^\dagger \hat{F}_4 \rangle, \\
D_{34} &= \langle \Delta\hat{a}_3 \Delta\hat{a}_4 \rangle = M_{31}^* M_{41} + M_{33}^* M_{43} + \langle \hat{F}_1 \hat{F}_4 \rangle.
\end{aligned} \tag{6.9}$$

We note that the two-mode interactions characterized by the coefficients D_{ij} and $\bar{D}_{ij}$ in Eq. (6.8) attain specific forms. While the coefficients D_{ij} reflect the presence of photon pairs in modes i and j, coefficients $\bar{D}_{ij}$ describe mutual transfer of individual photons between modes i and j.

The normal characteristic function $C_{\mathcal{N}}$ can be rewritten in the matrix form $\exp(\boldsymbol{\beta}^\dagger \mathbf{A} \boldsymbol{\beta}/2)$ by introducing the normally-ordered covariance matrix $\mathbf{A}$:

$$\mathbf{A} = \begin{pmatrix} \mathbf{A}_1 & \mathbf{D}_{12} & \mathbf{D}_{13} & \mathbf{D}_{14} \\ \mathbf{D}_{12}^\dagger & \mathbf{A}_2 & \mathbf{D}_{23} & \mathbf{D}_{24} \\ \mathbf{D}_{13}^\dagger & \mathbf{D}_{23}^\dagger & \mathbf{A}_3 & \mathbf{D}_{34} \\ \mathbf{D}_{14}^\dagger & \mathbf{D}_{24}^\dagger & \mathbf{D}_{34}^\dagger & \mathbf{A}_4 \end{pmatrix}, \tag{6.10}$$

where the 2×2 matrices are defined as:

$$\mathbf{A}_i = \begin{pmatrix} -B_i & 0 \\ 0 & -B_i \end{pmatrix}, \quad \mathbf{D}_{jk} = \begin{pmatrix} \bar{D}_{jk}^* & D_{jk} \\ D_{jk}^* & \bar{D}_{jk} \end{pmatrix}, \quad i,j,k = 1,\ldots,4. \tag{6.11}$$

The covariance matrix $\boldsymbol{\sigma}$ related to the symmetric ordering and corresponding to the phase space $(\hat{x}, \hat{p})$ is needed to perform easily partial transposition. It has the same structure as the covariance matrix $\mathbf{A}$ written in Eq. (6.10) with the blocks $\mathbf{A}_i$ ($\mathbf{D}_{jk}$) replaced by the blocks $\boldsymbol{\sigma_i}$ ($\boldsymbol{\varepsilon_{jk}}$) defined as:

$$\boldsymbol{\sigma_i} = \begin{pmatrix} B_i + \frac{1}{2} & 0 \\ 0 & B_i + \frac{1}{2} \end{pmatrix}, \quad \boldsymbol{\varepsilon_{jk}} = \begin{pmatrix} \mathrm{Re}(D_{jk} - \bar{D}_{jk}) & \mathrm{Im}(D_{jk} - \bar{D}_{jk}) \\ \mathrm{Im}(D_{jk} + \bar{D}_{jk}) & -\mathrm{Re}(D_{jk} + \bar{D}_{jk}) \end{pmatrix}, \quad i, j, k = 1, \ldots, 4. \tag{6.12}$$

Symbol Re (Im) denotes the real (imaginary) part of the argument.

In what follows, we consider the situation in which all four modes begin their interaction in the vacuum state. Moreover, we focus on the specific symmetric case in which $g_2 = g_3 \equiv g_{23}$. A note concerning the general case $g_2 \neq g_3$ is found at the end.

6.3 Nonclassicality

We first analyze the global nonclassicality of the whole four-mode system as it is relatively easy and, for the considered initial vacuum state, it implies entanglement (see below). Nonclassicality of the whole four-mode state described by the statistical operator $\hat{\rho}$ is conveniently quantified by the Lee nonclassicality depth τ [22]. This quantity gives the amount of noise, expressed in photon numbers, needed to conceal nonclassical properties exhibited by the Glauber-Sudarshan P function, which attains negative values in certain regions or even does not exist as an ordinary function. The Glauber-Sudarshan P function is determined by the Fourier transform of the normally-ordered characteristic function $C_{\mathcal{N}}$ given in Eq. (6.8). Technically, the Lee nonclassicality depth is given by the largest positive eigenvalue of the covariance matrix $\mathbf{A}$ defined in Eq. (6.10). So, it can be easily determined.

The Lee nonclassicality depth τ as a function of the coupling parameters $g_1 t$ and $g_{23} t$ is shown in Fig. 6.2. The increasing values of $g_1 t$ result in larger values of the nonclassicality depth τ, as the number of photons simultaneously generated in modes 1 and 2 increases. We note

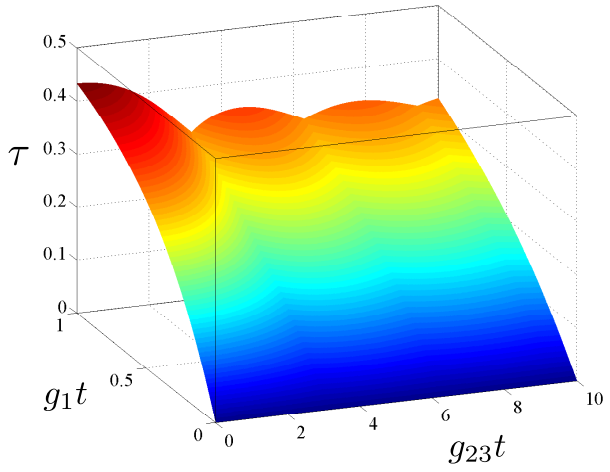

Figure 6.2: Nonclassicality depth τ as a function of the parameters $g_1 t$ and $g_{23} t$.

that this pairing of photons in the process of parametric down-conversion is the only source of nonclassicality in the analyzed four-mode system. On the contrary, nonzero values of parameter $g_{23}t$ only lead to the oscillations of the nonclassicality depth τ. This behavior occurs as the frequency up-conversion moves photons, and so also photon pairs, from modes 1 and 2 to modes 3 and 4 and vice versa (see the scheme in Fig. 6.1). This results in the nonclassical properties of modes 3 and 4, at the expenses of the nonclassical properties of modes 1 and 2.

The maximum value of the Lee nonclassicality depth $\tau = 0.5$ is reached for $g_{23}t = 0$ and ideally in the limit $g_1 t \to \infty$, i.e. when only the strong parametric down-conversion occurs. This is in agreement with the analysis of nonclassical properties of twin beams reported in Ref. [A1]. The value $\tau = 0.5$ can also be asymptotically reached in the limit $g_{23}t \to \infty$, in which we have

$$\tau_{g_{23}t\to\infty} = \frac{1}{2}\left[\sqrt{(B_1 - B_2)^2 + 4|D_{12}|^2} - (B_1 + B_2)\right] \tag{6.13}$$

with $B_3 \to B_1$, $B_4 \to B_2$ and $D_{34} \to D_{12}$. It is worth noting that formula (6.13) applies also for $g_{23}t = 0$. Nonclassicality is also strongly resistant against damping in the system. This means that even a low number of photon pairs is sufficient to have a nonclassical state. We demonstrate this resistance by considering the damping constants γ proportional to the nonlinear coupling constant g_1, which quantifies the speed of photon-pair generation. The graphs in Fig. 6.3 show that the generated states remain strongly nonclassical even though a considerable fraction of

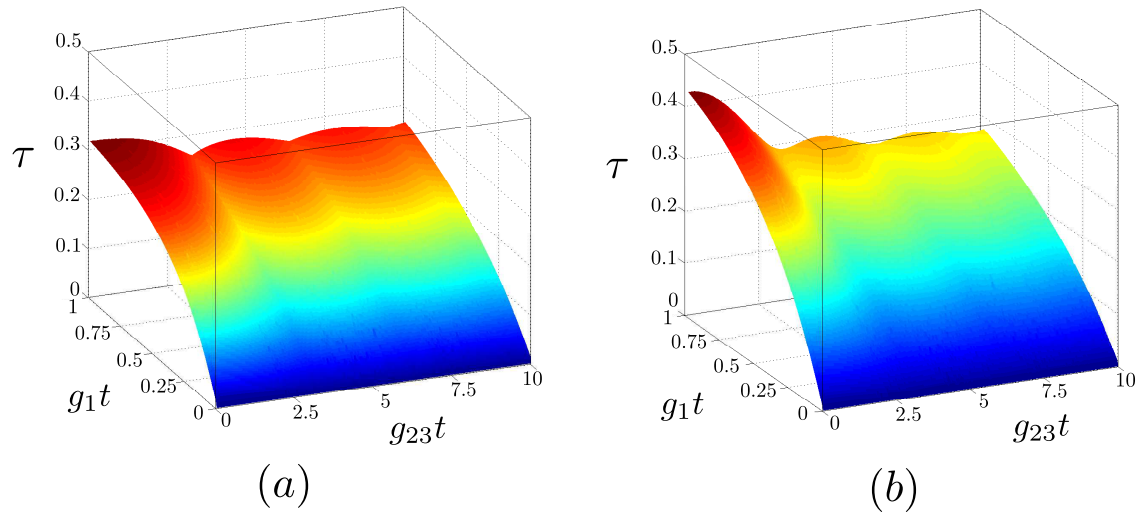

Figure 6.3: Nonclassicality depth τ as a function of the parameters g_1t and $g_{23}t$ for (a) $\gamma_1t = \gamma_2t = g_1t$, $\gamma_3t = \gamma_4t = 0$; (b) $\gamma_1t = \gamma_2t = 0$, $\gamma_3t = \gamma_4t = g_1t$, assuming $n_{dj} = 0$ for $j = 1, \ldots, 4$.

photon pairs is broken under these conditions. The comparison of graphs in Figs. 6.3(a) and (b) reveals that the damping is more detrimental in the down-converted modes 1 and 2 than in the up-converted modes 3 and 4.

At variance with nonclassicality, the determination and quantification of entanglement is more complex and it is technically accomplished by considering all possible bipartitions of the four-mode system (see the next Section). On the one side all bipartitions considered below are in principle sufficient to indicate entanglement, on the other side the application of the Van Loock and Furusawa inseparability criterion [109] to our system excludes the presence of genuine three- and four-mode entanglement. The analyzed Hamiltonian written in Eq. (6.1) together with the incident vacuum state also excludes the presence of nonclassical states in individual modes. In what follows, the bipartite entanglement is thus the only source of the global nonclassicality in the analyzed system. This situation considerably simplifies the possible experimental investigations as positive values of the Lee nonclassicality depth directly imply the presence of entanglement somewhere in the system.

6.4 Four-mode entanglement

In quantifying the entanglement in our four-mode Gaussian system, we rely on the following facts applicable to an arbitrary $(m+n)$-mode Gaussian state. It has been proven that positivity of the partially transposed (PPT) statistical operator describing any 2×2 or 2×3 bipartition of the state is a necessary condition for the separability of the state [24, 57]. Moreover, it has been shown that the violation of PPT condition occurring in any $1\times(m+n-1)$ bipartitions or $m\times n$ bisymmetric bipartitions for $m > 2$ and $n > 3$ is a sufficient condition for the entanglement in the analyzed $(m + n)$-mode state [90, 115]. For continuous variables systems, the PPT is simply accomplished when the symmetrically-ordered field operators are considered allowing to perform the PPT only by changing the signs of the momenta $\hat{p}$ [90]. Moreover, symplectic eiganvalues $\tilde{n}_i$ of the symmetrically-ordered covariance matrix $\boldsymbol{\sigma}$ can be conveniently used to quantify entanglement in bipartite systems via the logarithmic negativity E [42], defined in terms of eigenvalues $\tilde{n}_i < 1/2$:

$$E = \max\left\{0, -\sum_i \log(2\tilde{n}_i)\right\}, \tag{6.14}$$

where max gives the maximal value.

In the four-mode Gaussian state sketched in Fig. 6.1, we have two kinds of bipartitions. Either a single mode forms one subsystem and the remaining three modes belong to the other subsystem, or two modes are in one subsystem and the remaining two modes lie in the other subsystem. Due to the symmetry, only two members of each group are of interest for us. Namely, these are bipartitions 1×234 and 3×124 from the first group and bipartitions 12×34 and 13×24 from the second one. We note that, while the bipartition 12×34 is bisymmetric in our interaction configuration (provided that $g_2t = g_3t$), the bipartition 13×24 is not bisymmetric. Nevertheless, positive values of both the logarithmic negativities $E_{12\times34}$ and $E_{13\times24}$ reflect entanglement as both bipartitions involve two modes on both sides. Similarly, positive values of the logarithmic negativities $E_{1\times234}$ and $E_{3\times124}$ guarantee the presence of entanglement.

We first pay attention to the entanglement expressed in the logarithmic negativities $E_{1\times234}$ and

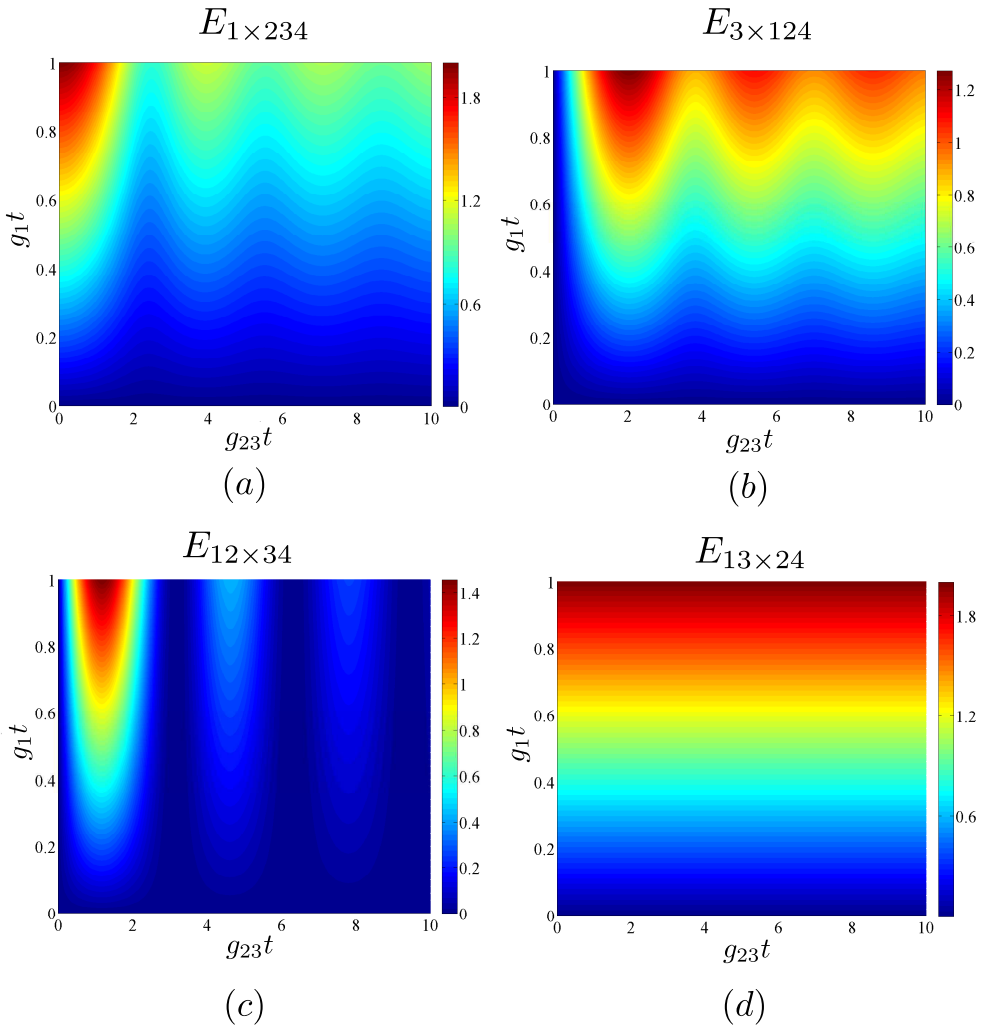

Figure 6.4: Logarithmic negativities $E_{1\times234}$ (a), $E_{3\times124}$ (b), $E_{12\times34}$ (c), and $E_{13\times24}$ (d) as functions of parameters g_1t and $g_{23}t$ for different bipartitions indicated in the subscripts.

$E_{3\times124}$. As suggested by the graphs in Figs. 6.4(a) and (b), the oscillating behavior of negativity $E_{1\times234}$ is complementary to that of negativity $E_{3\times124}$. This means that the larger values of negativity $E_{1\times234}$ are accompanied by the lower values of negativity $E_{3\times124}$ and vice versa. Such a result is a consequence of the fact that the entanglement is due to the presence of photon pairs and a photon created in mode 1 can move to mode 3 and later return back to mode 1. This movement leads to the oscillations with frequency g_{23}, which are clearly visible in Figs. 6.4(a) and (b). This explanation also suggests that no entanglement is possible between modes 1 and 3. Indeed, if we also determine the negativity $E_{1\times24}$ (or $E_{3\times24}$), we will get the same values already obtained for the negativity $E_{1\times234}$ ($E_{3\times124}$). The negativity $E_{12\times34}$, characterizing the entanglement between the twin beam in modes 1 and 2 and the up-converted beams in modes 3 and 4, is plotted in Fig. 6.4(c). It reflects the gradual movement of photon pairs from

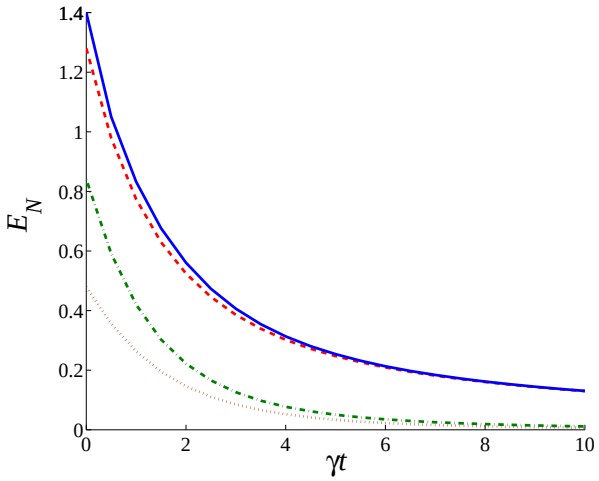

Figure 6.5: Logarithmic negativity E as a function of the damping coefficient γt for different bipartitions: 1×234 (dashed red line), 3×124 (brown dotted line), 12×34 (dashed-dotted green line), and 13×24 (solid blue line). We set $g_1 t = g_2 t = g_3 t = 0.7$, $\gamma \equiv \gamma_1 = \gamma_2 = \gamma_3 = \gamma_4$; $n_{dj} = 0$ for $j = 1, \ldots, 4$.

modes 1 and 2, where they are created, to modes 3 and 4. Note that the maxima of negativity $E_{12\times34}$ along the $g_{23}t$-axis occur inbetween the maxima of negativities $E_{1\times234}$ and $E_{3\times124}$. The origin of entanglement in photon pairing is confirmed in the graph of Fig. 6.4(d), showing that the negativity $E_{13\times24}$ is independent of parameter $g_{23}t$ and that the negativity $E_{13\times24}$ increases with the increasing parameter $g_1 t$. In certain sense, the independence of negativity $E_{13\times24}$ from parameter $g_{23}t$ represents the conservation law for nonclassical resources, as the negativities of the different two-mode reductions derived from this bipartition ($E_{1\times2}$, $E_{1\times4}$, $E_{3\times2}$, and $E_{3\times4}$) do depend on parameter $g_{23}t$.

The developed model also allows us to study the role of damping in the entanglement creation. The investigations based on equal damping constants γ and noiseless reservoirs ($n_d = 0$) just reveal the deterioration of entanglement in all the considered bipartitions with the increase of damping constants (see Fig. 6.5).

6.5 Two-mode entanglement and noise reduction factor

The results of the theoretical analysis suggest that, from the experimental point of view, the observation of entanglement between pairs of modes is substantial for the characterization of

the emitted entangled states. Formally, the theory describes such observations through the reduced two-mode statistical operators. The analysis shows that the behavior of two-mode negativities $E_{1\times2}$, $E_{3\times4}$, and $E_{1\times4}$ with respect to parameters g_1t and $g_{23}t$ is qualitatively similar to that of four-mode negativities $E_{1\times234}$, $E_{3\times124}$, and $E_{12\times34}$ plotted in Figs. 6.4(a), (b) and (c). This similarity originates in possible 'trajectories' of photon pairs born in modes 1 and 2 and responsible for the entanglement.

Additional insight into the generation of entanglement in the analyzed system is provided when the entanglement is related to the intensities of the interacting fields. As quantified in the graphs of Fig. 6.6, both mean photon numbers $B_1 \equiv B_2$ and $B_3 \equiv B_4$ are increasing functions of parameter g_1t and oscillating functions of parameter $g_{23}t$. This oscillating behavior is particularly interesting, as it reflects the flow of photons from modes 1 and 2 to modes 3 and 4, respectively, and vice versa. As we will see below, this is in agreement with the 'flow of the entanglement' among the modes.

The graph in Fig. 6.7(a) shows that the negativity $E_{1\times2}$ is on the one side an increasing function of the mean photon number B_1, on the other side it only weakly depends on the mean photon number B_3. This confirms that pairing of photons in parametric down-conversion is the only resource for entanglement creation. On the contrary, as shown in Fig. 6.7(b), the negativity $E_{3\times4}$ is an increasing function of the mean photon number B_3, whereas it weakly depends on the mean photon number B_1. This indicates that the entanglement in modes 34 comes from modes 12 through the transfer of photon pairs: The stronger the transfer is, the larger the value of negativity $E_{3\times4}$ is. Moreover, optimal conditions for the observation of entanglement in modes 1 and 4 occur provided that there is the largest available number of photon pairs with one photon in mode 1 and its twin in mode 4. According to the graph in Fig. 6.7(c) this occurs when the mean photon numbers B_4 ($B_4 \equiv B_3$) and B_1 are balanced, independently of their absolute values. In general, the experimental identification of two-mode entanglement is not easy, as it requires the simultaneous measurement of the entangled state in two complementary bases. Alternatively, entanglement can be inferred from the reconstructed two-mode phase-space quasi-distribution, which needs two simultaneous homodyne detectors [35], each one endowed with a local oscillator. However, the detection of entanglement, at least

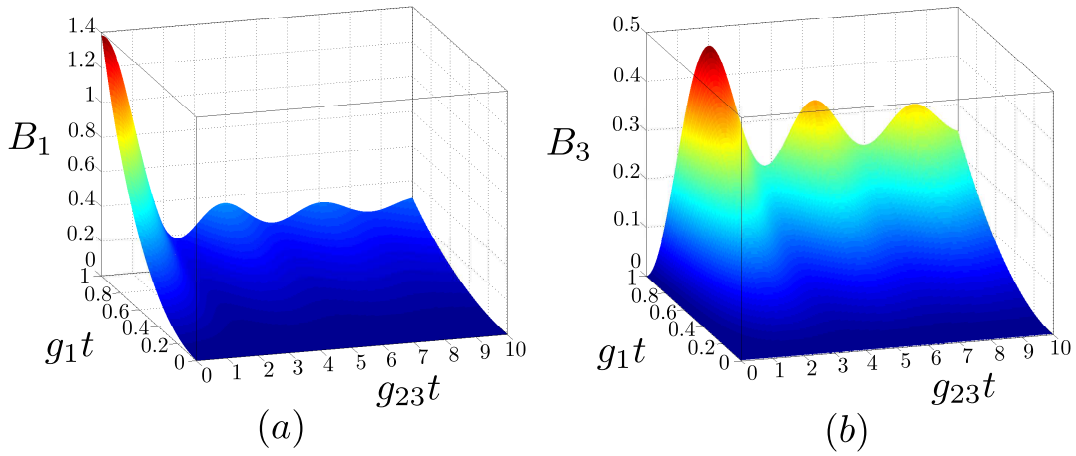

Figure 6.6: Mean photon numbers B_1 (a) and B_3 (b) plotted as functions of parameters g_1t and $g_{23}t$.

in some cases, can be experimentally accomplished by the observation of sub-shot-noise intensity correlations. This is a consequence of the detailed numerical analysis, which reveals that the majority of the reduced two-mode entangled states also exhibits sub-shot-noise intensity correlations. Nevertheless, it should be emphasized here that, in the analyzed system, there are also two-mode entangled states not exhibiting sub-shot-noise intensity correlations. On the contrary, we note that the reduced two-mode separable states do not naturally exhibit sub-shot-noise intensity correlations.

Sub-shot-noise intensity correlations are quantified by the noise reduction factor R [43, 45], that is routinely measured to recognize nonclassical intensity correlations of two optical fields. The noise reduction factor R expressed in the moments of photon numbers n_j and n_k of modes j and k, respectively, is defined by the formula:

$$R_{jk} = \frac{\langle \triangle (n_j - n_k)^2 \rangle}{\langle n_j \rangle + \langle n_k \rangle}. \tag{6.15}$$

Sub-shot-noise intensity correlations are described by the condition $R < 1$. We note that there exists the whole hierarchy of inequalities involving higher-order moments of photon numbers (or intensities) [101, 116, 102, 114] that indicate nonclassicality and, in our system, also entanglement. We mention here the inequality derived by Lee [20] as a practical example that is sometimes used in the experimental identification of nonclassicality. We note that this criterion

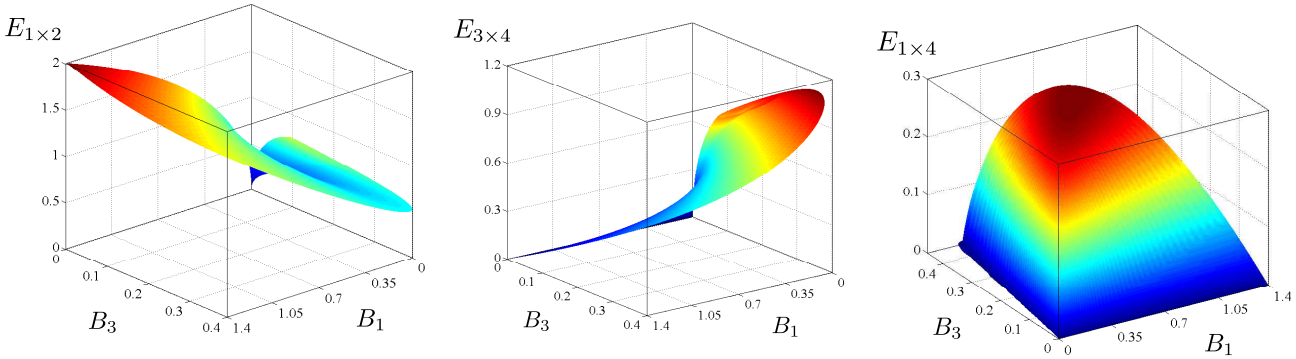

Figure 6.7: Logarithmic negativities $E_{1\times2}$ (a), $E_{3\times4}$ (b) and $E_{1\times4}$ (c) as functions of the mean photon numbers B_1 and B_3.

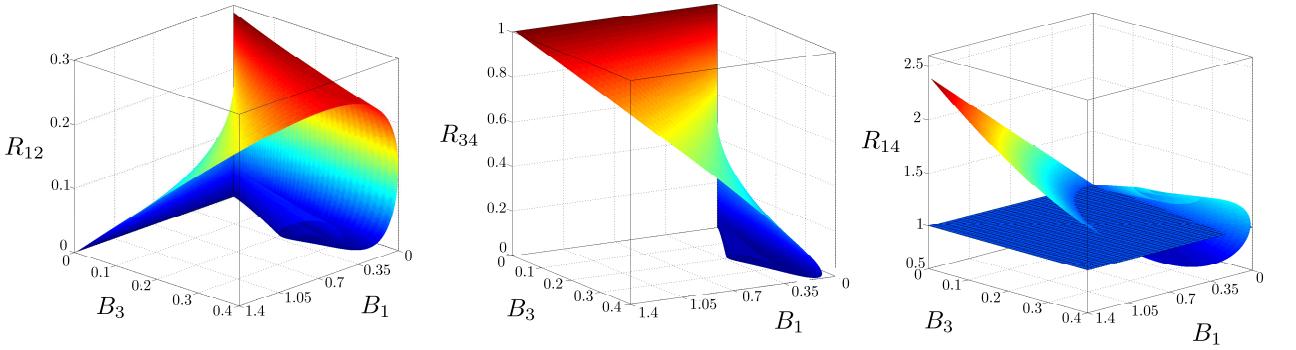

Figure 6.8: Noise reduction factors $R_{1\times2}$ (a), $R_{3\times4}$ (b) and $R_{1\times4}$ (c) as functions of the mean photon numbers B_1 and B_3. In (c), the plane defined as $R_{1\times4} = 1$ is represented by the blue mesh.

is stronger than the noise reduction factor R in revealing the nonclassicality [43]. The noise reduction factors $R_{1\times2}$, $R_{3\times4}$ and $R_{1\times4}$ describing the reduced two-mode fields with their negativities plotted in Fig. 6.7 are drawn in Fig. 6.8 for comparison. We can see complementary behavior of the negativities E and noise reduction factors R in the graphs in Figs. 6.7 and 6.8. An increase of the negativity E is accompanied by a decrease in the noise reduction factor R. A closer inspection of the curves in these graphs shows that the condition $R < 1$ identifies very well entangled states when the noise reduction factor is measured in modes 1×2 and 3×4. Nevertheless, there are entangled states with $R_{1\times4} > 1$, as shown in the graph of Fig. 6.9, in which the values of parameters $g_1 t$ and $g_{23} t$ appropriate for this situation occur in the areas I and III. On the other hand, the entangled states found in the area II in the graph of Fig. 6.9 have $R < 1$. It is worth noting that the relative amount of entangled states not detected via

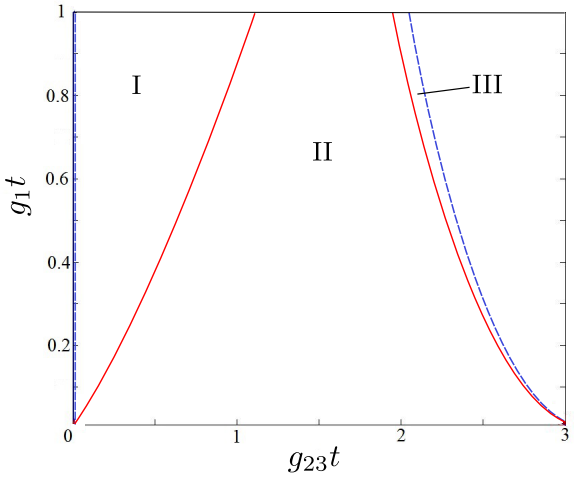

Figure 6.9: Solutions of the equations for logarithmic negativity $E_{1\times4} = 0$ (blue dashed line) and noise reduction factor $R_{1\times4} = 1$ (red solid line) in the plane spanned by parameters g_1t and $g_{23}t$. The two-mode field is entangled ($E_{1\times4} > 0$) inbetween the blue dashed lines, i.e. in the areas I, II, and III, whereas it is sub-shot-noise ($R_{1\times4} < 1$) inbetween the red solid lines, i.e. in the area II.

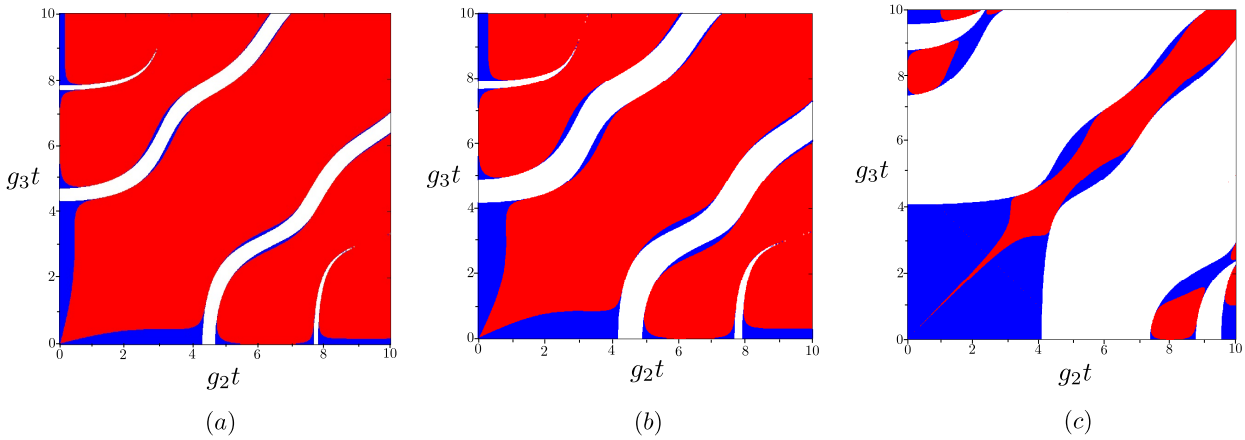

Figure 6.10: Planes given by $g_1t = 0.5$ (a), $g_1t = 1$ (b) and $g_1t = 5$ (c) in the 'phase diagram' identifying classical states (white areas), entangled states without sub-shot-noise intensity correlations (blue) and entangled states with sub-shot-noise intensity correlations (red) in the space spanned by the coupling constants g_jt, $j = 1, 2, 3$.

$R < 1$ increases with the increasing coupling constant g_1t and so with the increasing overall number of photons in the system. The observed relation between the entangled states and those exhibiting sub-shot-noise intensity correlations can even be explained theoretically, due to the specific form of the reduced two-mode Gaussian states analyzed in Ref. [A1]. According to Ref. [A1] entangled states in modes i and j are identified through the inequality $B_iB_j < |D_{ij}|^2$. On the other hand, the noise reduction factor R_{ij} defined in Eq. (6.15) attains for our modes

the form:

$$R_{ij} = 1 + \frac{B_i^2 + B_j^2 - 2|D_{ij}|^2}{B_i + B_j} \tag{6.16}$$

that assigns the sub-shot-noise intensity correlations to the states obeying the inequality $B_i^2 + B_j^2 < 2|D_{ij}|^2$. Thus, the inequality $B_i^2 + B_j^2 \geq 2B_iB_j$ implies that the states with sub-shot-noise intensity correlations form a subset in the set of all entangled states. Moreover, if $B_i = B_j$, both sets coincide as we have $B_i^2 + B_j^2 = 2B_iB_j$. Thus, the noise reduction factors R_{12} and R_{34} are reliable in identifying entangled states in the symmetric case, in which $B_1 = B_2$ and $B_3 = B_4$.

We note that, according to the theory developed for the modes without an additional internal structure [A1], the logarithmic negativity E_{ij} can be determined along the formula [A1]

$$E_{ij} = \max\left\{0, -\log\left(1 + B_i + B_j - \sqrt{(B_i - B_j)^2 + 4|D_{ij}|^2}\right)\right\}, \tag{6.17}$$

where $|D_{ij}|^2 = \langle \Delta n_i \Delta n_j \rangle$. According to Eq. (6.17) the logarithmic negativity E_{ij} can, in principle, be inferred from the measured mean intensities in modes i and j and the cross-correlation function of intensity fluctuations in this idealized case.

At the end, we make a note about the entanglement in the general four-mode system with different up-conversion coupling constants ($g_2 \neq g_3$). This is relevant when non-ideal phase-matching conditions of the three nonlinear interactions are met in the experiment (see below). According to our investigations, the largest values of negativities $E_{1\times2}$ and $E_{3\times4}$ are found in the symmetric four-mode system ($g_2 = g_3$) considered above. On the contrary, the largest values of negativities $E_{1\times4}$ and $E_{2\times3}$ are obtained for unbalanced g_2 and g_3 interactions.

Similarly to the symmetric case, separable states, entangled states without sub-shot-noise intensity correlations and entangled states exhibiting sub-shot-noise intensity correlations are found in the whole three-dimensional parametric space spanned by variables g_jt for $j = 1, 2, 3$. As an example, the distribution of different kinds of reduced two-mode states found in the up-converted modes 3 and 4 in this space is plotted in Fig. 6.10. The graphs in Fig. 6.10 indicate that, in accord with the symmetric case, the larger the value of constant g_1t, the larger the

relative amount of entangled states that cannot be identified through sub-shot-noise intensity correlations.

6.6 Experimental implementation

A possible experimental implementation of the four mode interaction described above can be achieved by using a BaB_2O_4 crystal as the nonlinear medium, a ps-pulsed laser (a mode-locked Nd:YLF laser regeneratively amplified at 500 Hz, High-Q Laser Production) to get the pump fields and hybrid photodetectors (mod. R10467U-40, Hamamatsu Photonics) as the photon-number-resolving detectors. A typical experimental setup can be built in analogy with other previous experiments [114]. The phase-matching conditions can be chosen so as to have $\omega_1 = \omega_2$ and a common pump field for both up-conversion processes so that $\omega_3 = \omega_4$. In this specific symmetric case we have $g_2 = g_3 \equiv g_{23}$.

We can estimate the range of coupling constants achievable in this setup based on the above-mentioned laser source. Let us consider the following parameters: wavelength of the pump for down-conversion $\lambda_{p1} = 349$ nm, $\lambda_1 = \lambda_2 = 698$ nm, wavelength of the pump for up-conversion $\lambda_{p2} = 1047$ nm, $\lambda_3 = \lambda_4 = 418.8$ nm, length of the BaB_2O_4 crystal $L = 4$ mm, diameters of the pumps 0.5 mm, pulse duration 4.5 ps. The coupling constants g_1 and g_{23} are linearly proportional to the corresponding pump field amplitudes so that $g_1 t = \kappa_1 A_{p1} L$ and $g_{23} t = \kappa_{23} A_{p2} L$, where κ_j $(j = 1, 23)$ are the nonlinear coupling coefficients and A_j $(j = p1, p2)$ are the pump amplitudes. For the considered parameters we can estimate $\kappa_j \approx 10^{-13} s^{1/2}$. The useful range of energies per pulse is up to 66 μJ in the UV and up to 240 μJ in the IR, corresponding to maximum values $g_1 t \approx 5.9$ and $g_2 t \approx 7$. The theoretical results discussed above predict an interesting behavior for this range of parameters, including the transfer of entanglement into the up-converted modes.

6.7 Conclusions

Four-mode Gaussian states generated via parametric down-conversion and frequency up-conversion have been analyzed in terms of nonclassicality, entanglement and entanglement transfer among the modes. While nonclassicality of the state has been described by the easily-computable Lee nonclassicality depth, logarithmic negativity for different bipartitions has been applied to monitor the occurrence of entanglement among different modes. It has been shown that whenever the analyzed system is nonclassical, it is also entangled. Moreover, the entanglement is present only in the form of bipartite entanglement. The analysis of the noise reduction factor identifying sub-shot-noise intensity correlations, in parallel with the logarithmic negativity quantifying two-mode entanglement, has shown that the noise reduction factor is a powerful indicator of the entanglement in the analyzed system. This is substantial for the experimental demonstration of the transfer of entanglement from the down-converted modes to the up-converted ones.

Appendix

The evolution matrix M

The evolution matrix **M** describing the operator solution of the Heisenberg equations written in Eq. (6.2) is derived in the form:

$$\mathbf{M} = \begin{pmatrix} \frac{xc_1-yc_2}{x-y} & \frac{ixy\left(\sqrt{y_1}s_2-\sqrt{x_1}s_1\right)}{(xy_1-x_1\,y)g_1} & \frac{i\left(y\sqrt{y_1}x_1\,s_2-x\sqrt{x_1}y_1\,s_1\right)}{g_2\,(xy_1-x_1\,y)} & \frac{xy(c_2-c_1)}{g_1\,g_3\,(x-y)} \\ \frac{ig_1\left(\sqrt{y_1}s_2-\sqrt{x_1}s_1\right)}{x-y} & \frac{xy_1\,c_2-x_1\,yc_1}{xy_1-x_1\,y} & \frac{g_1\,y_1\,x_1\,(c_2-c_1)}{g_2\,(xy_1-x_1\,y)} & \frac{i\left(\sqrt{y_1}xs_2-\sqrt{x_1}ys_1\right)}{(x-y)g_3} \\ \frac{ig_2\left(\sqrt{x_1}ys_2-\sqrt{y_1}xs_1\right)}{\sqrt{x_1}(x-y)\sqrt{y_1}} & -\frac{g_2\,xy(c_2-c_1)}{(xy_1-x_1\,y)g_1} & \frac{xy_1\,c_1-x_1\,yc_2}{xy_1-x_1\,y} & \frac{-ig_2\,xy\left(\sqrt{x_1}s_2-\sqrt{y_1}s_1\right)}{g_1\,g_3\,(x-y)\sqrt{x_1}\sqrt{y_1}} \\ \frac{g_1\,g_3\,(-c_2+c_1)}{x-y} & \frac{ig_3\left(\sqrt{y_1}xs_2-\sqrt{x_1}ys_1\right)}{xy_1-x_1\,y} & \frac{ig_1\,g_3\left(x_1\,\sqrt{y_1}s_2-y_1\,\sqrt{x_1}s_1\right)}{g_2\,(xy_1-x_1\,y)} & \frac{xc_2-yc_1}{x-y} \end{pmatrix}, \tag{6.18}$$

where $x = (a+b)/2$, $x_1 = (a_1+b)/2$, $y = (a-b)/2$, $y_1 = (a_1-b)/2$, $a = -g_1^2+g_2^2-g_3^2$, $a_1 = -g_1^2+g_2^2+g_3^2$, $b = \sqrt{{g_1}^4-2\,{g_1}^2{g_2}^2-2\,{g_1}^2{g_3}^2+{g_2}^4-2\,{g_2}^2{g_3}^2+{g_3}^4}$, $c_1 = \cos(\sqrt{x_1}t)$,

$c_2 = \cos(\sqrt{y_1}t)$, $s_1 = \sin(\sqrt{x_1}t)$, and $s_2 = \sin(\sqrt{y_1}t)$.

Chapter 7

Retrieving the covariance matrix of an unknown two-mode Gaussian state by means of a reference twin beam

Text adopted from *I. I. Arkhipov and J. Peřina Jr., Opt. Commun.* **375***, 29 (2016)* [A4].

7.1 Introduction

The reconstruction of a state of any quantum system belongs to the most important tasks in quantum physics [16, 117, 118]. For this reason, homodyne detection has been suggested and experimentally implemented for the first time in Ref. [119] for quantum light. This was the first successful example of the so-called quantum state tomography, that provides the full information about the analyzed quantum state. The knowledge of the quantum state of light is extraordinarily important, as such states are useful for testing the postulates of quantum mechanics, showing peculiar features of quantum states (teleportation [31], dense coding [120, 121], etc.), as well as applying them in metrology and other applications (cryptography [122, 123]).

The optical homodyne tomography both in its cw and pulsed variants has become the most advanced and also powerful method in quantum state tomography [35] and, as such, it has become an indispensable technique in the field of quantum optics. The method is based upon overlapping an unknown state with a classical light (coherent state) with a well-defined phase, that is called a local oscillator. The interference pattern depending on the varying phase of the local oscillator then allows to reconstruct the quantum state, in detail to reconstruct its Wigner function defined in the phase space [16, 35]. Subsequently, moments of the field operators can be obtained and used to fully characterize nonclassicality of the analyzed quantum state [124, 102]. However, the optical homodyne tomography is quite experimentally involved and requires extended experimental data sets [35].

For this reason, a simplified method still relying on the coherent local oscillator has been suggested for quantum state tomography in [125], and later elaborated in [126, 127]. In this method, one of the output ports of a beam splitter that mixes the analyzed light with the local oscillator is monitored in general by a photon-number resolving detector with the varying attenuation coefficient. Also an attempt to use the data measured under different levels of noise for quantum state tomography has been made [128].

In many cases, the light to be analyzed has specific properties that allow to apply simpler tools in the determination of its state. For example, when we analyze the properties of twin beams generated from the vacuum state by parametric down-conversion [28], the characterization by means of the measured photocount statistics is fully sufficient [68, 73]. This possibility originates in the generation process that does not 'prescribe' specific phases to the individual signal and idler fields. Here, the generated light is Gaussian without coherent components, i.e. it is completely characterized by means of its covariance matrix. Once the covariance matrix of a given state is obtained, all the properties of the state are easily derived. As useful examples, entanglement of a two-mode twin beam or local nonclassicalities of one-mode reduced states can be mentioned [A2],[A3]. Even phase-space quasidistributions of integrated intensities can be determined [61].

Whereas the analysis of covariance matrices of Gaussian two-mode twin beams is not difficult

since only certain elements of their covariance matrices are nonzero, the measurement of covariance matrices belonging to a general two-mode Gaussian state is more involved. To cope with this problem, we have developed a method for reconstructing the normally- or symmetrically-ordered covariance matrix of such a general two-mode Gaussian state based on mixing the analyzed state with a reference twin beam with the varying overall phase.

Moreover, the developed approach can be extended to multimode Gaussian states provided that the measurement on individual mode pairs can be performed. This is useful, e.g., for spectrally multimode twin beams composed of N paired modes. Even in this case, the genuine multimode entanglement of the state can be retrieved from its multimode covariance matrix [109, 76]. A specific example of this general approach was studied by Altepeter *et al.* [129] who reconstructed the polarization state of a photon pair by acquiring photon coincidence-count statistics.

Thechapter is organized as follows. Description of general two-mode Gaussian states through their covariance matrices is given in Sec. 7.2. Twin beams as the most common kind of two-mode Gaussian states are discussed in Sec. 7.3. The method for revealing the covariance matrix of a general two-mode Gaussian state is given in Sec. 7.4. Sec. 7.5 brings conclusions.

7.2 General two-mode Gaussian states

The normally-ordered characteristic function $C_{\mathcal{N}}$ for a general two-mode Gaussian state is defined as follows

$$C_{\mathcal{N}}(\beta_1, \beta_2) = \mathrm{Tr}\left[\hat{\rho}(0) \exp(\beta_1 \hat{a}_1^\dagger + \beta_2 \hat{a}_2^\dagger) \exp(-\beta_1^* \hat{a}_1 - \beta_2^* \hat{a}_2)\right], \tag{7.1}$$

where Tr stands for the operator trace and $\hat{a}_i$ ($\hat{a}_i^\dagger$) denote the boson annihilation (creation) operators of mode i, $i = 1, 2$.

The normally-ordered characteristic function $C_{\mathcal{N}}$ in Eq. (7.1) can be expressed via its complex

covariance matrix $\mathbf{A}_{\mathcal{N}}$,

$$\mathbf{A}_{\mathcal{N}} = \begin{bmatrix} \mathbf{B}_1 & \mathbf{D}_{12} \\ \mathbf{D}_{12}^{\dagger} & \mathbf{B}_2 \end{bmatrix}, \tag{7.2}$$

$$\mathbf{B}_j = \begin{bmatrix} -B_j & C_j \\ C_j^* & -B_j \end{bmatrix}, \quad j = 1, 2, \quad \mathbf{D}_{12} = \begin{bmatrix} \bar{D}_{12}^* & D_{12} \\ D_{12}^* & \bar{D}_{12} \end{bmatrix}, \tag{7.3}$$

in the form $C_{\mathcal{N}}(\hat{\boldsymbol{\beta}}) = \exp(\hat{\boldsymbol{\beta}}^{\dagger}\mathbf{A}_{\mathcal{N}}\hat{\boldsymbol{\beta}}/2)$, where $\hat{\boldsymbol{\beta}} = (\beta_1, \beta_1^*, \beta_2, \beta_2^*)^T$. The coefficients B_j, C_j, $j = 1, 2$, $\bar{D}_{12}$ and D_{12} occurring in Eq. (7.2) are defined as

$$\begin{aligned} B_j &= \langle \Delta\hat{a}_j^{\dagger}\Delta\hat{a}_j \rangle, \qquad C_j = \langle \Delta\hat{a}_j^2 \rangle, \\ D_{12} &= \langle \Delta\hat{a}_1\Delta\hat{a}_2 \rangle, \qquad \bar{D}_{12} = -\langle \Delta\hat{a}_1^{\dagger}\Delta\hat{a}_2 \rangle. \end{aligned} \tag{7.4}$$

Given the above coefficients for the normally-ordered covariance matrix $\mathbf{A}_{\mathcal{N}}$, the symmetrically-ordered covariance matrix $\mathbf{A}_{\mathcal{S}}$ is obtained in its block structure as follows:

$$\begin{aligned} \mathbf{A}_{\mathcal{S}} &= \begin{bmatrix} \mathbf{B}_{\mathcal{S}1} & \mathbf{D}_{\mathcal{S}} \\ \mathbf{D}_{\mathcal{S}}^T & \mathbf{B}_{\mathcal{S}2} \end{bmatrix}, \\ \mathbf{B}_{\mathcal{S}j} &= \begin{bmatrix} B_j + \mathrm{Re}(C_j) + 1/2 & \mathrm{Im}(C_j) \\ \mathrm{Im}(C_j) & B_j - \mathrm{Re}(C_j) + 1/2 \end{bmatrix}, \quad j = 1, 2, \\ \mathbf{D}_{\mathcal{S}} &= \begin{bmatrix} \mathrm{Re}(D_{12} - \bar{D}_{12}) & \mathrm{Im}(D_{12} + \bar{D}_{12}) \\ \mathrm{Im}(D_{12} - \bar{D}_{12}) & -\mathrm{Re}(D_{12} + \bar{D}_{12}) \end{bmatrix}; \end{aligned} \tag{7.5}$$

Re (Im) denotes the real (imaginary) part of the argument.

The determination of coefficients B_j and C_j, $j = 1, 2$, together with the coefficients D_{12} and $\bar{D}_{12}$ is thus sufficient to fully characterize a general two-mode Gaussian field without coherent components. All possible correlation functions can then be easily derived [28]. As it has been shown in [A2],[A3], determinant $I_4 \equiv \det(A_{\mathcal{S}})$ of the symmetrically-ordered covariance matrix along with the local unitary invariants I_j, $j = 1, 2, 3$, of the normally-ordered covariance matrix

$\mathbf{A}_{\mathcal{N}}$,

$$I_1 = \det(\mathbf{B}_1), \quad I_2 = \det(\mathbf{B}_2), \quad I_3 = \det(\mathbf{D}_{12}), \tag{7.6}$$

even completely determine the nonclassicality and entanglement of the state.

7.3 Pure twin beams

To determine the needed coefficients, we use as a reference a pure twin beam with a specific form of its covariance matrix. Pure twin beams represent a specific form of two-mode Gaussian states that is standardly generated in the process of parametric down-conversion. The boson operators characterizing the emitted signal ($\hat{a}_1^{\rm out}$) and idler ($\hat{a}_2^{\rm out}$) fields are written in the Heisenberg picture as follows [28]:

$$\begin{aligned} \hat{a}_1^{\rm out} &= \cosh(\sqrt{G})\hat{a}_1^{\rm in} + i\exp(i\phi)\sinh(\sqrt{G})\hat{a}_2^{\rm in\dagger}, \\ \hat{a}_2^{\rm out} &= \cosh(\sqrt{G})\hat{a}_2^{\rm in} + i\exp(i\phi)\sinh(\sqrt{G})\hat{a}_1^{\rm in\dagger}, \end{aligned} \tag{7.7}$$

where G is the gain of the parametric process, $\hat{a}_1^{\rm in}$ ($\hat{a}_2^{\rm in}$) denotes the incident signal- (idler-) field annihilation operator and ϕ stays for a phase that follows the phase of the coherent pump field.

Assuming the incident vacuum state in both the signal and idler fields, we arrive at the following only nonzero coefficients of the normally-ordered covariance matrix of this reference beam:

$$B_{1,2}^R = B_p, \quad D_{12}^R = i\exp(i\phi)\sqrt{B_p(B_p+1)}. \tag{7.8}$$

The problem how to reconstruct the coefficients of the normally-ordered covariance matrix $\mathbf{A}_{\mathcal{N}}^R$ of the reference twin beam has been discussed in detail in Refs. [89, 66, 73].

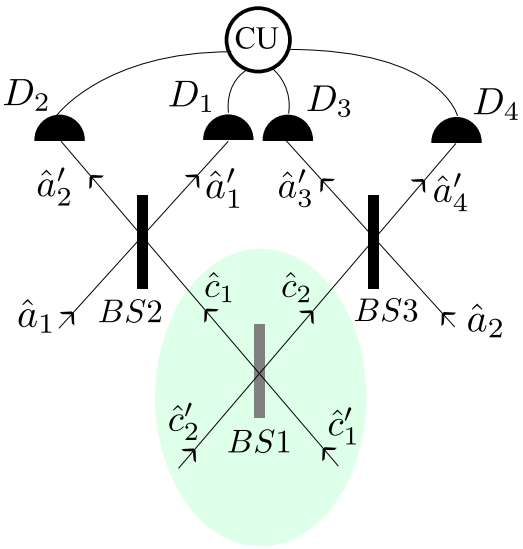

Figure 7.1: The experimental scheme. Two modes ($\hat{c}'_1$ and $\hat{c}'_2$) of a pure twin beam are mixed on beam splitter BS1 to provide a reference two-mode field ($\hat{c}_1$ and $\hat{c}_2$). The output modes $\hat{c}_1$ and $\hat{c}_2$ of beam splitter BS1 are combined with two modes $\hat{a}_1$ and $\hat{a}_2$ of an unknown two-mode Gaussian state at balanced beam splitters BS2 and BS3. The photocount statistics of four output modes $\hat{a}'_j$, $j = 1, \ldots, 4$, leaving beam splitters BS2 and BS3 are measured by detectors D_1, D_2, D_3, D_4 and correlation unit CU.

7.4 Retrieving the covariance matrix of an unknown two-mode Guaussian state

The scheme for retrieving the covariance matrix of an unknown Gaussian state with vanishing coherent components is shown in Fig. 7.1. It relies on mixing the analyzed state with a reference twin beam. However, a pure twin beam composed of only photon pairs and exhibiting the thermal photon-number statistics in the signal and idler fields is not sufficient for this task that requires all the coefficients of the reference covariance matrix being nonzero. For this reason, we first mix the signal (annihilation operator $\hat{c}'_1$) and idler ($\hat{c}'_2$) fields on a beam splitter BS1 with the varying transmissivity t_1. At the output ports of beam splitter BS1 and depending on the transmissivity t_1, there occur different kinds of states useful in the reconstruction [A2],[A3]. In the proposed method, the reference light at the output ports ($\hat{c}_1$ and $\hat{c}_2$) of beams splitter BS1 is superimposed with the analyzed two-mode Gaussian state at balanced beam splitters BS2 and BS3. The output ports ($\hat{a}'_j$, $j = 1, \ldots, 4$) of beam splitters BS2 and BS3 are then monitored by four detectors measured in coincidence.

The unitary transformations describing the functioning of three beam splitters BS_j with amplitude transmissivities t_j and phase shifts θ_j, $j = 1, 2, 3$, are expressed in general as follows:

$$\begin{aligned}
\begin{pmatrix} \hat{c}_1 \\ \hat{c}_2 \end{pmatrix} &= \begin{pmatrix} t_1 & r_1 \exp(i\theta_1) \\ -r_1 \exp(-i\theta_1) & t_1 \end{pmatrix} \begin{pmatrix} \hat{c}'_1 \\ \hat{c}'_2 \end{pmatrix}, \\
\begin{pmatrix} \hat{a}'_1 \\ \hat{a}'_2 \end{pmatrix} &= \begin{pmatrix} t_2 & r_2 \exp(i\theta_2) \\ -r_2 \exp(-i\theta_2) & t_2 \end{pmatrix} \begin{pmatrix} \hat{a}_1 \\ \hat{c}_1 \end{pmatrix}, \\
\begin{pmatrix} \hat{a}'_3 \\ \hat{a}'_4 \end{pmatrix} &= \begin{pmatrix} t_3 & r_2 \exp(i\theta_3) \\ -r_3 \exp(-i\theta_3) & t_3 \end{pmatrix} \begin{pmatrix} \hat{a}_2 \\ \hat{c}_2 \end{pmatrix},
\end{aligned} \tag{7.9}$$

where the annihilation operators $\hat{a}_1$ and $\hat{a}_2$ belong to the modes of the analyzed two-mode Gaussian state.

Assuming the balanced beam splitters BS2 and BS3 ($t_2 = t_3 = 1/\sqrt{2}$) with zero phase shifts ($\theta_2 = \theta_3 = 0$) and applying the relations in Eqs. (7.9), we reveal the following formulas giving the number operators $\hat{n}'_j$ of fields at the detectors as functions of the operators of the analyzed state and the reference state:

$$\begin{aligned}
\hat{n}'_1 &= \hat{a'}_1^{\dagger} \hat{a}'_1 = \frac{1}{2}\left(\hat{a}_1^{\dagger}\hat{a}_1 + \hat{a}_1^{\dagger}\hat{c}_1 + \hat{a}_1\hat{c}_1^{\dagger} + \hat{c}_1^{\dagger}\hat{c}_1\right), \\
\hat{n}'_2 &= \hat{a'}_2^{\dagger} \hat{a}'_2 = \frac{1}{2}\left(\hat{a}_1^{\dagger}\hat{a}_1 - \hat{a}_1^{\dagger}\hat{c}_1 - \hat{a}_1\hat{c}_1^{\dagger} + \hat{c}_1^{\dagger}\hat{c}_1\right), \\
\hat{n}'_3 &= \hat{a'}_3^{\dagger} \hat{a}'_3 = \frac{1}{2}\left(\hat{a}_2^{\dagger}\hat{a}_2 + \hat{a}_2^{\dagger}\hat{c}_2 + \hat{a}_2\hat{c}_2^{\dagger} + \hat{c}_2^{\dagger}\hat{c}_2\right), \\
\hat{n}'_4 &= \hat{a'}_4^{\dagger} \hat{a}'_4 = \frac{1}{2}\left(\hat{a}_2^{\dagger}\hat{a}_2 - \hat{a}_2^{\dagger}\hat{c}_2 - \hat{a}_2\hat{c}_2^{\dagger} + \hat{c}_2^{\dagger}\hat{c}_2\right).
\end{aligned} \tag{7.10}$$

The normally-ordered characteristic function $C_{\mathcal{N}}$ of the four-mode Gaussian state characterizing the four fields in front of detectors is written as

$$C_{\mathcal{N}}(\beta_1, \beta_2, \beta_3, \beta_4) = \mathrm{Tr}\left[\hat{\rho}'(0) \exp\left(\sum_{i=1}^{4} \beta_i \hat{a}_i'^{\dagger}\right) \exp\left(-\sum_{i=1}^{4} \beta_i^* \hat{a}'_i\right)\right]. \tag{7.11}$$

The quantum-mechanical averaging in Eq. (7.11) is performed by the statistical operator $\hat{\rho}'(0) = \hat{\rho}_{12}(0) \otimes \hat{\rho}^R(0)$, where $\hat{\rho}_{12}$ is the statistical operator of the unknown two-mode Gaussian state

and the operator $\hat{\rho}^R$ describes the incident reference twin beam.

Given Eqs. (7.4) and (7.11), the normally-ordered characteristic function $C_{\mathcal{N}}$ is obtained in the form:

$$C_{\mathcal{N}}(\beta_1,\beta_2,\beta_3,\beta_4) = \exp\left\{-\sum_{i=1}^{4} B'_i|\beta_i|^2 + \left[\frac{1}{2}\sum_{i=1}^{4} C'_i\beta_i^{*2} + \sum_{j<k}^{4} D'_{jk}\beta_j^*\beta_k^* + \sum_{j<k}^{4}\bar{D}'_{jk}\beta_j\beta_k^* + \text{c.c.}\right]\right\}, \tag{7.12}$$

where the coefficients B'_i, C'_i, D'_{jk}, and $\bar{D}'_{jk}$ are determined by the formulas written in Eqs. (7.4).

Second-order correlations of the integrated-intensity fluctuations ΔW in different modes are easily derived from Eq. (7.12) [28]:

$$\begin{aligned}\langle\Delta W_j\Delta W_k\rangle_{\mathcal{N}} &= \langle\hat{a'}_j^{\dagger}\hat{a'}_k^{\dagger}\hat{a}'_j\hat{a}'_k\rangle - \langle\hat{a'}_j^{\dagger}\hat{a}'_j\rangle\langle\hat{a'}_k^{\dagger}\hat{a}'_k\rangle \\ &= \left.\frac{\partial^4 C_{\mathcal{N}}}{\partial\beta_j\partial(-\beta_j^*)\partial\beta_k\partial(-\beta_k^*)}\right|_{\{\beta_j\}=\{\beta_j^*\}=0} - \left.\frac{\partial^2 C_{\mathcal{N}}}{\partial\beta_j\partial(-\beta_j^*)}\frac{\partial^2 C_{\mathcal{N}}}{\partial\beta_k\partial(-\beta_k^*)}\right|_{\{\beta_j\}=\{\beta_j^*\}=0} \\ &= |D'_{jk}|^2 + |\bar{D}'_{jk}|^2, \quad j\neq k.\end{aligned} \tag{7.13}$$

Now, applying the photodetection theory [28] for the detectors with quantum detection efficiencies η_j and dark-count rates n_{dj}, we arrive at the following second-order moments of photocount fluctuations at all four detectors:

$$\langle\Delta\hat{m}_j\Delta\hat{m}_k\rangle = \eta_j\eta_k\langle\Delta W_j\Delta W_k\rangle_{\mathcal{N}}, \quad j\neq k. \tag{7.14}$$

Applying further Eqs. (7.4), (7.9) and (7.13), we reveal the following second-order moments of

photocount fluctuations:

$$\begin{aligned}
\langle \Delta\hat{m}_1 \Delta\hat{m}_2 \rangle &= \frac{\eta_1\eta_2}{4}\Big(B_1^2 + |C_1|^2 + B_1^{R2} + |C_1^R|^2 - 2B_1 B_1^R - 2\mathrm{Re}\{C_1 C_1^{R*}\}\Big), \\
\langle \Delta\hat{m}_3 \Delta\hat{m}_4 \rangle &= \frac{\eta_3\eta_4}{4}\Big(B_2^2 + |C_2|^2 + B_2^{R2} + |C_2^R|^2 - 2B_2 B_2^R - 2\mathrm{Re}\{C_2 C_2^{R*}\}\Big), \\
\langle \Delta\hat{m}_1 \Delta\hat{m}_3 \rangle &= \frac{\eta_1\eta_3}{4}\Big(|D_{12}|^2 + |\bar{D}_{12}|^2 + |D_{12}^R|^2 + |\bar{D}_{12}^R|^2 + 2\mathrm{Re}\{D_{12} D_{12}^{R*}\} + \\
&\quad 2\mathrm{Re}\{\bar{D}_{12}\bar{D}_{12}^{R*}\}\Big), \\
\langle \Delta\hat{m}_1 \Delta\hat{m}_4 \rangle &= \frac{\eta_1\eta_4}{4}\Big(|D_{12}|^2 + |\bar{D}_{12}|^2 + |D_{12}^R|^2 + |\bar{D}_{12}^R|^2 - 2\mathrm{Re}\{D_{12} D_{12}^{R*}\} - \\
&\quad 2\mathrm{Re}\{\bar{D}_{12}\bar{D}_{12}^{R*}\}\Big), \\
\langle \Delta\hat{m}_2 \Delta\hat{m}_3 \rangle &= \frac{\eta_2\eta_3}{4}\Big(|D_{12}|^2 + |\bar{D}_{12}|^2 + |D_{12}^R|^2 + |\bar{D}_{12}^R|^2 - 2\mathrm{Re}\{D_{12} D_{12}^{R*}\} - \\
&\quad 2\mathrm{Re}\{\bar{D}_{12}\bar{D}_{12}^{R*}\}\Big), \\
\langle \Delta\hat{m}_2 \Delta\hat{m}_4 \rangle &= \frac{\eta_2\eta_4}{4}\Big(|D_{12}|^2 + |\bar{D}_{12}|^2 + |D_{12}^R|^2 + |\bar{D}_{12}^R|^2 + 2\mathrm{Re}\{D_{12} D_{12}^{R*}\} + \\
&\quad 2\mathrm{Re}\{\bar{D}_{12}\bar{D}_{12}^{R*}\}\Big). \qquad (7.15)
\end{aligned}$$

The formulas in Eqs. (7.15), when applied to the analyzed two-mode Gaussian state and the reference twin beam, allow to recover all coefficients of the covariance matrix of the analyzed state. The determination of the coefficients is naturally split into the following four steps.

Retrieving the coefficients B_1 and B_2 — These coefficients give the mean numbers of photons present in both modes of the analyzed state. If the inputs of the reference field are replaced by the vacuum, we immediately arrive at the values of these coefficients using the relations in Eqs. (7.10):

$$B_1 = 2\left(\langle \hat{m}_1 \rangle - n_{d1}\right)/\eta_1, \qquad B_2 = 2\left(\langle \hat{m}_3 \rangle - n_{d3}\right)/\eta_3. \qquad (7.16)$$

Retrieving the coefficients C_1 and C_2 — To reveal these coefficients, we exploit the fact that a pure twin beam with the mean photon-pair number B_p gives two separable squeezed states with opposite phases ϕ when its constituents are combined at the balanced beam splitter BS1 [95]. Thus, the reference field attains the coefficients $B_1^R = B_2^R = B_\mathrm{p}$, $C_1^R = -C_2^R = i\exp(i\phi)\sqrt{B_\mathrm{p}(B_\mathrm{p}+1)}$ [A2] and the suitable relations in Eqs. (7.15) can be recast into the

form:

$$\begin{aligned}\langle \Delta\hat{m}_1 \Delta\hat{m}_2 \rangle &= \frac{\eta_1\eta_2}{4}\Big(2B_{\rm p}^2 + B_{\rm p}(1-2B_1) + \langle \Delta W_1^2 \rangle_{\mathcal{N}}\Big) - \\ &\quad \frac{\eta_1\eta_2\sqrt{B_{\rm p}(B_{\rm p}+1)}}{2}{\rm Im}\left\{\exp\left(-i\phi\right) C_1\right\}, \qquad (7.17)\\ \langle \Delta\hat{m}_3 \Delta\hat{m}_4 \rangle &= \frac{\eta_3\eta_4}{4}\Big(2B_{\rm p}^2 + B_{\rm p}(1-2B_2) + \langle \Delta W_2^2 \rangle_{\mathcal{N}}\Big) + \\ &\quad \frac{\eta_3\eta_4\sqrt{B_{\rm p}(B_{\rm p}+1)}}{2}{\rm Im}\left\{\exp\left(-i\phi\right) C_2\right\}. \qquad (7.18)\end{aligned}$$

The formulas in Eqs. (7.18) allow us to determine the variances $\langle \Delta W_j^2 \rangle_{\mathcal{N}}$ for $j = 1, 2$ of the constituents of the analyzed field provided that the reference field is absent. The absolute values $|C_j|$ can immediately be derived using the relations $|C_j|^2 = \langle \Delta W_j^2 \rangle_{\mathcal{N}} - B_j^2$. For the complex coefficients C_j, we need to vary the phase ϕ of the reference field, that is derived from the pump field that created the reference pure twin beam. The obtained interference pattern then gives us both the magnitudes and phases of both coefficients.

If the analyzed state is known to be symmetric ($B_1 = B_2$ and $C_1 = C_2 \equiv C$), we can even apply the following simpler formula to arrive at the coefficient C:

$$\frac{1}{\sqrt{B_{\rm p}(B_{\rm p}+1)}}\left(\frac{\langle \Delta\hat{m}_3 \Delta\hat{m}_4 \rangle}{\eta_3\eta_4} - \frac{\langle \Delta\hat{m}_1 \Delta\hat{m}_2 \rangle}{\eta_1\eta_2}\right) = {\rm Im}\left\{\exp\left(-i\phi\right) C\right\}. \qquad (7.19)$$

Retrieving the coefficient D_{12} — We need as a reference field the original pure twin beam for which D_{12}^R is given in Eq. (7.8) and $\bar{D}_{12}^R$ vanishes. The third and fourth relations in Eqs. (7.15) can be rearranged into the formula:

$$\frac{1}{\sqrt{B_{\rm p}(B_{\rm p}+1)}}\left(\frac{\langle \Delta\hat{m}_1 \Delta\hat{m}_3 \rangle}{\eta_1\eta_3} - \frac{\langle \Delta\hat{m}_1 \Delta\hat{m}_4 \rangle}{\eta_1\eta_4}\right) = {\rm Im}\left\{\exp\left(-i\phi\right) D_{12}\right\}. \qquad (7.20)$$

According to Eq. (7.20), the variation of the pump phase ϕ provided both the magnitude and phase of coefficient D_{12}. We note that also other combinations of the second-order moments in Eqs. (7.15) can be used to reveal the coefficient D_{12}.

Retrieving the coefficient $\bar{D}_{12}$ — To retrieve the coefficient $\bar{D}_{12}$ one needs a nonzero coefficient

$\bar{D}_{12}^{R}$ of the reference field. Such coefficient cannot be obtained by a simple mixing of the constituents of a pure twin beam on beam splitter BS1. However, if we consider only one constituent of the pure twin beam and mix it with the vacuum state of beam splitter BS1 with transmissivity $t_1 = 1/\sqrt{2}$, we arrive at the fields with zero values D_{12}^{R}, C_1^{R} and C_2^{R}, but nonzero coefficients $B_1^{R} = B_2^{R} = B_{\mathrm{p}}/2$ and $\bar{D}_{12}^{R} = \pm B_{\mathrm{p}}/2$, where the plus (minus) sign is taken for mode $\hat{c}_2'$ ($\hat{c}_1'$) in the vacuum state. In this case, the following relation is revealed:

$$\frac{\langle \Delta\hat{m}_1 \Delta\hat{m}_3 \rangle}{\eta_1 \eta_3} - \frac{\langle \Delta\hat{m}_1 \Delta\hat{m}_4 \rangle}{\eta_1 \eta_4} = \mathrm{Re}\{\bar{D}_{12}^{R} \bar{D}_{12}^{*}\}. \tag{7.21}$$

The formula in Eq. (7.21) suggests that the variation of complex phase of the reference coefficient $\bar{D}_{12}^{R}$ allows to recover the coefficient $\bar{D}_{12}$ of the analyzed field. This can easily be accomplished by imposing a variable phase shift θ to, e.g., mode $\hat{c}_1$ by a phase modulator placed between the beam splitters BS1 and BS2 [$\hat{c}_1 \to \exp(i\theta)\hat{c}_1$]. In this case, Eq. (7.21) is transformed into the form

$$\frac{2}{B_{\mathrm{p}}} \left(\frac{\langle \Delta\hat{m}_1 \Delta\hat{m}_3 \rangle}{\eta_1 \eta_3} - \frac{\langle \Delta\hat{m}_1 \Delta\hat{m}_4 \rangle}{\eta_1 \eta_4} \right) = \pm \mathrm{Re}\{\exp(-i\theta) \bar{D}_{12}^{*}\}, \tag{7.22}$$

where again the plus (minus) sign is taken for the mode $\hat{c}_2'$ ($\hat{c}_1'$) in the vacuum state. According to Eq. (7.22) the variation of phase θ then provides both the real and imaginary part of the coefficient $\bar{D}_{12}$.

We note that the reference pure twin beam can be characterized in the suggested scheme provided that its copy is obtained. Such auto-characterization allows to check the quality of the applied reference twin beam, that is ideally composed only of photon pairs.

At the end, we note that the developed method can be generalized to allow for the characterization of two-mode Gaussian states with nonzero coherent components. In this case, the coherent components in both modes of the analyzed state have to be identified first, by applying the homodyne detection scheme. Then, the above written formulas can be generalized to include the coherent components. So the contributions from coherent components can easily be subtracted.

7.5 Conclusions

We have suggested a method for characterizing a general two-mode Gaussian state with vanishing coherent components. The coefficients of its normally-ordered covariance matrix are revealed by mixing the analyzed state with a reference beam obtained from a pure twin beam, by using two balanced beam splitters. The variation of the phase of the pump beam that generates the reference twin beam together with the variation of the phase of one mode of the reference beam are needed in the method that monitors the first- and second-order moments of photocounts at four detectors placed in the experimental setup.

Chapter 8

Conclusions

- First, we have shown how the nonclassicality, entanglement, and dimensionality of a noisy twin beam can be determined using a characteristic function of the twin beam written in the Fock basis instead of using the covariance matrix approach. We have found a one-to-one correspondence between the negativity quantifying entanglement and the nonclassicality depth, and thus for the first time we have shown that the nonclassicality of the twin beams is completely determined by their entanglement. Using Fock states basis we were able to see the internal structure of the entanglement of the twin beams defined in the subspaces of the Fock Hilbert space. We also compared the dimensionality of the twin beam quantified by the participation ratio with the dimensionality of entanglement determined from the negativity. We also considered the extension of the developed theory to the multimode case and thus we have demonstrated how our model can be directly applied to the experiment, therefore showing the model's experimental significance.

- Second, we have investigated the behavior of general nonclassical two-mode Gaussian states at a beam splitter and thus we have studied various states which can be generated at the output of the beam splitter. We have proposed new suitable quantifiers to analyze single-mode nonclassicality as well as two-mode entanglement of both input and output states. These new quantifiers have been derived from local and global invariants of linear unitary two-mode transformations such that the sum of input (or output) local

nonclassicality measures and entanglement measure gives a global invariant. Moreover we showed that this new invariant quantifies the global nonclassicality resource. We have demonstrated the applicability of such global nonclassicality invariant considering mutual transformations of local nonclassicalities and entanglement induced by the beam splitter for incident noisy twin beams, single-mode noisy squeezed vacuum states, and states encompassing both squeezed states and twin beams, and as such, a variety of new possible states have been predicted.

- Third, we have considered one of the states that can be obtained from the twin beam, namely single-mode nonclassical states, which were experimentally generated from a twin beam by postselection based on detecting a given number of photocounts in one arm by using an iCCD camera. For such states we have derived the nonclassicality criteria based on intensity moments from the usual matrix approach and compared them with those provided by the majorization theory. Our analysis has revealed that the majorization theory gives a greater number of more suitable nonclassicality criteria. We have experimentally identified fifteen useful criteria of the majorization theory containing the intensity moments up to the fifth order. As such, we have also experimentally confirmed the usefulness of our derived criteria to detect nonclassicality of single-mode states, which resides in the intensity domain.

- At fourth, we have provided the study of the multipartite entanglement and nonclassicality of four-mode Gaussian states generated in two simultaneous nonlinear processes involving parametric frequency down-conversion and frequency up-conversion assuming the vacuum as the initial state. Most importantly, we have found suitable conditions for the generation of highly entangled states, which can be useful for future quantum telecommunication when the problem of transfer of the state from one frequency domain into another one will play a crucial role. We have also demonstrated the process of the flow of the entanglement from the down-converted modes into the up-converted. The analysis of the whole set of the obtained states shows that one can apply the common sub-shot noise intensity correlations as an entanglement measure to uniquely identify the entanglement between the equally-populated down-converted modes, as well as the equally-populated up-converted modes.

- At fifth, we have developed a method for reconstruction of the Gaussian states making use of the nonclassicality properties of the twin beam. Namely we have found a scheme which allows to reveal the covariance matrix of an unknown two-mode Gaussian state. The method is based on the interference of the unknown states with a reference twin beam whose covariance matrix is known. Our approach relies on the first- and second-order cross-correlation intensity moments, which are determined by varying the overall phase of the reference twin beam. In other words, we have proposed the experimental scheme which does not require the homodyne detection, and where the role of the phase of the local oscillator is played by the phase of twin beams, which, in turn, is controlled by the phase of the pump field in SPDC process. Thus, our method can utilize photon-counting detectors instead of homodyne photodetectors which are demanding from the experimental point of view.

List of author's publications

[A1] I. I. Arkhipov, J. Peřina Jr., J. Peřina, and A. Miranowicz, "Comparative study of nonclassicality, entanglement, and dimensionality of multimode noisy twin beams," Phys. Rev. A **91**, 033837 (2015).

[A2] I. I. Arkhipov, J. Peřina Jr., J. Svozilík, and A. Miranowicz, "Nonclassicality invariant of general two-mode Gaussian states," Sci. Rep. **6**, 26523 (2016).

[A3] I. I. Arkhipov, J. Peřina Jr., J. Peřina, and A. Miranowicz, "Interplay of nonclassicality and entanglement of two-mode Gaussian fields generated in optical parametric processes," Phys. Rev. A **94**, 013807 (2016).

[A4] I. I. Arkhipov and J. Peřina Jr., "Retrieving the covariance matrix of an unknown two-mode Gaussian state by means of a reference twin beam," Opt. Commun. **375**, 29—33 (2016).

[A5] I. I. Arkhipov, J. Peřina Jr., O. Haderka, A. Allevi, and M. Bondani, "Entanglement and nonclassicality in four-mode Gaussian states generated via parametric down-conversion and frequency up-conversion," Sci. Rep. **6**, 33802 (2016).

[A6] I. I. Arkhipov, J. Peřina Jr., O. Haderka, and V. Michálek, "Experimental detection of nonclassicality of single-mode fields via intensity moments," Opt. Express **24**, 29496–29505 (2016).

[A7] I. Arkhipov, J. Peřina Jr., A. Miranowicz, and J. Peřina, "Entanglement and nonclassicality of twin beams containing noise," Proc. SPIE, **9441**, 94410Y–94410Y–7 (2014).

Bibliography

[1] A. Einstein, "Über einen die Erzeugung und Verwandlung des Lichtes betreffenden heuristischen Gesichtspunkt," Annalen der Physik **322**, 132–148 (1905).

[2] R. J. Glauber, "Coherent and incoherent states of the radiation field," Phys. Rev. **131**, 2766—2788 (1963).

[3] E. C. G. Sudarshan, "Equivalence of semiclassical and quantum mechanical descriptions of statistical light beams," Phys. Rev. Lett. **10**, 277 (1963).

[4] H. J. Kimble, M. Dagenais, and L. Mandel, "Photon antibunching in resonance fluorescence," Phys. Rev. Lett. **39**, 691–695 (1977).

[5] R. E. Slusher, L. W. Hollberg, B. Yurke, J. C. Mertz, and J. F. Valley, "Observation of squeezed states generated by four-wave mixing in an optical cavity," Phys. Rev. Lett. **55**, 2409–2412 (1985).

[6] L.-A. Wu, M. Xiao, and H. J. Kimble, "Squeezed states of light from an optical parametric oscillator," J. Opt. Soc. Am. B **4**, 1465–1475 (1987).

[7] M. D. Levenson, R. M. Shelby, A. Aspect, M. Reid, and D. F. Walls, "Generation and detection of squeezed states of light by nondegenerate four-wave mixing in an optical fiber," Phys. Rev. A **32**, 1550–1562 (1985).

[8] A. Einstein, B. Podolsky, and N. Rosen, "Can quantum-mechanical description of physical reality be considered complete?" Phys. Rev. **47**, 777 (1935).

[9] E. Schrödinger, "Die gegenwartige Situation in der Quantenmechanik," Naturwissenschaften **23**, 807 (1935).

[10] S. J. Freedman and J. F. Clauser, "Experimental test of local hidden-variable theories," Phys. Rev. Lett. **28**, 938–941 (1972).

[11] A. Aspect, P. Grangier, and G. Roger, "Experimental realization of einstein-podolsky-rosen-bohm gedankenexperiment: A new violation of bell's inequalities," Phys. Rev. Lett. **49**, 91–94 (1982).

[12] C. H. Bennett, G. Brassard, C. Crépeau, R. Jozsa, A. Peres, and W. K. Wootters, "Teleporting an unknown quantum state via dual classical and EPR channels," Phys. Rev. Lett. **70**, 1895 (1993).

[13] D. Bouwmeester, J.-W. Pan, K. Mattle, M. Eibl, H. Weinfurter, and A. Zeilinger, "Experimental quantum teleportation," Nature **390**, 575 (1997).

[14] M. A. Nielsen and I. L. Chuang, *Quantum Computation and Quantum Information* (Cambridge University Press, Cambridge, 2000).

[15] L. Mandel and E. Wolf, *Optical Coherence and Quantum Optics* (Cambridge University Press, Cambridge, 1995).

[16] G. Agarwal, *Quantum Optics* (Cambridge University Press, Cambridge, UK, 2013).

[17] R. J. Glauber, "Coherent and incoherent states of the radiation field," Phys. Rev. **131**, 2766 (1963).

[18] E. C. G. Sudarshan, "Equivalence of semiclassical and quantum mechanical descriptions of statistical light beams," Phys. Rev. Lett. **10**, 277 (1963).

[19] L. Mandel, "Sub-poissonian photon statistics in resonance fluorescence," Opt. Lett. **4**, 205–207 (1979).

[20] C. T. Lee, "Higher-order criteria for nonclassical effects in photon statistics," Phys. Rev. A **41**, 1721—1723 (1990).

[21] H. P. Yuen, "Two-photon coherent states of the radiation field," Phys. Rev. A **13**, 2226–2243 (1976).

[22] C. T. Lee, "Measure of the nonclassicality of nonclassical states," Phys. Rev. A **44**, R2775 (1991).

[23] S. L. Braunstein and P. van Loock, "Quantum information with continuous variables," Rev. Mod. Phys. **77**, 513–577 (2005).

[24] A. Peres, "Separability criterion for density matrices," Phys. Rev. Lett **77**, 1413 (1996).

[25] G. Adesso, A. Serafini, and F. Illuminati, "Multipartite entanglement in three-mode gaussian states of continuous-variable systems: Quantification, sharing structure, and decoherence," Phys. Rev. A **73**, 032345 (2006).

[26] K. Audenaert, M. B. Plenio, and J. Eisert, "Entanglement cost under positive-partial-transpose-preserving operations," Phys. Rev. Lett. **90**, 027901 (2003).

[27] L. Mandel and E. Wolf, *Optical Coherence and Quantum Optics* (Cambridge Univ. Press, Cambridge, 1995).

[28] J. Peřina, *Quantum Statistics of Linear and Nonlinear Optical Phenomena* (Kluwer, Dordrecht, 1991).

[29] J. Peřina, Z. Hradil, and B. Jurčo, *Quantum Optics and Fundamentals of Physics* (Kluwer, Dordrecht, 1994).

[30] D. F. Walls and G. J. Milburn, *Quantum Optics* (Springer, Berlin, 1994).

[31] D. Bouwmeester, J. W. Pan, K. Mattle, M. Eibl, H. Weinfurter, and A. Zeilinger, "Experimental quantum teleportation," Nature **390**, 575–579 (1997).

[32] G. Weihs, T. Jennewein, C. Simon, H. Weinfurter, and A. Zeilinger, "Violation of Bell's inequality under strict einstein locality conditions," Phys. Rev. Lett. **81**, 5039—5043 (1998).

[33] A. Lukš, V. Peřinová, and J. Peřina, "Principal squeezing of vacuum fluctuations," Opt. Commun. **67**, 149 (1988).

[34] C. T. Lee, "Nonclassical photon statistics of two mode squeezed states," Phys. Rev. A **42**, 1608—1616 (1990).

[35] A. I. Lvovsky and M. G. Raymer, "Continuous-variable optical quantum state tomography," Rev. Mod. Phys. **81**, 299 (2009).

[36] O. Jedrkiewicz, Y. K. Jiang, E. Brambilla, A. Gatti, M. Bache, L. A. Lugiato, and P. Di Trapani, "Detection of sub-shot-noise spatial correlation in high-gain parametric down-conversion," Phys. Rev. Lett. **93**, 243601 (2004).

[37] M. Bondani, A. Allevi, G. Zambra, M. G. A. Paris, and A. Andreoni, "Sub-shot-noise photon-number correlation in a mesoscopic twin beam of light," Phys. Rev. A **76**, 013833 (2007).

[38] J. Peřina Jr., O. Haderka, and V. Michálek, "Sub-Poissonian-light generation by postselection from twin beams," Opt. Express **21**, 19387—19394 (2013).

[39] M. Lamperti, A. Allevi, M. Bondani, R. Machulka, V. Michálek, O. Haderka, and J. Peřina Jr., "Optimal sub-Poissonian light generation from twin beams by photon-number resolving detectors," JOSA B **31**, 20–25 (2014).

[40] M. Lamperti, A. Allevi, M. Bondani, R. Machulka, V. Michálek, O. Haderka, and J. Peřina Jr., "Generation of sub-Poissonian non-Gaussian states from multimode twin beams by photon-number-resolving detector," Int. J. Quant. Inf. **31**, 1461017 (2014).

[41] A. S. K. Życzkowski, P. Horodecki and M. Lewenstein, "Volume of the set of separable states," Phys. Rev. A **58**, 883 (1998).

[42] G. Vidal and R. F. Werner, "Computable measure of entanglement," Phys. Rev. A **65**, 032314 (2002).

[43] I. P. Degiovanni, M. Bondani, E. Puddu, A. Andreoni, and M. G. A. Paris, "Intensity correlations, entanglement properties, and ghost imaging in multimode thermal-seeded parametric down-conversion: Theory," Phys. Rev. A **76**, 062609 (2007).

[44] M. Bondani, E. Puddu, I. P. Degiovanni, and A. Andreoni, "Chaotically seeded parametric downconversion for ghost imaging," J. Opt. Soc. Am. B **25**, 1203—1213 (2008).

[45] I. P. Degiovanni, M. Genovese, V. Schettini, M. Bondani, A. Andreoni, and M. G. A. Paris, "Monitoring the quantum-classical transition in thermally seeded parametric down-conversion by intensity measurements," Phys. Rev. A **79**, 063836 (2009).

[46] C. Eltschka and J. Siewert, "Negativity as an estimator of entanglement dimension," Phys. Rev. Lett. **111**, 100503 (2013).

[47] K. Życzkowski, "Volume of the set of separable states. ii," Phys. Rev. A **60**, 3496–3507 (1999).

[48] M. V. Fedorov, M. A. Efremov, A. E. Kazakov, K. W. Chan, C. K. Law, and J. H. Eberly, "Packet narrowing and quantum entanglement in photoionization and photodissociation," Phys. Rev. A **69**, 052117 (2004).

[49] M. V. Fedorov, M. A. Efremov, P. A. Volkov, E. V. Moreva, S. S. Straupe, and S. P. Kulik, "Anisotropically and high entanglement of biphoton states generated in spontaneous parametric down-conversion," Phys. Rev. Lett. **99**, 063901 (2007).

[50] K. W. Chan, J. P. Torres, and J. H. Eberly, "Transverse entanglement migration in hilbert space," Phys. Rev. A **75**, 050101 (2007).

[51] H. Di Lorenzo Pires, C. H. Monken, and M. P. van Exter, "Direct measurement of transverse-mode entanglement in two-photon states," Phys. Rev. A **80**, 022307 (2009).

[52] K. Bartkiewicz, K. Lemr, and A. Miranowicz, "Direct method for measuring of purity, superfidelity, and subfidelity of photonic two-qubit mixed states," Phys. Rev. A **88**, 052104 (2013).

[53] F. Just, A. Cavanna, M. V. Chekhova, and G. Leuchs, "Transverse entanglement of biphotons," New Journal of Physics **15**, 083015 (2013).

[54] K. Bartkiewicz, J. c. v. Beran, K. Lemr, M. Norek, and A. Miranowicz, "Quantifying entanglement of a two-qubit system via measurable and invariant moments of its partially transposed density matrix," Phys. Rev. A **91**, 022323 (2015).

[55] K. Bartkiewicz, P. Horodecki, K. Lemr, A. Miranowicz, and K. Życzkowski, "Method for universal detection of two-photon polarization entanglement," Phys. Rev. A **91**, 032315 (2015).

[56] J. Peřina and J. Křepelka, "Multimode description of spontaneous parametric down-conversion," J. Opt. B: Quantum Semiclass. Opt. **7**, 246 (2005).

[57] P. Horodecki, "Separability criterion and inseparable mixed states with positive partial transposition," Phys. Lett. A **232**, 333 (1997).

[58] R. Horodecki, P. Horodecki, M. Horodecki, and K. Horodecki, "Quantum entanglement," Rev. Mod. Phys. **81**, 865 (2009).

[59] A. Lukš, J. Peřina Jr., W. Leoński, and V. Peřinová, "Entanglement between an autoionizing system and a neighboring atom," Phys. Rev. A **85**, 012321 (2012).

[60] V. Peřinová, A. Lukš, J. Křepelka, and J. Peřina Jr., "Quantum correlation and entanglement between an ionizing system and a neighboring tom interacting directly and via a quantized field," Phys. Rev. A **90**, 033428 (2014).

[61] J. Peřina Jr., O. Haderka, V. Michálek, and M. Hamar, "State reconstruction of a multimode twin beam using photodetection," Phys. Rev. A **87**, 022108 (2013).

[62] C. K. Law and J. H. Eberly, "Analysis and interpretation of high transverse entanglement in optical parametric down conversion," Phys. Rev. Lett. **92**, 127903 (2004).

[63] A. Gatti, T. Corti, E. Brambilla, and D. B. Horoshko, "Dimensionality of the spatiotemporal entanglement of parametric down-conversion photon pairs," Phys. Rev. A **86**, 053803 (2012).

[64] M. Chekhova, G. Leuchs, and M. Żukowski, "Bright squeezed vacuum: Entanglement of macroscopic light beams," Optics Communications **337**, 27 – 43 (2015).

[65] D. B. Horoshko, G. Patera, A. Gatti, and M. I. Kolobov, "X-entangled biphotons: Schmidt number for 2d model," The European Physical Journal D **66**, 239 (2012).

[66] A. Allevi, M. Lamperti, M. Bondani, J. Peřina Jr., V. Michálek, O. Haderka, and R. Machulka, "Characterizing the nonclassicality of mesoscopic optical twin-beam states," Phys. Rev. A **88**, 063807 (2013).

[67] A. M. Pérez, T. S. Iskhakov, P. Sharapova, S. Lemieux, O. V. Tikhonova, M. V. Chekhova, and G. Leuchs, "Bright squeezed-vacuum source with 1.1 spatial mode," Opt. Lett. **39**, 2403–2406 (2014).

[68] O. Haderka, J. Peřina Jr., M. Hamar, and J. Peřina, "Direct measurement and reconstruction of nonclassical features of twin beams generated in spontaneous parametric down-conversion," Phys. Rev. A **71**, 033815 (2005).

[69] J. Peřina Jr., O. Haderka, M. Hamar, and V. Michálek, "Absolute detector calibration using twin beams," Opt. Lett. **37**, 2475—2477 (2012).

[70] Arvind, N. Mukunda, and R. Simon, "Gaussian-Wigner distributions and hierarchies of nonclassical states in quantum optics: The single-mode case," Phys. Rev. A **56**, 5042–5052 (1997).

[71] Arvind, N. Mukunda, and R. Simon, "Characterizations of classical and nonclassical states of quantized radiation," Journal of Physics A: Mathematical and General **31**, 565 (1998).

[72] V. Dodonov and V. Man'ko, *Theory of Nonclassical States of Light* (Taylor & Francis, New York, 2003).

[73] J. Peřina Jr., M. Hamar, V. Michálek, and O. Haderka, "Photon-number distributions of twin beams generated in spontaneous parametric down-conversion and measured by an intensified CCD camera," Phys. Rev. A **85**, 023816 (2012).

[74] C. K. Hong, Z. Y. Ou, and L. Mandel, "Measurement of subpicosecond time intervals between two photons by interference," Phys. Rev. Lett **59**, 2044 (1987).

[75] S. L. Braunstein, "Squeezing as an irreducible resource," Phys. Rev. A **71**, 055801 (2005).

[76] G. Adesso, A. Serafini, and F. Illuminati, "Multipartite entanglement in three-mode gaussian states of continuous-variable systems: Quantification, sharing structure, and decoherence," Phys. Rev. A **73**, 032345 (2006).

[77] M. B. Plenio, "Logarithmic negativity: A full entanglement monotone that is not convex," Phys. Rev. Lett. **95**, 090503 (2005).

[78] P. Marian and T. A. Marian, "Bures distance as a measure of entanglement for symmetric two-mode Gaussian states," Phys. Rev. A **77**, 062319 (2008).

[79] J. K. Asbóth, J. Calsamiglia, and H. Ritsch, "Squeezing as an irreducible resource," Phys. Rev. Lett. **94**, 173602 (2005).

[80] M. Brunelli, C. Benedetti, S. Olivares, A. Ferraro, and M. Paris, "Single- and two-mode quantumness at a beam splitter," Phys. Rev. A **91**, 062315 (2015).

[81] A. Miranowicz, K. Bartkiewicz, A. Pathak, J. Peřina, Y. Chen, and F. Nori, "Statistical mixtures of states can be more quantum than their superpositions: Comparison of nonclassicality measures for single-qubit states," Phys. Rev. A **91**, 042309 (2015).

[82] A. Miranowicz, K. Bartkiewicz, N. Lambert, Y. Chen, and F. Nori, "Increasing relative nonclassicality quantified by standard entanglement potentials by dissipation and unbalanced beam splitting," Phys. Rev. A **92**, 062314 (2015).

[83] W. Vogel and J. Sperling, "Quantum optics in the phase space," Phys. Rev. A **89**, 052302 (2014).

[84] W. Ge, M. E. Tasgin, and M. S. Zubairy, "Conservation relation of nonclassicality and entanglement for gaussian states in a beam splitter," Phys. Rev. A **92**, 052328 (2015).

[85] E. S. Polzik, J. Carri, and H. J. Kimble, "Spectroscopy with squeezed light," Phys. Rev. Lett. **68**, 3020 (1992).

[86] T. C. Ralph and P. K. Lam, "Teleportation with bright squeezed light," Phys. Rev. Lett. **81**, 5668 (1998).

[87] F. Wolfgramm, A. Ceré, F. A. Beduini, A. Predojević, M. Koschorreck, and M. W. Mitchell, "Squeezed-light optical magnetometry," Phys. Rev. Lett. **105**, 053601 (2010).

[88] J. Peřina, Jr. and J. Peřina, "Quantum statistics of nonlinear optical couplers," Prog. Opt. **41**, 361 (2000).

[89] J. Peřina and J. Křepelka, "Joint probability distribution and entanglement in optical parametric processes," Opt. Commun. **284**, 4941 (2011).

[90] R. Simon, "Peres-Horodecki separability criterion for continuous variable systems," Phys. Rev. Lett **84**, 2726 (2000).

[91] P. Marian, T. A. Marian, and H. Scutaru, "Inseparability of mixed two-mode gaussian states generated with a SU (1,1) interferometer," Journal of Physics A: Mathematical and General **34**, 6969 (2001).

[92] S. Olivares, "Quantum optics in the phase space," Eur. Phys. J. Special Topics **203**, 3 (2012).

[93] D. N. Klyshko, "Quantum optics: Quantum, classical, and metaphysical aspects," Physics-Uspekhi **37**, 1097 (1994).

[94] T. S. Iskhakov, K. Y. Spasibko, and M. V. Chekhova, "Macroscopic Hong-Ou-Mandel interference," New J. Phys. **15**, 093036 (2013).

[95] M. G. A. Paris, "Joint generation of identical squeezed states," Phys. Lett. A **225**, 28 (1997).

[96] A. Allevi, M. Bondani, and A. Andreoni, "Photon-number correlations by photon-number resolving detectors," Opt. Lett. **35**, 1707–1709 (2010).

[97] J. Laurat, T. Coudreau, N. Treps, A. Maitre, and C. Fabre, "Conditional preparation of a quantum state in the continuous variable regime: Generation of a sub-Poissonian state from twin beams," Phys. Rev. Lett. **91**, 213601 (2003).

[98] M. Hamar, J. Peřina Jr., O. Haderka, and V. Michálek, "Transverse coherence of photon pairs generated in spontaneous parametric down-conversion," Phys. Rev. A **81**, 043827 (2010).

[99] G. S. Agarwal and K. Tara, "Nonclassical character of states exhibiting no squeezing or sub-poissonian statistics," Phys. Rev. A **46**, 485–488 (1992).

[100] E. Shchukin and W. Vogel, "Nonclassical moments and their measurement," Phys. Rev. A **72**, 043808 (2005).

[101] W. Vogel, "Nonclassical correlation properties of radiation fields," Phys. Rev. Lett. **100**, 013605 (2008).

[102] A. Miranowicz, M. Bartkowiak, X. Wang, X.-Y. Liu, and F. Nori, "Testing nonclassicality in multimode fields: A unified derivation of classical inequalities," Phys. Rev. A **82**, 013824 (2010).

[103] A. W. Marshall, I. Olkin, and B. C. Arnold, *Inequalities: Theory of Majorization and its Application, sec. ed.* (Springer, New York, 2010).

[104] A. P. Dempster, N. M. Laird, and D. B. Rubin, "Maximum likelihood from incomplete data via the em algorithm," J. R. Statist. Soc. B **39**, 1—38 (1977).

[105] B. R. Frieden, *Science from Fisher Information: A Unification* (Cambridge University Press, Cambridge, UK, 2004).

[106] R. W. Boyd, *Nonlinear Optics, 2nd edition* (Academic Press, New York, 2003).

[107] C. Langrock, E. Diamanti, R. V. Roussev, Y. Yamamoto, M. M. Fejer, and H. Takesue, "Highly efficient single-photon detection at communication wavelengths by use of upconversion in reverse-proton-exchanged periodically poled LiNbO3 waveguides," Opt. Lett. **30**, 1725–1727 (2005).

[108] S. Ramelow, A. Fedrizzi, A. Poppe, N. K. Langford, and A. Zeilinger, "Polarization-entanglement-conserving frequency conversion of photons," Phys. Rev. A **85**, 013845 (2012).

[109] P. van Loock and A. Furusawa, "Detecting genuine multipartite continuous-variable entanglement," Phys. Rev. A **67**, 052315 (2003).

[110] S. Hill and W. K. Wootters, "Computable entanglement," Phys. Rev. Lett. **78**, 5022 (1997).

[111] E. Waks, E. Diamanti, B. C. Sanders, S. D. Bartlett, and Y. Yamamoto, "Direct observation of nonclassical photon statistics in parametric down-conversion," Phys. Rev. Lett. **92**, 113602 (2004).

[112] M. Avenhaus, H. B. Coldenstrodt-Ronge, K. Laiho, W. Mauerer, I. A. Walmsley, and C. Silberhorn, "Photon number statistics of multimode parametric down-conversion," Phys. Rev. Lett. **101**, 053601 (2008).

[113] J. Sperling, W. Vogel, and G. S. Agarwal, "True photocounting statistics of multiple on-off detectors," Phys. Rev. A **85**, 023820 (2012).

[114] A. Allevi, S. Olivares, and M. Bondani, "Measuring high-order photon-number correlations in experiments with multimode pulsed quantum states," Phys. Rev. A **85**, 063835 (2012).

[115] A. Serafini, G. Adesso, and F. Illuminati, "Unitarily localizable entanglement of gaussian states," Phys. Rev. A. **71**, 032349 (2005).

[116] T. Richter and W. Vogel, "Nonclassicality of quantum states: A hierarchy of observable conditions," Phys. Rev. Lett. **89**, 283601 (2002).

[117] C. W. Helstrom, *Quantum Detection and Estimation Theory* (Academic Press, New York, 1976).

[118] R. J. Glauber, *Quantum Theory of Optical Coherence: Selected Papers and Lectures* (Wiley-VCH, Weinheim, 2007).

[119] M. G. Raymer, M. Beck, and D. McAlister, "Complex wave-field reconstruction using phase-space tomography," Phys. Rev. Lett. **72**, 1137–1140 (1994).

[120] S. L. Braunstein and H. J. Kimble, "Dense coding for continuous variables," Phys. Rev. A **61**, 042302 (2000).

[121] D. Bruß, G. M. D'Ariano, M. Lewenstein, C. Macchiavello, A. Sen(De), and U. Sen, "Distributed quantum dense coding," Phys. Rev. Lett. **93**, 210501 (2004).

[122] T. Jennewein, C. Simon, G. Weihs, H. Weinfurter, and A. Zeilinger, "Quantum cryptography with entangled photons," Phys. Rev. Lett. **84**, 4729–4732 (2000).

[123] N. Gisin, G. Ribordy, W. Tittel, and H. Zbinden, "Quantum cryptography," Rev. Mod. Phys. **74**, 145—195 (2011).

[124] E. Shchukin, T. Richter, and W. Vogel, "Nonclassicality criteria in terms of moments," Phys. Rev. A **71**, 011802(R) (2005).

[125] K. Banaszek and K. Wódkiewicz, "Direct probing of quantum phase space by photon counting," Phys. Rev. Lett. **76**, 4344–4347 (1996).

[126] G. Zambra, A. Andreoni, M. Bondani, M. Gramegna, M. Genovese, G. Brida, A. Rossi, and M. G. A. Paris, "Experimental reconstruction of photon statistics without photon counting," Phys. Rev. Lett. **95**, 063602 (2005).

[127] M. Bondani, A. Allevi, and A. Andreoni, "Wigner function of pulsed fields by direct detection," Opt. Lett. **34**, 1444–1446 (2009).

[128] G. Harder, D. Mogilevtsev, N. Korolkova, and C. Silberhorn, "Tomography by noise," Phys. Rev. Lett. **113**, 070403 (2014).

[129] J. B. Altepeter, D. Branning, E. Jeffrey, T. C. Wei, P. G. Kwiat, R. T. Thew, J. L. O'Brien, M. A. Nielsen, and A. G. White, "Ancilla-assisted quantum process tomography," Phys. Rev. Lett. **90**, 193601 (2003).

Appendix

Co-author statement

As a co-author I, Ondřej Haderka, hereby confirm that Ievgen Arkhipov made major contribution to the theory and writing the following publication

- I. I. Arkhipov, J. Peřina Jr., O. Haderka, A. Allevi, and M. Bondani, "Entanglement and nonclassicality in four-mode Gaussian states generated via parametric down-conversion and frequency up-conversion," Sci. Rep. **6**, 33802 (2016).
- I. I. Arkhipov, J. Peřina Jr., O. Haderka, and V. Michálek, "Experimental detection of nonclassicality of single-mode fields via intensity moments," Opt. Express **24**, 29496–29505 (2016).

.....

Co-author statement

As a co-author I, Jan Peřina Jr., hereby confirm that Ievgen Arkhipov made considerable contribution to the theory and writing the following publications:

- I. I. Arkhipov, J. Peřina Jr., J. Peřina, and A. Miranowicz, "Comparative study of nonclassicality, entanglement, and dimensionality of multimode noisy twin beams," Phys. Rev. A **91**, 033837 (2015).
- I. I. Arkhipov, J. Peřina Jr., J. Svozilík, and A. Miranowicz, "Nonclassicality invariant of general two-mode Gaussian states," Sci. Rep. **6**, 26523 (2016).
- I. I. Arkhipov, J. Peřina Jr., J. Peřina, and A. Miranowicz, "Interplay of nonclassicality and entanglement of two-mode Gaussian fields generated in optical parametric processes," Phys. Rev. A **94**, 013807 (2016).
- I. I. Arkhipov and J. Peřina Jr., "Retrieving the covariance matrix of an unknown two-mode Gaussian state by means of a reference twin beam," Opt. Commun. **375**, 29—33 (2016).
- I. I. Arkhipov, J. Peřina Jr., O. Haderka, A. Allevi, and M. Bondani, "Entanglement and nonclassicality in four-mode Gaussian states generated via parametric down-conversion and frequency up-conversion," Sci. Rep. **6**, 33802 (2016).
- I. I. Arkhipov, J. Peřina Jr., O. Haderka, and V. Michálek, "Experimental detection of nonclassicality of single-mode fields via intensity moments," Opt. Express **24**, 29496–29505 (2016).
- I. Arkhipov, J. Peřina Jr., A. Miranowicz, and J. Peřina, "Entanglement and nonclassicality of twin beams containing noise," Proc. SPIE, **9441**, 94410Y–94410Y–7 (2014).

.....

Co-author statement

As a co-author I, Jan Peřina, hereby confirm that Ievgen Arkhipov made considerable contribution to the theory and writing the following publications:

- I. I. Arkhipov, J. Peřina Jr., J. Peřina, and A. Miranowicz, "Comparative study of nonclassicality, entanglement, and dimensionality of multimode noisy twin beams," Phys. Rev. A **91**, 033837 (2015).
- I. I. Arkhipov, J. Peřina Jr., J. Svozilík, and A. Miranowicz, "Nonclassicality invariant of general two-mode Gaussian states," Sci. Rep. **6**, 26523 (2016).
- I. I. Arkhipov, J. Peřina Jr., J. Peřina, and A. Miranowicz, "Interplay of nonclassicality and entanglement of two-mode Gaussian fields generated in optical parametric processes," Phys. Rev. A **94**, 013807 (2016).

.....

Co-author statement

As a co-author I, Adam Miranowicz, hereby confirm that Ievgen Arkhipov made considerable contribution to the theory and writing the following publications:

- I. I. Arkhipov, J. Peřina Jr., J. Peřina, and A. Miranowicz, "Comparative study of nonclassicality, entanglement, and dimensionality of multimode noisy twin beams," Phys. Rev. A **91**, 033837 (2015).
- I. I. Arkhipov, J. Peřina Jr., J. Svozilík, and A. Miranowicz, "Nonclassicality invariant of general two-mode Gaussian states," Sci. Rep. **6**, 26523 (2016).
- I. I. Arkhipov, J. Peřina Jr., J. Peřina, and A. Miranowicz, "Interplay of nonclassicality and entanglement of two-mode Gaussian fields generated in optical parametric processes," Phys. Rev. A **94**, 013807 (2016).

Adam Miranowicz

.....